

Graphical performance characterization of membrane modules for RO and PRO processes

by

Luiz Fernando Moreira
M.Sc., Pontifical Catholic University of Minas Gerais, 2018

A Project Report Submitted in Partial Fulfillment
of the Requirements for the Degree of

MASTER OF ENGINEERING

in the Department of Mechanical Engineering

© Luiz Fernando Moreira, 2022
University of Victoria

All rights reserved. This Dissertation may not be reproduced in whole or in part, by
photocopy or other means, without the permission of the author.

Graphical performance characterization of membrane modules for RO and PRO processes

by

Luiz Fernando Moreira

M.Sc., Pontifical Catholic University of Minas Gerais, 2018

Supervisory Committee

Dr. Ing. Henning Struchtrup, Department of Mechanical Engineering
Supervisor

Dr. Ben Nadler, Department of Mechanical Engineering
Committee Member

Abstract

Environmental issues have been stricken our planet in different areas. Current worldwide problems, for instance, water shortage and the increasing demand for energy can be mitigated by employing technological mechanisms, such as a well-established osmotic process for salt water desalination known as reverse osmosis (RO), and a promising technology for generating power from salinity gradient sources, called pressure retarded osmosis (PRO). This work aims to mathematically model the core component of RO and PRO systems, which is the membrane module, working in different conditions and graphically characterize its efficiency using performance indicators to support researchers and people in industry to design and implement RO and PRO systems in a less complex and more reliable way. To reach this goal, segmented mathematical models of a 5-inch scale Toyobo HP5255SI-H3K hollow fibers membrane module were developed for the RO and PRO processes using the solution-diffusion and friction-concentration polarization transport models, mass balances and pressure drop equations. After validating the models and performing simulations, the performance curves obtained were able to provide the optimum values of inlet parameters for both RO and PRO processes that led to generate the best results in terms of volume flow rate and salinity of permeate, recovery ratio, salt rejection rate, power density and net power output. In addition, some interesting discoveries were acquired from the results such as an unused portion of membrane area in the radial direction and the influence of flow velocities on entropy generation, salt and water fluxes within the membrane module in the RO process, as well as how input parameters as hydraulic pressures and flow rates impact power generation in PRO systems and how to mitigate the reverse salt flux in this process. Finally, the possibility of integrating RO and PRO systems to desalinate salt water and produce power from the resulting permeate and brine solutions is also discussed and arguments on the reasons why such systems would not work with current technology are presented.

Keywords: Reverse Osmosis, Pressure Retarded Osmosis, Performance Curves

Contents

Abstract	iii
Table of Contents	iv
List of Tables	vi
List of Figures	vii
List of Symbols	ix
Acknowledgements.....	xii
1. Introduction	13
1.1 Environmental background.....	13
1.2 Desalination and Reverse Osmosis (RO)	14
1.3 Salinity gradient energy and Pressure Retarded Osmosis (PRO).....	15
1.4 Objectives	16
2. Concepts and equations for RO and PRO systems	18
2.1 Overview of RO and PRO processes	18
2.2 Osmosis and osmotic pressure	19
2.3 Semipermeable membrane	22
2.4 Osmotic processes	25
2.5 Limiting factors on osmotic processes	26
2.5.1 Concentration polarization.....	26
2.5.1.1 Concentration polarization in RO	26
2.5.1.2 Concentration polarization in PRO.....	29
2.5.2 Membrane fouling.....	31
2.6 Transport models.....	32
2.7 Performance indicators.....	35
2.8 Pressure drop equations	36
2.9 Internal losses in the membrane module	37
3. Mathematical modelling.....	40
3.1 Segmentation.....	40
3.2 Model development.....	44
3.2.1 Main assumptions.....	44
3.2.2 Mass balances.....	44
3.2.2.1 RO mass balances.....	45
3.2.2.2 PRO mass balances	46
3.2.3 Flow rates.....	47
3.2.4 Concentrations	48
3.2.5 Membrane transport.....	48
3.2.5.1 RO transport equations	49

3.2.5.2	PRO transport equations.....	50
3.2.6	<i>Pressure drops</i>	51
3.3	Membrane module parameters	52
3.4	Validation	55
3.5	Computational resources	56
4.	Results and discussion	58
4.2	Results for the RO membrane module	58
4.2.1	<i>Validation for RO</i>	58
4.2.2	<i>Sectional distribution of pressures, flows and fluxes for RO</i>	59
4.2.3	<i>Performance curves for RO</i>	63
4.3	Results for the PRO membrane module	68
4.3.1	<i>Validation for PRO</i>	68
4.3.2	<i>Sectional distribution of pressures, flows and fluxes for PRO</i>	69
4.3.3	<i>Performance curves for PRO</i>	72
4.4	Remarks on integrated RO-PRO systems	74
5.	Conclusions and suggestions for future work	76
	Bibliography	78
	Appendix A	84
	Appendix B	85
	Appendix C	87

List of Tables

Table 1.1: Osmotic power generation capacity of rivers around the world [5].	15
Table 3.1: Membrane module parameters used in the RO and PRO simulations.	52
Table 3.2: Constants used in the RO and PRO simulations.	53
Table 3.3: Operational input parameters to the membrane module of the RO process.	53
Table 3.4: Operational input parameters to the membrane module of the PRO process.	54
Table 3.5: Input and output parameters for the RO and PRO models.	54
Table 3.6: Input parameters for validating the RO model from [42], unless otherwise noted. ...	55
Table 3.7: Input parameters for validating the PRO model from [31], unless otherwise noted. .	56
Table 4.1: Average inlet parameters for understanding the behavior of certain quantities within the membrane module of the RO process.	59
Table 4.2: Average inlet parameters for understanding the behavior of certain quantities within the membrane module of the PRO process.	69

List of Figures

Figure 2.1: General diagram of the RO process.....	18
Figure 2.2: General diagram of the PRO process.	19
Figure 2.3: Schematics representation of the osmosis phenomenon.	20
Figure 2.4: Main groups and types of semipermeable membranes [29].	22
Figure 2.5: Commonly used configurations for semipermeable membranes [33].....	23
Figure 2.6: Schematic representation of the osmotic processes considered in this study.	25
Figure 2.7: Schematic representation of local concentration polarization in RO processes.	27
Figure 2.8: Schematic representation of concentration polarization in PRO processes.....	29
Figure 2.9: Solution-diffusion model used to describe permeation across a semipermeable membrane [54].	32
Figure 2.10: Detailed view of a single hollow fiber of a membrane module.....	36
Figure 2.11: Diagram for accounting losses in the membrane module for the RO process.....	37
Figure 2.12: Diagram for accounting losses in the membrane module for the PRO process.	38
Figure 3.1: Directions of the flows in the hollow fibers membrane module for RO and PRO processes.....	40
Figure 3.2: Sample of cells within the membrane module and related dimensions.	42
Figure 3.3: Illustration of the method used for segmentizing the hollow fiber membrane module.	43
Figure 3.4: Mass balances of water and salt over a single cell for the RO process.	45
Figure 3.5: Mass balances of water and salt over a single cell for the PRO process.....	46
Figure 4.1: Comparison between experimental and produced results from the proposed RO model.	58
Figure 4.2: Sectional distribution of pressures for each cell within the membrane module.	60
Figure 4.3: Sectional distribution of volume flow rates for each cell within the membrane module.	61
Figure 4.4: Sectional distribution of salinities for each cell within the membrane module.	61
Figure 4.5: Sectional distribution of fluxes for each cell within the membrane module.....	62
Figure 4.6: Performance curve for the Toyobo HP5255SI-H3K membrane module in terms of permeate outlet volume flow rate and salinity for different inlet parameters.	63
Figure 4.7: Performance curve for the Toyobo HP5255SI-H3K membrane module in terms of recovery ratio and permeate salinity for different inlet parameters.....	65

Figure 4.8: Performance curve for the Toyobo HP5255SI-H3K membrane module in terms of salt rejection and permeate salinity for different inlet parameters.	66
Figure 4.9: Performance curve for the Toyobo HP5255SI-H3K membrane module in terms of power loss and permeate salinity for different inlet parameters.	67
Figure 4.10: Performance curve for the Toyobo HP5255SI-H3K membrane module in terms of extra cost work and permeate salinity for different inlet parameters.	68
Figure 4.11: Comparison between experimental and produced results from the proposed PRO model	69
Figure 4.12: Sectional distribution of pressures for each cell within the membrane module.	70
Figure 4.13: Sectional distribution of volume flow rates for each cell within the membrane module	70
Figure 4.14: Sectional distribution of salinities for each cell within the membrane module.....	71
Figure 4.15: Sectional distribution of fluxes for each cell within the membrane module.	72
Figure 4.16: Performance curve for the Toyobo HP5255SI-H3K membrane module in terms of power density and net power output for different inlet parameters.	73
Figure 4.17: Performance curve for the Toyobo HP5255SI-H3K membrane module in terms net power output and power loss for different inlet parameters.....	74
Figure A.1: Toyobo HP5255SI-H3K membrane module specification sheet.....	84
Figure B.1: Performance curves for the Toyobo HP5255SI-H3K membrane module working in the RO process in terms of permeate outlet volume flow rate and its salinity for inlet feed solution with salinities of 0.020 kg/kg (a) and 0.050 kg/kg (b)	85
Figure B.2: Performance curves for the Toyobo HP5255SI-H3K membrane module working in the RO process in terms of recovery ratio and permeate salinity for inlet feed solution with salinities of 0.020 kg/kg (a) and 0.050 kg/kg (b)	85
Figure B.3: Performance curves for the Toyobo HP5255SI-H3K membrane module working in the RO process in terms of salt rejection and permeate salinity for inlet feed solution with salinities of 0.020 kg/kg (a) and 0.050 kg/kg (b)	85
Figure B.4: Performance curves for the Toyobo HP5255SI-H3K membrane module working in the RO process in terms of power loss and permeate salinity for inlet feed solution with salinities of 0.020 kg/kg (a) and 0.050 kg/kg (b)	86
Figure B.5: Performance curves for the Toyobo HP5255SI-H3K membrane module working in the RO process in terms of extra cost work and permeate salinity for inlet feed solution with salinities of 0.020 kg/kg (a) and 0.050 kg/kg (b)	86
Figure C.1: Performance curve for the Toyobo HP5255SI-H3K membrane module working in the PRO process in terms of power density and net power output for inlet draw solution with salinities of 0.020 kg/kg (a) and 0.050 kg/kg (b)	87
Figure C.2: Performance curve for the Toyobo HP5255SI-H3K membrane module working in the PRO process in terms net power output and power loss for inlet draw solution with salinities of 0.020 kg/kg (a) and 0.050 kg/kg (b)	87

List of Symbols

a	Activity coefficient	-
A	Water permeability coefficient	m/s-Pa
A_m	Total membrane area	m ²
$A_{m,vol}$	Active membrane area per unit of volume	m ² /m ³
B	Salt permeability coefficient	m/s
C	Mass concentration	kg/m ³
d	Diameter of the hollow fiber	m
D_s	Diffusion coefficient of salt	m ² /s
E	Total energy of a system	J
h	Enthalpy	J/kg
i	Van't Hoff factor	-
J_s	Salt flux	kg/m ² -s
J_v	Permeate flux	m/s
J_w	Water flux	m ³ /m ² -s
k	External mass transfer coefficient of salt	m/s
K	Internal mass transfer coefficient of salt	s/m
L	Axial or radial length	m
L_{mod}	Active length of the membrane module	m
m	Mass	kg
\dot{m}	Mass flow rate	kg/s
M	Molar mass	kg/mol
\widehat{M}	Molality	mol/kg
n_{fib}	Number of fibers within the membrane module	-
$n_{fib,cell}$	Number of fibers per cell	-
n_r	Number of radial segments	-
n_z	Number of axial segments	-
P	Pressure	Pa
r	Radius	m
R	Gas constant	J/kg-K
\overline{R}	Molar gas constant	J/mol-K
R_{ct}	Radius of the perforated central tube	m
Re	Reynolds number	-
R_{mod}	Active radius of the membrane module	m
\mathbb{R}_{recov}	Recovery ratio	%
\mathbb{R}_{rejec}	Salt rejection rate	%
s	Specific entropy	J/kg-K
S	Structure factor of the support layer	-
\dot{S}_{gen}	Entropy generation rate	W
sal	Salinity	kg of salt/kg of solution
Sc	Schmidt number	-
Sh	Sherwood number	-

t	Thickness of the support layer	m
T	Temperature	K
u	Superficial velocity	m/s
U	Velocity	m/s
v	Specific volume	m ³ /kg
V_{cell}	Volume of a cell	m ³
\dot{V}	Volume flow rate	m ³ /s
W	Work	J
\dot{W}	Power	W
W_s	Weighted average of the molecular weight of each dissolved solute in salt water	g/mol

Greek letters

γ	Osmotic coefficient of the solution	-
δ	Boundary layer of fluid near the membrane	-
Δ	Difference	-
Δr	Radial length of a cell	m
Δz	Axial length of a cell	m
ε	Void fraction	-
θ	Coefficient of proportionality	-
μ	Specific chemical potential	J/kg
ν	Dynamic viscosity	Pa-s
Π	Osmotic pressure	Pa
ρ	Density	kg/m ³
σ	Porosity of the support layer	-
τ	Tortuosity of the support layer	-
φ	Concentration polarization coefficient	-

Subscripts

0	Reference state
α	Particles in a mixture
β	Particles in a mixture different from α particles
<i>avg</i>	Average length
<i>b</i>	Bulk
<i>br</i>	Brine
<i>D</i>	Draw solution
<i>dens</i>	Refers to the power density of the membrane module in PRO
<i>EC</i>	Refers to the Extra Cost work
<i>ext</i>	External diameter
<i>F</i>	Feed solution
<i>fac</i>	Refers to the osmotic pressure factor
<i>fib</i>	Refers to the fibers

<i>fw</i>	Solution with lower concentration or freshwater
<i>I</i>	Refers to the internal concentration polarization
<i>in</i>	Inlet flow
<i>int</i>	Internal diameter
<i>loss</i>	Refers to losses within the system
<i>m</i>	Refers to the membrane surface
<i>net</i>	Refers to the net power output by the PRO process
<i>out</i>	Outlet flow
<i>P</i>	Permeate
<i>PRO</i>	Refers to the PRO process
<i>pw</i>	Refers to pure water
<i>RO</i>	Refers to the RO process
<i>s</i>	Salt
<i>sh</i>	Refers to the shell side
<i>sol</i>	Refers to the solution
<i>sw</i>	Solution with higher concentration or salt water
<i>tot</i>	Refers to a total amount
<i>w</i>	Water

Superscripts

<i>i</i>	Row index of variables within the membrane module
<i>j</i>	Column index of variables within the membrane module

Acknowledgements

Firstly, I thank God for His endless love, mercy, peace that surpasses all understanding and wonderful grace manifested through our Lord Jesus Christ.

I also thank my wonderful wife Amanda, my parents Luiz and Sônia, my aunt Maria da Consolação, my sister Tatiane, my brother-in-law Eduardo and my nephew Rodrigo for their love, encouragement and patience during this time.

I would like to express my sincere appreciation and gratitude to my supervisor Dr. Henning Struchtrup for granting this opportunity to me, as well as for his great support and guidance in this journey.

I thank the examination committee for their advice and comments on this work.

Finally, I thank all my friends and colleagues from UVic for their assistance and support.

Chapter 1

Introduction

This work characterizes graphically the efficiency of membrane modules to be used in Reverse Osmosis (RO) and Pressure Retarded Osmosis (PRO) processes using performance indicators. It was divided into five chapters as follows:

- Chapter 1 introduces current concerning environmental issues (i.e. quality water scarcity worldwide and dependency on fossil fuels for producing energy) and presents a solution for mitigating these problems, which is by employing osmotic processes as RO and PRO systems. The objectives of this study are also presented in this chapter;
- Chapter 2 explains the working principles of RO and PRO processes, main concepts related to them, and the equations used for mathematically modelling their core component (membrane module);
- Chapter 3 demonstrates how the mathematical models were developed and presents the inlet parameters and validation procedure for the models;
- Chapter 4 is dedicated to present and discuss the results of the simulations, validation and performance curves;
- Chapter 5 ends this study with the conclusions obtained from the results and offers suggestions for future work on this topic.

1.1 Environmental background

Our planet faces serious environmental challenges in a wide range of areas. One of the major concerning areas is the availability of natural resources (e.g. water), which have been scarcer each day. Water scarcity in many regions worldwide is a severe problem these days. Quality water shortage affects more than one-third of the world population, and this amount is expected to rise significantly in the upcoming years [1]. Studies have shown that 1.2 billion people have no access to safe potable water and 2.6 billion have poor sanitation conditions, resulting in numerous deaths every year [2]. Another current environmental issue is the global demand for energy, which has been increasing substantially due to world population growth linked to the economic development of many countries [3]. The worldwide demand for primary energy source reached the highest rate since 2010 and fossil fuels represent the main energy source

consumed [4]. This increased greenhouse gases emissions and accelerated climate change on the planet [5]. Fortunately, according to current estimations, around 30% of the total global energy generation comes from renewable energy sources [6]. Before these concerning scenarios, it must be acknowledged that there is a strong necessity to address global water supply in water-stressed regions, as well as energy needs in different parts of the globe while decreasing the worldwide dependence on fossil fuels.

1.2 Desalination and Reverse Osmosis (RO)

In order to mitigate the overload on water supply, technological mechanisms must be employed. The only technologies that allow increasing the amount of water available for human consumption are water reuse and desalination [1], which is a process for producing water with proper quality in terms of salt concentration (salinity) for human consumption from salt water [7]. Between these two alternatives, salt water desalination is able to provide a clearly stable and unlimited source of quality water.

The main water reservoir on Earth is the oceans. Salt water accounts for approximately 97% of all existing water on the planet, while around 2% of water supply is locked in icecaps and only another 0.5% is available as freshwater [8]. There are also large quantities of water under the Earth's surface, however many of them are located too deeply and may not be economically feasible to be obtained. Given the massive amount of salt water available on the planet, desalination is an important method for obtaining fresh water [9]. Currently, there are approximately 15,900 fully operational desalination plants in 177 countries, supplying nearly 95 million m³/day of fresh water for human consumption [10], which corresponds to only 3% of the overall daily water usage on the planet [11]. Despite of this, some countries, e.g. Saudi Arabia, United Arab Emirates, China, etc. [7], strongly rely on desalination systems to address their freshwater demands [9].

Currently, the most commercially dominant technologies for desalination are Multi-Stage Flash (MSF) distillation and the membrane-based process named Reverse Osmosis (RO) [9]. Over the years, the use of RO processes has increased significantly due to membrane technology improvements, which provide several advantages for such systems due to its simpler construction and operation, good efficiency, compactness, ease of process automation and economical feasibility [9, 12, 13]. This set of assets has made the RO technology the most popular and reliable state-of-the-art technique for salt water desalination [13]. Nowadays, approximately 84% of the operational desalination plants worldwide are based on RO technology and produce around 65 million m³/day of desalinated water, which corresponds to 69% of the total volume of desalinated water produced around the world [7].

However, RO processes present some limitations. The main drawback is membrane fouling, which might lead to a reduction on fluxes, interfere on the permeate quality, reduce the membrane lifespan, and raise maintenance costs. Also there might be a need for feed water pre-treatment or brine treatment before discharge in some cases [13], which are common obstacles in other desalination methods.

1.3 Salinity gradient energy and Pressure Retarded Osmosis (PRO)

From the energy point of view, renewable energy usage must be increased to reduce the dependence on fossil fuels. Nowadays, renewable energy can be obtained from different sources as wind, solar, hydro, etc. A novel renewable energy source that has drawn attention from the research community over the past few decades is the salinity gradient source. This energy source is based on mixing two solutions with different salinities which allows energy to be released due to the chemical potential difference between the two solutions [14]. Thanks to recent technologies capable of controlling the mixture of these two solutions, energy can be produced and converted into a more convenient form as electricity [15].

The principle of applying mechanisms to extract salinity gradient energy from the mixture of two solutions with different salinities (e.g. water from sea and rivers) to generate power has been investigated since the 1970's. It is acknowledged that there are rivers all over the world with massive potential for salinity gradient energy production [16]. The estimated amount of global energy released by the mixture between water from sea and rivers is estimated to be approximately 2 TW [15], which corresponds to nearly 8.5% of the world electricity demand in 2020 [17]. Table 1.1 shows the potential power generation capacity for some major rivers worldwide. According to Table 1.1, it would be theoretically possible that the mentioned rivers would be able to supply up to 42,070 MW, which would be sufficient to provide electric energy for more than 470 million households in different parts of the world. Of course, it is not feasible to deviate the course of such large rivers in economic, practical or environmental terms, but this gives an idea of the potential of electricity production for remote areas that could be achieved using medium or small-scale plants.

River	Average flow rate [$\times 10^3 \text{ m}^3/\text{s}$]	Power capacity [MW]	Electricity supply [$\times 10^3$ households] ^a
Amazon river, Brazil	200	20,800	77,600
La Plata river, Argentina	80	8,320	29,100
Congo river, Congo	57	5,930	282,300
Yangtze river, China	22	2,290	5,800
Ganges river, Bangladesh	20	2,080	74,300
Mississippi river, USA	18	1,870	1,300
Columbia river, USA	7.5	780	550

Table 1.1: Osmotic power generation capacity of rivers around the world [5].

^a This estimative is based on household's average consumption in each country.

A suitable and promising solution to make effective use of this opportunity is the implementation of another membrane-based process, called Pressure Retarded Osmosis (PRO). PRO systems, have been proven to achieve superior efficiency compared to other technologies for extracting energy from salinity gradient sources [18]. PRO also offer advantages over other systems for energy recovery and power generation (e.g. solar and wind) such as: steady and reliable source of power production; flexibility to control power generation and possibility to be integrated to desalination processes [3, 5, 19].

The main limitation of PRO systems is their modest efficiency with current membrane technology [20]. The practical feasibility of PRO systems is another concern because it may not be economically and/or environmentally advantageous to make changes in the course of a river to implement such process. Another limitation on PRO processes is the necessity of pre-treating the incoming flows. One of the incoming solutions needs to be treated (usually it is not clean enough) for avoiding membrane fouling, while the other requires pre-treatment before entering the process due to its higher concentration of salt in some cases [21].

1.4 Objectives

Currently, RO processes are a consolidated technology for desalination [12] and they are crucial for many countries across the globe for allowing them to meet a humanitarian function of supplying freshwater to their population. Whereas PRO systems are still a concept in development for producing power from a renewable energy source. In order to properly fulfill their environmental and humanitarian roles, these systems should operate as efficiently as possible.

The initial intention of this work was to perform computational optimizations of RO, PRO and combined RO-PRO, also called Osmotic Energy Storage (OES), systems working with different sets of input parameters. After analysing this plan, it was observed that what the optimization process would do was to simulate the models repeatedly using different input parameters. This would take too much time to obtain only a small set of results with the best values for each simulated condition, which seemed to be not worthy due to the high computational costs.

From this initial plan, a more appealing opportunity was identified. Instead of running a massive number of simulations only varying the input parameters to find the optimum results, it was decided that a more feasible and meaningful option in terms of computational costs and practical application, would be to simulate the models with the range of input parameters only once and collect the results in a database. Then, use the obtained results for future optimization processes. This way, simulations would be resolved and the computational efforts required for the optimization process would be significantly smaller.

However, encouraged by a demand from the RO industry on how to graphically quantify the efficiency of the core component used in RO and PRO systems (the membrane module), then we decided to mathematically model this component on MATLAB and use the results from the simulations to create meaningful plots, that is, to graphically characterize the efficiency of membrane modules using performance indicators, especially for the RO process since it is already an established technology. This is the purpose of this work. By doing this, it was possible to gain a broader understanding on how the membrane module work in RO and PRO systems for a variety of different conditions, since manufacturers of this component only provide a very selective set of data due to internal confidential reasons.

This research is useful for researchers and people in industry to make the design and implementation of RO and PRO systems less complex and more reliable. Because it allows them to totally focus on other aspects of their systems and improve them with no need for spending too much time and resources on performing countless simulations.

Hence, to reach the goal of graphically characterizing the efficiency of membrane modules for RO and PRO systems, the following specific objectives were established:

- a) Mathematically model and simulate a membrane module using actual data;
- b) Validate the proposed models by using the same input parameters as experimental studies found in literature;
- c) Generate meaningful plots from the results that describe the performance of the membrane module working on RO and PRO processes under different conditions;
- d) Discuss what relevant information can be understood from those plots, e.g., if the whole available membrane area is being fully used, the influence of flow velocities within the membrane module over the output results, the feasibility on integrating RO and PRO systems to perform desalination and produce power, etc.

Chapter 2

Concepts and equations for RO and PRO systems

This chapter presents the working principles of RO and PRO processes, as well as main concepts related to them. The governing laws and equations used for modeling these processes are also presented and explained.

2.1 Overview of RO and PRO processes

As previously mentioned, the RO process is used for desalination, while PRO is a process for producing power from salinity gradient sources. Both processes, respectively depicted in Figures 2.1 and 2.2, work based on the osmotic pressures of their inlet solutions, which is a colligative property that depends on the fluids temperature and concentration as presented ahead in section 2.2.

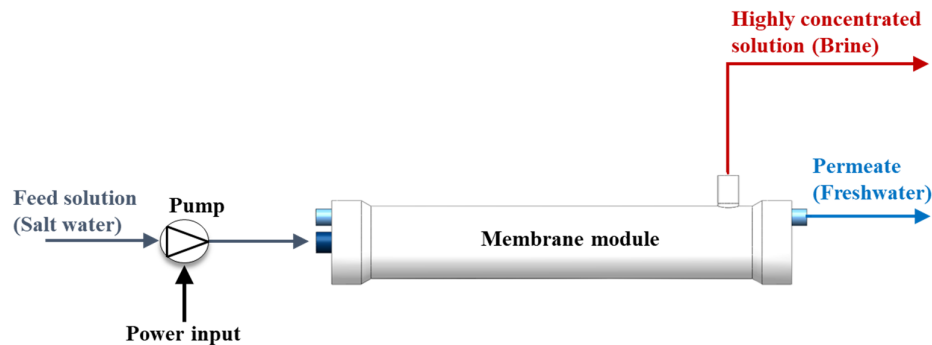


Figure 2.1: General diagram of the RO process.

The RO process shown in Figure 2.1 uses hydraulic pressure differences and a phenomenon called osmosis, which is also explained in detail ahead in section 2.2, to produce water with suitable salinity for human consumption from salt water. This process, composed by a hydraulic pump and a membrane module, presents one inlet and two outlet flows. The inlet flow, also called feed solution, is salt water or high salinity water, which is pressurized by the hydraulic pump to enter the membrane module. Inside this component, salt water is forced against a semipermeable membrane allowing water molecules to pass through, leaving major part of salt particles behind. The first outlet flow is the output freshwater or lower salinity water produced, named permeate. The other outlet flow is the highly concentrated remaining solution of the process, so called brine.

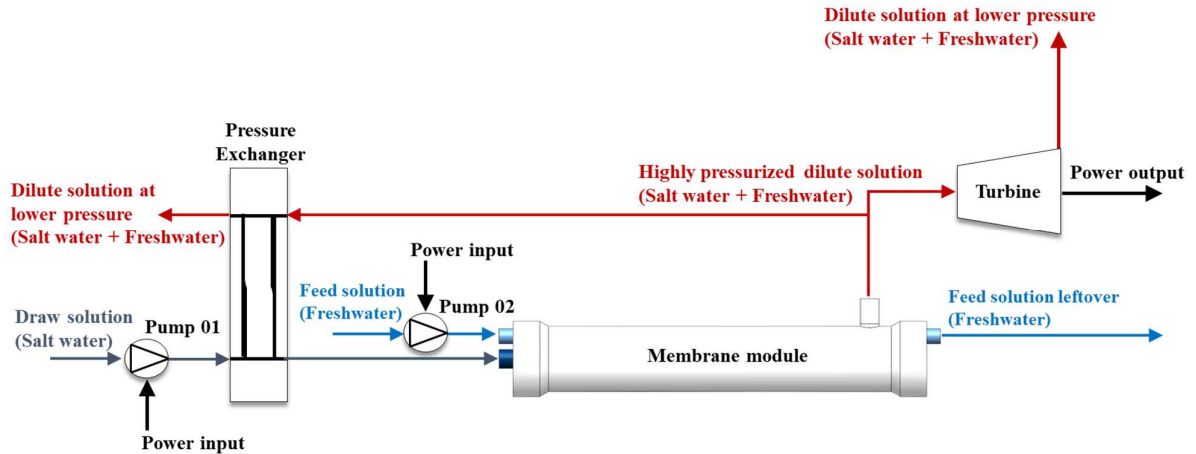


Figure 2.2: General diagram of the PRO process.

The PRO process shown in Figure 2.2 also uses hydraulic pressure differences and the osmosis phenomenon, but to produce power. This process, which presents two inlet and three outlet flows, is composed by two hydraulic pumps, a pressure exchanger and a hydraulic turbine. The first inlet flow, also called feed solution, is freshwater or lower salinity water. The freshwater is pressurized by a hydraulic pump to enter the membrane module and once inside, a portion of it is drawn through a semipermeable membrane by salt water or high salinity water coming from the second inlet, which is named draw solution. Before entering the membrane module, the incoming salt water is pressurized by a hydraulic pump and sent to the pressure exchanger device to raise its hydraulic pressure a bit more. A highly pressurized mixture of salt water and freshwater flows out of the membrane module and is divided into two streams. The first stream is sent to the hydraulic turbine to generate power, while the second stream is sent to the pressure exchanger to pressurize the incoming stream of salt water. These are the two first outflows from the PRO process. The third and last outflow is the remaining portion of feed solution that was not utilized in the process. A salt water salinity of 0.035 kg of salt/kg of solution [22] was used as the reference salinity.

2.2 Osmosis and osmotic pressure

Osmosis is the phenomenon in which RO and PRO technologies are based on, and it is presented in Figure 2.3. Consider two salt water solutions of different composition (i.e. freshwater as the solvent and salt water as the solution) in a container at a time zero. The external pressure is the atmosphere pressure P_0 . The two fluids present equal hydraulic pressures, but different chemical potentials due to their distinct concentrations of salt, and are separated by a semipermeable membrane, which allows only water molecules to pass through (Figure 2.3a) [16].

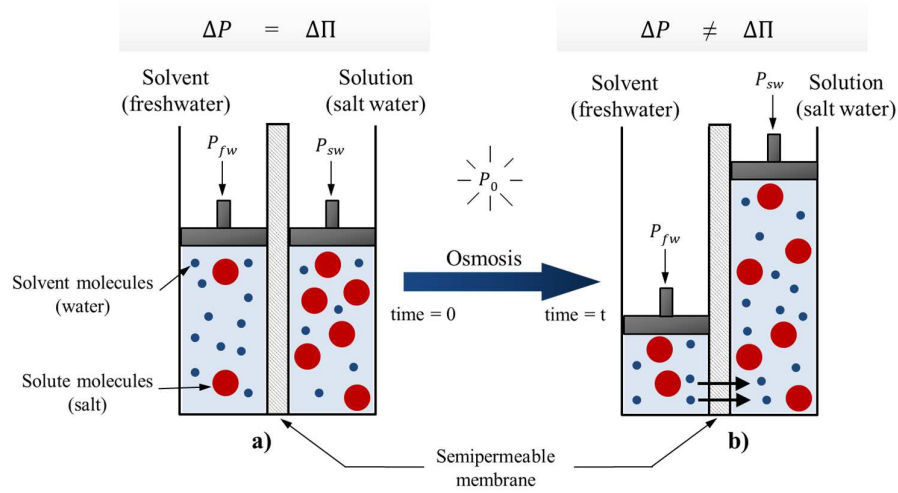


Figure 2.3: Schematics representation of the osmosis phenomenon.

The term osmosis is used to describe the flux of solvent (water) molecules from the higher chemical potential side (freshwater) to the lower one (salt water) until their chemical potentials reach equilibrium after a certain time (Figure 2.3b). The chemical potential difference between these two substances caused by their different concentrations of solute (salt) is the mechanism that causes the flow of solvent (water) from one side to the other, that is, the osmosis phenomenon [23].

In general terms, the specific mass based chemical potential of a certain component α in a mixture is expressed as [16]:

$$\mu_{\alpha} = \mu_{\alpha}(T, P, C) , \quad (2.1)$$

where μ_{α} is the chemical potential of component α at a temperature T , pressure P and mass concentration C . Note that these and all the other properties and variables introduced in this work with their respective units are presented in the first pages of this document on the list of symbols section on page ix. For an isothermal process, an infinitesimal change in chemical potential of component α is written as:

$$d\mu_{\alpha} = R_{\alpha} T d\ln(a_{\alpha} C_{\alpha}) + v_{\alpha} dP , \quad (2.2)$$

where a_{α} , C_{α} and v_{α} are the activity coefficient, mass concentration and specific volume of component α respectively; and R_{α} is the gas constant of component α , which is calculated as:

$$R_{\alpha} = \frac{\bar{R}}{M_{\alpha}} , \quad (2.3)$$

where \bar{R} is the molar gas constant; and M_{α} is the molar mass of component α .

The presence of a solute dissolved in the substances on both sides of the semipermeable membrane not only is a parameter in which their chemical potentials depend on, but it also provides another property named osmotic pressure (Π). The term osmotic pressure refers to the hydraulic pressure difference between a solution and the solvent in equilibrium, when separated by a semipermeable membrane that allows only solvent particles to pass through [16]. In other words, osmotic pressure is a pressure that must be applied to the solution with the purpose of preventing solvent molecules to cross the membrane [5]. This is a colligative property, which means it is a function of concentration and temperature of the substance. Considering the equilibrium condition between freshwater and salt water shown in Figure 2.3a where $\Delta P = \Delta \Pi$, the chemical potential of water is constant across the semipermeable membrane and is related to its osmotic pressure as [24]:

$$\mu_{fw}(T, P) = \mu_{sw}(T, P + \Pi, a_w) , \quad (2.4)$$

where μ_{fw} is the chemical potential of freshwater as a function of its temperature and hydraulic pressure; μ_{sw} is the chemical potential of salt water as a function of its temperature, pressure and activity coefficient of water molecules. Here, $P + \Pi$ is the total hydraulic pressure on salt water, where P is the hydraulic pressure on water alone and Π is the osmotic pressure of the solution. The hydraulic pressures on both sides of the membrane differ by the osmotic pressure (Π).

An empirical and general relation for the osmotic pressure as a function of the temperature and mass concentration of a solution is defined as [25]:

$$\Pi(T, C) = \gamma(T, C)RT \rho(T, C, P) \widehat{M} , \quad (2.5)$$

where $\gamma(T, C)$ is the osmotic coefficient of the solution as a function of its temperature and mass concentration; and $\rho(T, C, P)$ is the density of the solution as a function of its temperature, mass concentration and pressure. These two parameters were acquired from experimental research [25]. \widehat{M} is the molality of the solution, that is the number of mols of solute per kilograms of solvent, and it is empirically expressed as [25]:

$$\widehat{M} = \frac{10^3 sal}{W_s (10^3 - sal)} , \quad (2.6)$$

where W_s is the weighted average of the molecular weight of each dissolved solute in salt water, which is equal to 31.4038 g/mol [26]; and sal is the salinity of salt water as a function of its mass concentration and density:

$$sal = \frac{C}{\rho(T, C, P)} . \quad (2.7)$$

For a dilute solution (i.e., the solute concentration is considerably smaller than the solvent concentration in the mixture) at constant temperature, the osmotic pressure can be expressed by a commonly used simplified relation, which is the van't Hoff equation given by [24, 27]:

$$\Pi = iRTC , \quad (2.8)$$

where i is the van't Hoff factor, which describes the number of particles the solute dissolves into. In the case of NaCl in water, for example, it values 2.

2.3 Semipermeable membrane

A semipermeable membrane is a flat and thin structure, which separates two substances and restricts the passage of one or more chemical species acting as a selective barrier while allowing others to pass. The mechanisms of mass transport through a membrane are either a diffusion of specific molecules or a fluid motion that results from electrical potential, concentration, pressure or temperature gradients [28]. The semipermeable membrane can be homogeneous, that is totally uniform throughout in terms of composition and structure, heterogeneous, with different chemical or physical compositions containing pores of various dimensions, or even a layered structure [29]. Current commercial materials for membranes production are polymers due to their thermal and chemical stabilities, as well as mechanical properties [30].

The two main groups, in which membranes can be classified, are symmetrical, also called isotropic, and asymmetrical, also known as anisotropic. These two groups are shown in Figure 2.4.

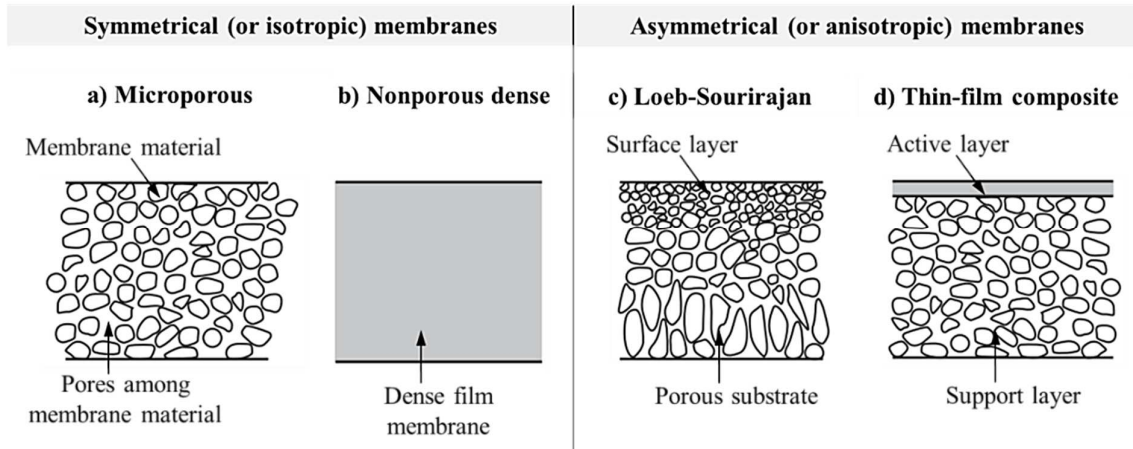


Figure 2.4: Main groups and types of semipermeable membranes [29].

Symmetrical membranes are composed of the same structure throughout. In microporous membranes (Figure 2.4a), only particles smaller than the smallest orifice cross the membrane as in a filter. Nonporous dense membrane (Figure 2.4b) is a dense film, which allows transport of substances by diffusivity and solubility in the membrane material due to a driving force.

Asymmetrical membranes are layered and the structure of the base is different from that on the surface. The selective characteristics are established by the surface layer, while the substrate works as mechanical resistance support due to large pressure differences [28-30]. Loeb-Sourirajan membranes are comprised of a thinner surface layer followed by a thicker and loose porous substrate (Figure 2.4c). Thin-film composite membranes (Figure 2.4d) present a substrate (support layer) attached to a surface (active layer) made of different materials.

Asymmetrical membranes are more commonly used commercially because they bear higher water fluxes compared to symmetrical membranes [29]. The semipermeable membrane used here was the thin-film composite type made of a cellulose triacetate material, which allows usage in both RO and PRO processes [31]. In the case of RO processes, this type of semipermeable membrane can reach salt rejection rates higher than 96%. This means that less than 4% of salt particles in salt water passes through the semipermeable membrane, which is a common efficiency parameter presented by most current commercial thin-film composite cellulose triacetate semipermeable membranes. The salt rejection rate depends mainly on the exposure time of the membrane to the solution, as well as the concentrations of feed solution and permeate. This is an important parameter for measuring the performance of semipermeable membranes in RO systems, since it determines the amount of salt removed from the inlet salt water. The salt rejection rate is presented in more detail ahead in section 2.7.

The geometry on which semipermeable membranes are produced is also relevant because of their performance characteristics, costs and type of application. The most commonly used geometries of semipermeable membranes for osmotic systems are flat sheet and hollow fibers [32]. The three main configurations of membrane modules, in which these geometries are used, are shown in Figure 2.5.

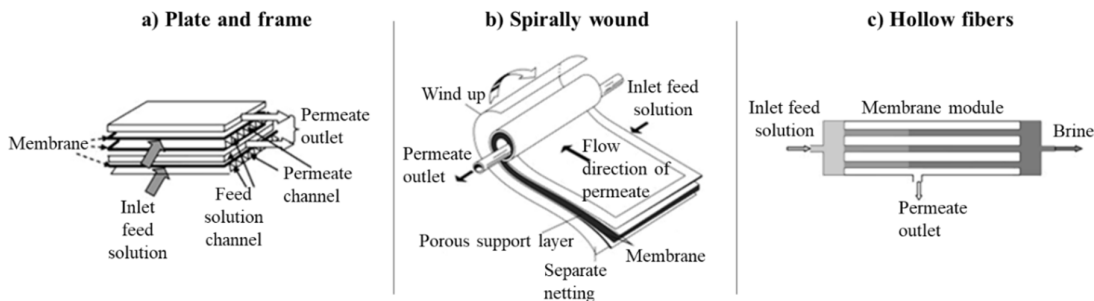


Figure 2.5: Commonly used configurations for semipermeable membranes [33]

The plate and frame configuration (Figure 2.5a) is a set of two flat sheet semipermeable membranes piled up with their feed sides in front of each other and a spacer between them. A number of sets is piled up according to the application. Its main drawback is the lower membrane surface per unit volume compared to the other configurations [34], between 45 and 150 ft²/ft³ [35].

The spirally wound configuration (Figure 2.5b) consists in a bag made of two large flat sheet semipermeable membranes sealed on three sides and separated by a porous support layer that allows the outlet permeate to flow. This assembly is rolled up spirally to form a cylindrical membrane module. A central bored tube is placed in the middle of the rolled bag to collect the outlet permeate, while the brine solution flows through the channel created by the separate netting, or mesh spacer, between the rolled-up membrane and porous layer sets. The membrane surface per unit volume of the spirally wound configuration is higher than that one in the plate and frame configuration [33], ranging from 150 to 380 ft²/ft³ [35].

The hollow fiber configuration (Figure 2.5c) presents a construction of capillary size tubular semipermeable membranes, called hollow fibers, which are as small as human hair in terms of outside diameter [35]. These hollow fibers are cross wound around a perforated central tube. The hollow fibers are attached to perforated end plates and the whole set is inserted into a vessel. The inlet feed solution enters the membrane module through the central tube where it is distributed along its length. Then, it flows radially through the small holes of the central tube to occupy the empty spaces of the shell while crossing the hollow fibers, leaving the major part of salt behind. Finally, the output permeate flows through the hollow fibers out of the module to be collected and the brine solution leaves from another outlet [33]. The main advantages of hollow fiber membranes are [36-38]:

- a) greater membrane surface per unit volume (between 150 and 1500 ft²/ft³ [35]), which results in higher productivity;
- b) lower cost per unit membrane area due to its large packing density;
- c) it bears higher pressure differentials compared to the spirally wound configuration, which increases the possibilities of different operating conditions;
- d) possibility to reverse the flux in order to clean and recover the hollow fiber membranes;
- e) easier module fabrication and operation.

Due to these outstanding advantages, along with a wider availability of technical data found both in literature and in official sources from membrane manufacturing companies, as well as capability to be used in both RO and PRO systems, the hollow fibers arrangement was chosen as the membrane module configuration.

2.4 Osmotic processes

Processes driven by osmotic pressure differences are called osmotic processes, in which deviations from equal hydraulic and osmotic pressures differences ($\Delta P \neq \Delta \Pi$) results in a process towards equilibrium. The osmotic processes studied here are depicted in Figure 2.6, which shows freshwater and salt water in a container separated by a semipermeable membrane. In this picture, the semipermeable membrane is represented by the white crosshatched rectangle and the black arrows in the middle in front of it indicate the direction of water flux. There are also pistons on both sides of the container in which hydraulic pressures are applied. These osmotic processes are described as [5, 32]:

- a) RO: Salt water is pressurized against the semipermeable membrane. A larger hydraulic pressure difference (ΔP) is used to overcome the osmotic pressure difference ($\Delta \Pi$) on both sides, forcing water molecules to pass through the semipermeable membrane while it restrains the passage of salt. The output permeate is freshwater or lower salinity water (Figure 2.6a);
- b) PRO: Salt water is pressurized to a value below its osmotic pressure on one side of the semipermeable membrane. In this process, the hydraulic pressure differential (ΔP) on both sides is smaller than the osmotic pressure difference ($\Delta \Pi$) of the fluids, allowing water molecules to cross the semipermeable membrane from the freshwater to the salt water side. This results in an outgoing diluted flow with larger pressure than the inlet flows (Figure 2.6b).

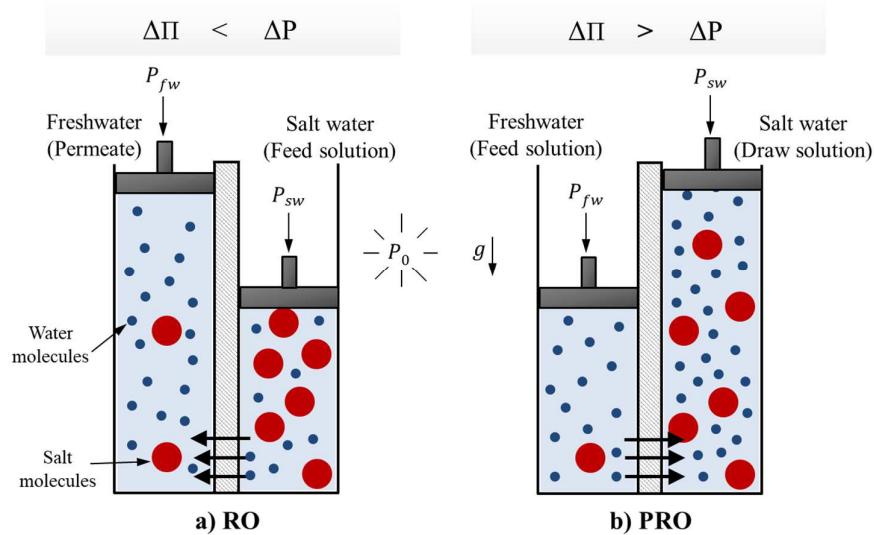


Figure 2.6: Schematic representation of the osmotic processes considered in this study.

2.5 Limiting factors on osmotic processes

The semipermeable membrane is the core component in RO and PRO systems and it is unanimous that it plays a key role in these systems performance. In theory, RO and PRO processes share similar working principle with respect to fluxes across the semipermeable membrane and they also present similar limitations. The main constraints in such processes are concentration polarization and membrane fouling, which are described as follows.

2.5.1 Concentration polarization

An ideal semipermeable membrane with perfect selectivity would reject all salt particles and allow only water molecules to pass through. In addition, if there were perfect mixing in the solutions on both sides of this ideal membrane, the concentrations on its surfaces would be the same as in the rest of the bulk solutions. However, in real semipermeable membranes, a phenomenon called concentration polarization is one of the most limiting factors for RO and PRO processes [23].

2.5.1.1 Concentration polarization in RO

In an ongoing RO process, along with the flow of bulk feed solution within the membrane module at concentration ($C_{F,b}$), there is also a convective flow of salt from the bulk feed solution towards the surface of the semipermeable membrane as illustrated in Figure 2.7. As the flux of water (J_w) crosses the semipermeable membrane, it carries some small amount of salt (J_s) with it. The salt left behind makes the concentration of salt on the membrane surface ($C_{F,m}$) in the feed side to increase, resulting in a boundary layer (δ) with higher salinity than the bulk feed solution in this region. This leads to a diffusional back-transport of salt away from the membrane. Therefore, there is an accumulation of salt in this boundary layer, as well as on the membrane surface. Consequently, the concentration at the membrane surface is greater compared to that on the bulk feed solution and, of course, also higher than the concentration of permeate arriving (C_P) on the other side of the membrane. This phenomenon is known as concentration polarization [13].

The accumulation of salt at the membrane surface increases the osmotic pressure of the solution within the boundary layer on the feed solution side and therefore, the osmotic pressure difference across the membrane. This decreases the driving force, and therefore the flow of permeate through the membrane, since the net osmotic pressure difference on both sides of the membrane is reduced [13, 35]. The relation between the osmotic pressure difference and water flux across the membrane is shown ahead in Eq. (2.26).

To reduce the effective osmotic pressure difference in front of the membrane and consequently, concentration polarization in RO it is necessary to support flow mixing. This can be achieved by adjusting the velocity of the inlet flows, applying ultrasound, pulsation or electric field techniques, and vibrating or rotating the membrane module. [39, 40].

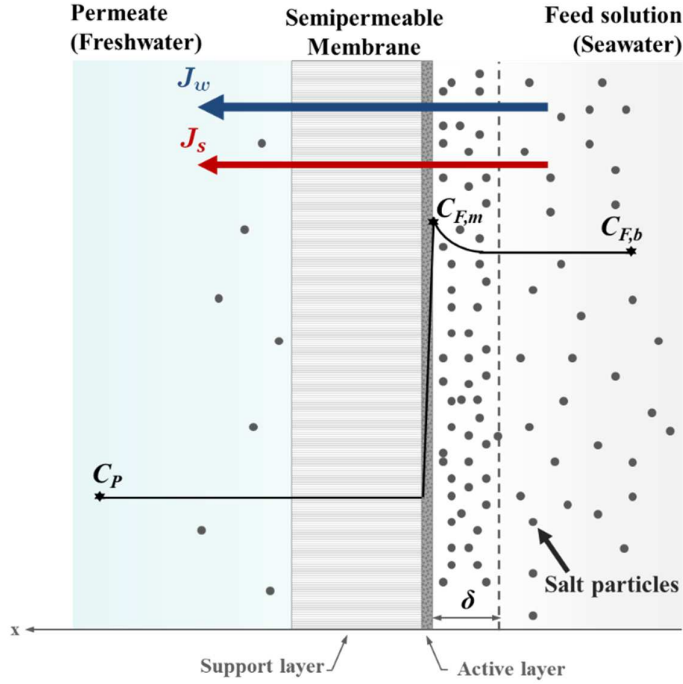


Figure 2.7: Schematic representation of local concentration polarization in RO processes.

The mass balance of salt over the semipermeable membrane for the RO process can be written as [41]:

$$J_s = J_w C(x) + D_s \frac{dC(x)}{dx}, \quad (2.9)$$

where $J_w C(x)$ is the convective flow of salt, $C(x)$ is the concentration of salt in the convective flow at a position x ; $D_s \frac{dC(x)}{dx}$ is the diffusional back-transport of salt away from the membrane, D_s is the diffusion coefficient of salt, and $\frac{dC(x)}{dx}$ is the gradient in concentration along the membrane thickness. Integration of Eq. (2.9) over the concentration polarization boundary layer leads to:

$$C_{F,m} = \left(C_{F,b} - \frac{J_s}{J_w} \right) \exp\left(\frac{J_w \delta_F}{D_s} \right) + \frac{J_s}{J_w}. \quad (2.10)$$

Since the thickness of the boundary layer is difficult to measure, the ratio $\frac{\delta_F}{D_s}$ is replaced by the mass transfer coefficient of salt in the feed solution (k). Then, Eq. (2.10) is rewritten as:

$$C_{F,m} = \left(C_{F,b} - \frac{J_s}{J_w} \right) \exp \left(\frac{J_w}{k} \right) + \frac{J_s}{J_w}, \quad (2.11)$$

where, k is calculated as:

$$k = \frac{Sh D_s}{d_{fib,ext}}, \quad (2.12)$$

where $d_{fib,ext}$ is the external diameter of the hollow fiber; and Sh is the Sherwood number, which is an empirical relation that depends on experimental data such as the type of process, membrane module characteristics, composition of the solution and flow patterns. The equation used here, provided by [42], meets the membrane module specifications used in the simulations for the RO process and it is given by:

$$Sh = 0.048 Re^{0.6} Sc^{1/3}, \quad (2.13)$$

where, Re is the Reynolds number and Sc is the Schmidt number. The Reynolds number is defined as:

$$Re = \frac{d_{fib,ext} U \rho}{\nu}, \quad (2.14)$$

where ρ and ν are the density and the dynamic viscosity of higher salinity water, respectively; U is the velocity of the concentrated water in the shell, and it is given by:

$$U = u\varepsilon, \quad (2.15)$$

where ε is the void fraction of the module, that means, the volume within the membrane module free of hollow fibers; and u is the superficial velocity of the higher salinity water, which is the velocity as if there were no hollow fibers within the membrane module, and it is given by:

$$u = \frac{\dot{V}}{2\pi r L}, \quad (2.16)$$

where \dot{V} is the volume flow rate of fluid at a radial and an axial lengths r and L , respectively, within the membrane module.

Lastly, the Schmidt number is calculated as:

$$Sc = \frac{\nu}{\rho D_s} . \quad (2.17)$$

2.5.1.2 Concentration polarization in PRO

As in RO processes, concentration polarization in PRO processes is also an issue, but here it reduces the osmotic pressure difference across the membrane and consequently, the possible work output. Figure 2.8 illustrates the concentration polarization phenomenon present in PRO processes, where two types of concentration polarization occur: internal and external represented by the red and yellow regions, respectively.

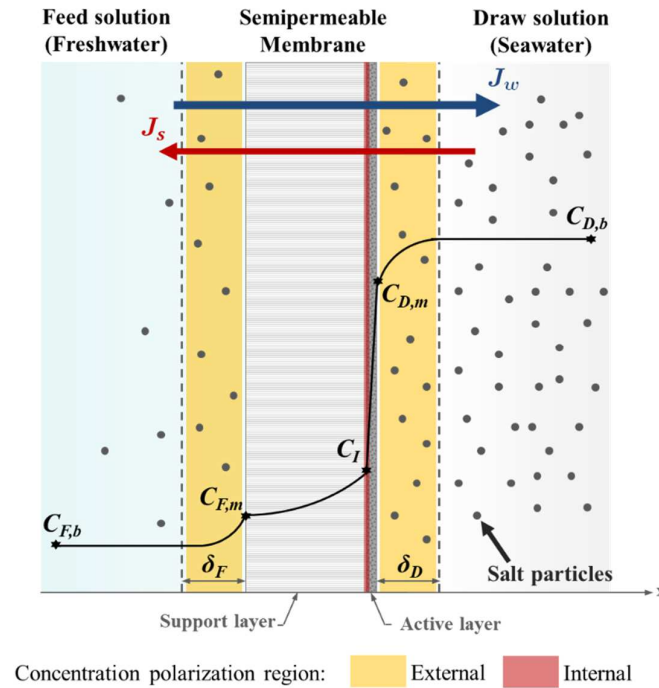


Figure 2.8: Schematic representation of concentration polarization in PRO processes.

The internal concentration polarization can be understood as the salt concentration on the interface between the support and active layers (C_I). As a result of the salinity gradient across the membrane, a salt flux (J_s) crosses the membrane from the draw to the feed solution side. This phenomenon, called reverse salt flux, makes part of the salt to be retained between the active and support layers of the semipermeable membrane, which increases the salinity in the red colored region. This contributes for a smaller driving force pushing water to cross the membrane, since the osmotic pressure difference across the membrane is reduced. External concentration polarization (yellow regions) occurs differently either within the feed (δ_F) and draw

(δ_D) boundary layers on both sides of the membrane. In the feed solution side, salt accumulation along the support layer produces a phenomenon named concentrative external concentration polarization, which increases the salt concentration of the bulk feed solution ($C_{F,b}$) near the support layer surface ($C_{F,m}$). While in the draw solution side, the water flux across the membrane (J_w) from the feed to draw solution dilutes the amount of salt near the surface of the active layer. Consequently, the concentration on the active layer surface ($C_{D,m}$) is lower than that in the bulk draw solution ($C_{D,b}$). Hence, the presence of concentration polarization reduces the osmotic pressure gradient through the membrane, decreasing its efficiency [23, 28, 43].

It is possible to minimize external concentration polarization by using enhanced mixing and proper velocity for the flows along the membrane surface. To reduce the internal concentration polarization, some modifications in membrane parameters are necessary, for instance: lower thickness, low salt leakage and less tortuous support layers [44].

It is important to mention that Figures 2.7 and 2.8 represent an infinitesimal segment of a flat semipermeable membrane. For hollow fibers, which are very narrow and their curvature is much larger than their diameter, the curvature effects for the flow inside of it can be ignored. Also, small segments of hollow fibers can be treated as a plane interface [45]. This approach is supported by the related literature [31, 46, 47].

Analogously to the RO process, a mass balance of salt over the semipermeable membrane for PRO (refer to Figure 2.8) is written as [41]:

$$-J_s = D_s \frac{dC(x)}{dx} + J_w C(x) . \quad (2.18)$$

That is, the salt flux is composed of diffusive and convective contributions. The negative sign in front of the salt flux is because it is in the opposite direction relative to the horizontal axis shown in Figure 2.8.

Using a similar approach for integration as the one presented in section 2.5.1.1, integration of Eq. (2.18) over the boundary layers on the feed and draw sides for the PRO process gives:

$$C_{F,m} = \left(C_{F,b} + \frac{J_s}{J_w} \right) \exp \left(\frac{J_w}{k} \right) - \frac{J_s}{J_w} , \quad (2.19)$$

$$C_{D,m} = \left(C_{D,b} + \frac{J_s}{J_w} \right) \exp \left(- \frac{J_w}{k} \right) - \frac{J_s}{J_w} . \quad (2.20)$$

Here, the mass transfer coefficients (k) at the two membrane interfaces are assumed to be equal, since their dependency on concentration are not significant and their values do not vary much compared to each other [41, 45, 48].

The Sherwood number, which is a parameter within the mass transfer coefficient as seen in Eq. (2.12), is obtained experimentally and depends on the nature of the process, membrane module, concentration of the solution, etc. For the PRO process it is given by [31]:

$$Sh = 0.45 Re^{0.1} Sc^{1/3} . \quad (2.21)$$

For the internal concentration polarization, some parameters of the support layer must be considered. Integration of Eq. (2.18) over the thickness of the support layer provides:

$$C_I = \left(C_{F,m} + \frac{J_s}{J_w} \right) \exp \left(J_w \frac{\tau t}{\sigma D_s} \right) - \frac{J_s}{J_w} , \quad (2.22)$$

where τ , t and σ are the tortuosity, thickness and porosity of the support layer, respectively. The term $\frac{\tau t}{\sigma D_s}$ is also written as:

$$\frac{\tau t}{\sigma D_s} = \frac{S}{D_s} , \quad (2.23)$$

where S is the structure factor of the support layer of the semipermeable membrane. Finally, the term $\frac{S}{D_s}$ is replaced by another coefficient of mass transfer (K), which measures the resistance of transport of salt in the porous support layer. Combining Eqs. (2.22) and (2.23), it leads to:

$$C_I = \left(C_{F,m} + \frac{J_s}{J_w} \right) \exp(J_w K) - \frac{J_s}{J_w} . \quad (2.24)$$

2.5.2 Membrane fouling

Another challenging issue that figures as drawback during the operation of RO and PRO systems is membrane fouling, since it affects the operation and maintenance costs of such systems. Membrane fouling occurs due to deposition of materials inside the semipermeable membrane pores or on its surface and it can be grouped in four categories [49]:

- a) Organic fouling is due to natural organic materials present in fresh or salt water (e.g., polysaccharides, proteins, lipides, cell components, etc.);
- b) Inorganic fouling is caused by scaling formation in the membrane module (i.e., crystalized salts, oxides, hydroxides, other minerals, etc.);

- c) Colloidal fouling is due to accumulation of colloids, which adhere the membrane surface and it is linked to the shape, charge and interaction with ions of these colloids (e.g., silt, clay, etc.);
- d) Biofouling occurs because of biofilm formation on the membrane surface, which is formed by grown microorganisms.

Not only membrane fouling reduces the overall system performance by decreasing the water flux across the membrane and raising the operating pressure required for the process, but it also reduces the membrane lifespan, since it would have to go through chemical cleaning more often. A number of studies have been carried out over the years to better comprehend and mitigate membrane fouling [50-53]. However, it is still one of the most obstacles to be tackled in RO and PRO plants [49]. That is why performing pre-treatment of the feed solutions before inputting them into the systems is so important, since it allows to avoid membrane fouling. Unfortunately, pre-treatment processes might be costly, making the implementation and/or operation of RO or PRO systems economically unfeasible in some cases.

2.6 Transport models

The main characteristic of semipermeable membranes is their capability of blocking passage of certain particles while allowing others to pass easily [54]. Transport models are crucial methods to explain the transport of particles through semipermeable membranes [13]. Among the different transport models available for describing the mechanism of permeation through membranes, the base model selected for this work was the solution-diffusion model. This model was proposed in the 1960's and over the years it became the most accepted and extensively model used for RO and PRO applications due to better expressing the non-porous behavior of the semipermeable membranes used in actual applications, which presented diffusion as their major transport mechanism [13, 54]. Figure 2.9 presents a schematic of the solution-diffusion transport model.

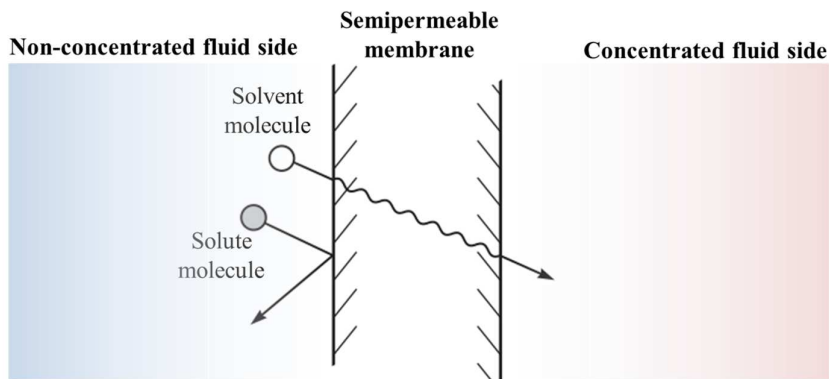


Figure 2.9: Solution-diffusion model used to describe permeation across a semipermeable membrane [54].

In the solution-diffusion model, molecules are separated because of the differences in their solubilities and diffusivities through the semipermeable membrane. It considers that molecules dissolve and diffuse through the membrane material driven by a concentration difference [55]. In this sense, the flux of component α through the semipermeable membrane is proportional to the reduction in chemical potential across the membrane as:

$$J_{\alpha} = -\theta_{\alpha} \frac{d\mu_{\alpha}}{dx} , \quad (2.25)$$

where J_{α} is the flux of component α through the membrane; θ_{α} is the transport coefficient of proportionality that relates the chemical potential to the flux of component, which is not necessarily constant; and the term $\frac{d\mu_{\alpha}}{dx}$ represents the gradient in chemical potential of component α along the membrane thickness. Note that Eq. (2.25) presents the same form as the first Fick's law [45, 56, 57].

By combining Eqs. (2.2) and (2.25) along with the appropriate boundary conditions, the equations for water and salt fluxes across an idealized semipermeable membrane for the RO process could be developed [55, 58]. The water flux is given by:

$$J_w = A(\Delta P - \Delta \Pi) , \quad (2.26)$$

where J_w is the flux of water through the membrane; A is the water permeability coefficient of the membrane; ΔP and $\Delta \Pi$ are the hydraulic and osmotic pressure differences across the membrane, respectively. Observe that the water flux across the membrane decreases as the osmotic pressure difference increases due to the concentration polarization phenomenon as explained earlier in section 2.5.1.1.

The salt flux is expressed as:

$$J_s = B(C_{B,m} - C_P) , \quad (2.27)$$

where J_s is the flux of salt through the membrane; B is the salt permeability coefficient of the membrane; $C_{B,m}$ is the concentration of salt in the bulk solution at the membrane interface; and C_P is the concentration of permeate. Note that while the water flux across a semipermeable membrane is driven by hydraulic and osmotic pressure differences, the salt flux occurs due to the salt concentration gradient through the membrane. This difference is because of the nature of the substance. Water molecules in a fluid require pressure difference to be displaced. On the other hand, in salt flux the chemical potential difference due to the applied pressures are negligible in comparison with the chemical potential difference due to a concentration gradient [48].

The solution-diffusion model [48] was historically relevant in terms of describing the transport of mass through a semipermeable membrane in RO processes, however it did not account for some crucial factors, which are known these days, due to technological constraints and lack of specialized literature and data from that time. Because of these limitations, a more precise approach derived from the solution-diffusion model was chosen to be used for the RO process. This is the friction-concentration polarization model [59]. This widespread method was verified to better predict the actual performance of membrane modules for RO applications, since it considers the effect of concentration polarization on water and salt fluxes, as well as it uses mass transfer coefficients obtained from experimental data.

Therefore, the water flux is rewritten as:

$$J_w = A(\Delta P - \varphi \Delta \Pi) , \quad (2.28)$$

where φ is the concentration polarization coefficient, which accounts for the concentration polarization effect on water and salt fluxes in the RO, and it is given by:

$$\varphi = \frac{C_{F,m} - C_P}{C_{F,b} - C_P} = \exp\left(\frac{J_v}{k}\right) , \quad (2.29)$$

where J_v is the total flux of permeate (i.e., water and salt) across the semipermeable membrane:

$$J_v = \frac{J_s + (J_w \rho_{pw})}{\rho} . \quad (2.30)$$

where ρ_{pw} is the density of pure water; and ρ is the mass density of the mixture. Note that J_s is the mass flux of salt, but J_w is the volume flow of water.

Similarly, the flux of salt across the semipermeable membrane considering the influence of concentration polarization is adjusted to

$$J_s = B\varphi(C_{F,m} - C_P) . \quad (2.31)$$

On the other hand, since the PRO technology is still not mature enough and requires more research and development, this work was restricted to a simpler analysis of the PRO process. The focus here is on RO processes because it is already a consolidated technology and widely used in commercial desalination plants around the world as mentioned previously in section 1.2.

The solution-diffusion model was selected as the transport model to express the mass transport through the semipermeable membrane in the PRO process. In order to use Eq. (2.26) to describe the flux of water for PRO processes, a small adjustment

needs to be made to maintain the water flux positive. Since the osmotic pressure difference ($\Delta\Pi$) is larger than the hydraulic pressure difference (ΔP) for such systems, these terms are exchanged. The fluxes of water and salt through an idealized membrane for the PRO process according to the solution-diffusion model are respectively defined as:

$$J_w = A(\Delta\Pi - \Delta P) , \quad (2.32)$$

and

$$J_s = B(C_{D,m} - C_I) . \quad (2.33)$$

2.7 Performance indicators

The efficiency of membrane modules working in RO and PRO processes are measured using input and output parameters as flow rates and concentrations. Two important indicators for the membrane module performance in the RO process are the salt rejection rate (\mathbb{R}_{rejec}), which measures the amount of salt removed from the inlet feed solution, and the recovery ratio (\mathbb{R}_{recov}), which is the ratio between the flow rates of permeate produced and feed solution entering the membrane module. These two performance indicators are given as percentages respectively,

$$\mathbb{R}_{rejec} = \left(1 - \frac{C_P}{C_{F,b}}\right) \cdot 100\% , \quad (2.34)$$

and

$$\mathbb{R}_{recov} = \left(\frac{\dot{m}_P}{\dot{m}_{F,b}}\right) \cdot 100\% , \quad (2.35)$$

here \dot{m}_P is the mass flow rate of permeate produced; and $\dot{m}_{F,b}$ is the mass flow rate of feed solution supplied to the membrane module.

The salt rejection rate (\mathbb{R}_{rejec}) is commonly used in industry to measure the performance of membrane modules in RO systems, since it describes the ability of the membrane to separate salt from salt water [54], which is directly linked to the membrane module lifespan. The recovery ratio (\mathbb{R}_{recov}) is also a useful performance indicator because it measures the amount of permeate produced relative to the inlet feed solution. For both indicators, it is better to have higher values because it means that the quality and amount of permeate produced are favorable. Unfortunately, it is not possible to reach 100% on them due to imperfections in the semipermeable membrane material and losses during the process.

For membrane modules working in PRO systems, an important indicator of efficiency is their power density (\dot{W}_{PRO}). This stands for the osmotic energy output per unit membrane area given by:

$$\dot{W}_{PRO} = J_w \Delta P = A(\Delta\Pi - \Delta P)\Delta P , \quad (2.36)$$

2.8 Pressure drop equations

The passage of the solutions through the membrane module generates hydraulic losses due to friction between the fluid with the materials of the semipermeable membrane and the internal walls of the module. Different measures related to the hollow fibers are used to express the pressure drops within the fibers and the membrane module shell. These measures are shown in Figure 2.10.

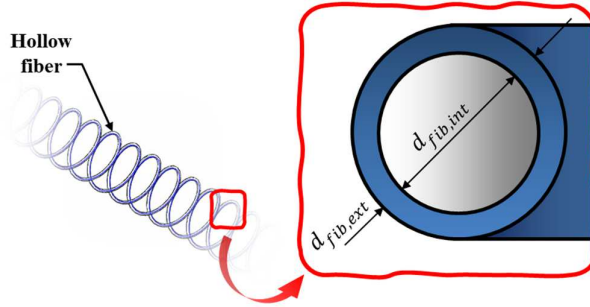


Figure 2.10: Detailed view of a single hollow fiber of a membrane module.

The pressure drop along the length of hollow fibers is expressed in its differential form by the Hagen-Poiseuille equation as:

$$\frac{\partial P}{\partial L_{fib}} = - \frac{128 \nu \dot{V}}{\pi d_{fib,int}^4} , \quad (2.37)$$

where ∂L_{fib} and $d_{fib,int}$ are an infinitesimal axial length and the internal diameter of the hollow fiber, respectively.

The pressure drop for fluids flowing through the shell of the membrane module is described by the Ergun equation in its differential form as [60]:

$$\frac{\partial P}{\partial L_{sh}} = \frac{150 (1 - \varepsilon)^2 \nu u}{\varepsilon^3 (1.5 d_{fib,ext})^2} + \frac{1.75 (1 - \varepsilon) \rho u^2}{\varepsilon^3 (1.5 d_{fib,ext})} , \quad (2.38)$$

here ∂L_{sh} is an infinitesimal radial length in the shell of the membrane module. The first term on the right-hand side in Eq. (2.38) accounts for the viscous energy losses, while the second term represents the kinetic energy losses. Note that terms as superficial velocity (u), void fraction (ε), dynamic viscosity (ν), external diameter of the hollow fiber ($d_{fib,ext}$), etc. were introduced previously in section 2.5.1.1.

2.9 Internal losses in the membrane module

In actual RO and PRO systems, entropy is generated within the membrane module due to friction between the solutions and the walls of the hollow fibers and shell, so called friction losses. There are also losses related to the flux of water across the membrane caused by concentration polarization, which increases the local osmotic pressure of the mixture [23, 36]. As a result, the work requirement to run these processes is larger and more amount of work is necessary to overcome these losses. There are further losses due to pressure drops and entropy generation within pipes, pumps, turbines, and other equipment in these systems [16], however these are out of the scope of this study.

Figure 2.11 illustrates the diagram used to account for the losses within the membrane module alone for the RO process. Consider the membrane module alone as an open system. It has an incoming flow of salt water ($\dot{m}_{sw,in}$) at a pressure ($P_{sw,in}$) and temperature (T), and outgoing flows of concentrated brine ($\dot{m}_{br,out}$) at a pressure ($P_{br,out}$) and temperature (T) and fresh or less concentrated water ($\dot{m}_{fw,out}$) at environmental pressure and temperature (P_0, T_0).

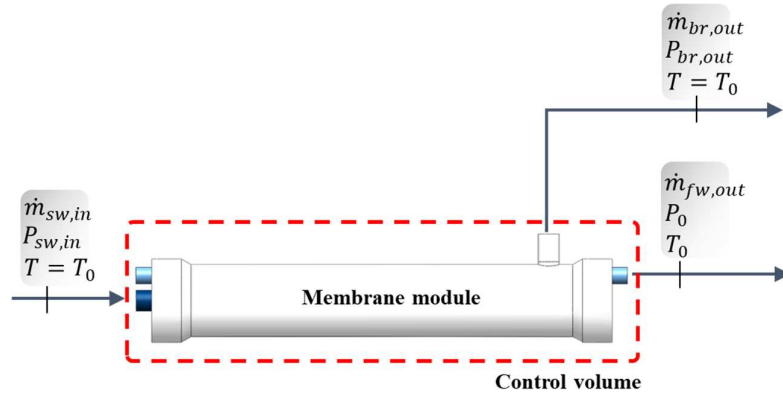


Figure 2.11: Diagram for accounting losses in the membrane module for the RO process.

For the purpose of simplicity, consider that the membrane module alone shown in Figure 2.11 undergoes an isothermal process at steady state with negligible changes in specific kinetic and potential energies. Also, the total entropy generation due to heat transfer over the system boundary occurs at environmental temperature (T_0). The total internal losses within the membrane module alone for the RO process reads:

$$T_0 \dot{S}_{gen} = \sum_{in} \dot{m}_{in} (h_{in} - T_0 s_{in}) - \sum_{out} \dot{m}_{out} (h_{out} - T_0 s_{out}) = \dot{W}_{loss} , \quad (2.39)$$

here \dot{S}_{gen} is the entropy generation rate caused by irreversibilities within the membrane module; \dot{m}_{in} and \dot{m}_{out} are the mass flow rates entering and leaving the membrane module alone; h_{in} and h_{out} are the specific enthalpies of the flow entering and leaving

the membrane module; and s_{in} and s_{out} are the specific entropies associated with the mass flows entering and leaving the membrane module. Eq. (2.39) shows that the total internal losses within the membrane module alone ($T_0 \dot{S}_{gen}$) is given by the difference in enthalpies and entropies between the incoming and outgoing flows. The total internal losses within the membrane module alone are also written as power losses (\dot{W}_{loss}).

The extra cost work for the RO process, which measures the extra work input per liter of permeate produced to be provided to this open system to overcome the total internal losses, is given by:

$$\dot{W}_{EC} = \frac{\dot{W}_{loss}}{\dot{V}_P}, \quad (2.40)$$

where \dot{W}_{EC} is the extra cost work for the RO process; and \dot{V}_P is the volume flow rate of permeate produced.

Similarly for the PRO system, Figure 2.12 exhibits the diagram used for calculating the losses within the membrane module alone for the PRO process. The membrane module alone shown in Figure 2.12 has two inlet flows at a same temperature (T). The first is salt water ($\dot{m}_{sw,in}$) at a pressure ($P_{sw,in}$) and the other is freshwater ($\dot{m}_{fw,in}$) at a pressure ($P_{fw,in}$). There are also two outgoing flows. One is the diluted salt water ($\dot{m}_{sw,out}$) at a pressure ($P_{sw,out}$), while the other is the remaining freshwater that did not cross the hollow fibers ($\dot{m}_{fw,out}$) at an environmental pressure (P_0). The two outlets leave the membrane module at the same temperature ($T = T_0$).

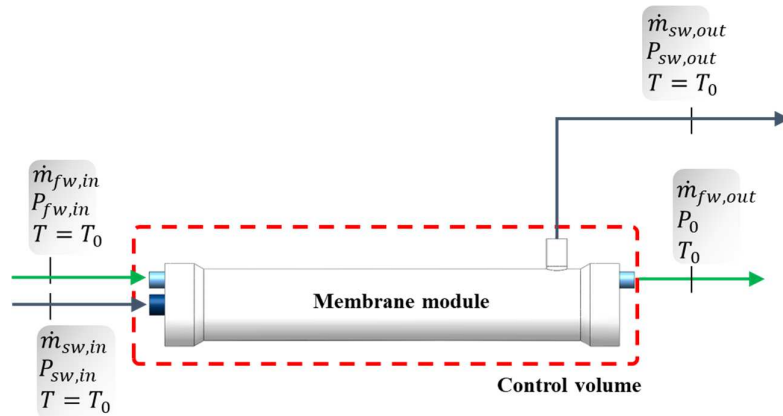


Figure 2.12: Diagram for accounting losses in the membrane module for the PRO process.

Using analogous simplification as done for the membrane module in RO, the membrane module alone displayed in Figure 2.12 for PRO also undergoes an isothermal process at steady state. The total entropy generation due to heat transfer over the system boundary occurs at environmental temperature (T_0) and changes in specific kinetic and potential energies are also negligible. The total internal losses (\dot{W}_{loss})

within the membrane module alone for the PRO process is expressed by the difference in enthalpies and entropies between the inlet and outlet flows as given in Eq. (2.39).

After presenting the key concepts to understand how RO and PRO processes operate, this work aims to visually characterize the efficiency of membrane modules using performance parameters in order to comprehend on which conditions this component performs in the most effective way for its purposed application as mentioned in section 1.4. This study is intended to guide researchers and professionals to select more accurately the appropriate membrane modules according to their needs for on-site application. This way, their RO and PRO plants will be respectively able to produce quality freshwater and generate energy more efficiently from the energy and economic perspectives.

Chapter 3

Mathematical modelling

This chapter presents the steps used for developing this study. These steps comprise the procedure for segmenting the membrane module, as well as the way in which the governing equations presented in chapter 2 were applied for describing the mass balances, flow rates and pressure drops within the membrane module for the RO and PRO processes. The technical information of the selected membrane module is also provided, as well as the procedure for verifying the accuracy of the proposed models. Finally, the computational resources used here are presented.

3.1 Segmentation

The segmentation method for the hollow fibers membrane module configuration considered a radially symmetric module for both RO and PRO processes. The directions of the flows for each process are indicated in Figure 3.1 and are described in the following paragraphs. Note that for the RO process, saltwater (feed solution) flows in the shell side of the membrane module, while freshwater (permeate) flows within the hollow fibers. For the PRO process, freshwater (feed solution) also flows inside the hollow fibers and saltwater (draw solution) is the one flowing in the shell side. That is, in any case freshwater flows within the hollow fibers and saltwater flows outside. In order to prevent any misunderstanding in terms of location, some variables in the equations for modeling both processes use the subscripts *sh* and *fib* to indicate shell and fibers sides, respectively.

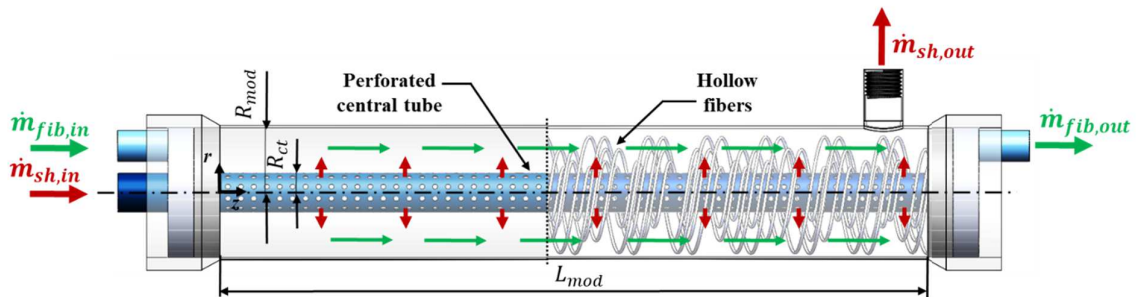


Figure 3.1: Directions of the flows in the hollow fibers membrane module for RO and PRO processes.

In the RO process, the flow rate of salt water ($\dot{m}_{sh,in}$) enters the membrane module through the perforated central pipe, escapes through the holes and flows radially only within the module towards the outer radius to be collected at the outlet tube ($\dot{m}_{sh,out}$). Meanwhile, a major part of water and some small portion of salt cross the hollow fibers membranes. Within the hollow fibers, the permeate is considered to flow only axially towards the length of the membrane module ($\dot{m}_{fib,out}$) and collected at the outlet. For the hollow fibers configuration, the curvature effects on the flow inside the hollow fibers were neglected in both RO and PRO processes, since the curvature of the fibers are considerably larger than their capillary diameter.

In the PRO process, the flow rate of salt water ($\dot{m}_{sh,in}$), which enters the membrane module via the perforated central pipe and flows only radially within the module as in the RO process. However, due to the difference in salinity, the flow rate of freshwater, which enters the module through the hollow fibers inlet ($\dot{m}_{fib,in}$) and flows only axially, crosses the hollow fibers in order to equilibrate the salt concentration of salt water in the shell. This makes the pressure of the fluid within the shell of the membrane module to increase. These two mixed streams flow only radially to be collected at the module outlet tube ($\dot{m}_{sh,out}$) at a higher pressure than their respective inlet pressures to produce power, while the remaining freshwater that did not cross the hollow fibers ($\dot{m}_{fib,out}$) continues to flow only axially towards the end of the module length.

As a result of these flows patterns, a two-dimensional model for the hollow fibers membrane module based on previous research [47] was considered as a reference for this study, since it presents good accuracy and acceptable computational costs. The membrane module for both RO and PRO processes was segmented into a number of axial (n_z) and radial (n_r) ring-shaped cells (i.e. a $n_z = 10 \times n_r = 10$ grid). This choice presented a suitable balance between computational costs and accuracy during the simulations. The axial length of the cells is given by:

$$\Delta z = \frac{L_{mod}}{n_z}, \quad (3.1)$$

here Δz is the axial length of each cell; L_{mod} is the active length of the membrane module shown in Figure 3.1, which is the length of the membrane module that allows the contact of the hollow fibers with the feed solution in the shell; and n_z is the number of axial segments.

The radial length of the cells is expressed as:

$$\Delta r = \frac{R_{mod} - R_{ct}}{n_r}, \quad (3.2)$$

where Δr is the radial length of each cell; R_{mod} is the membrane module active radius and R_{ct} is the radius of the perforated central tube, both displayed in Figure 3.1; and n_r is the number of radial segments. A partial interior view of the membrane module showing the main dimensions of a single cell is provided in Figure 3.2. In this figure, r is the inner radius of a given cell. Note that the cells present larger volume towards the outer radius of the membrane module, since the radial coordinate (r) increases and the radial length (Δr) of each cell is constant.

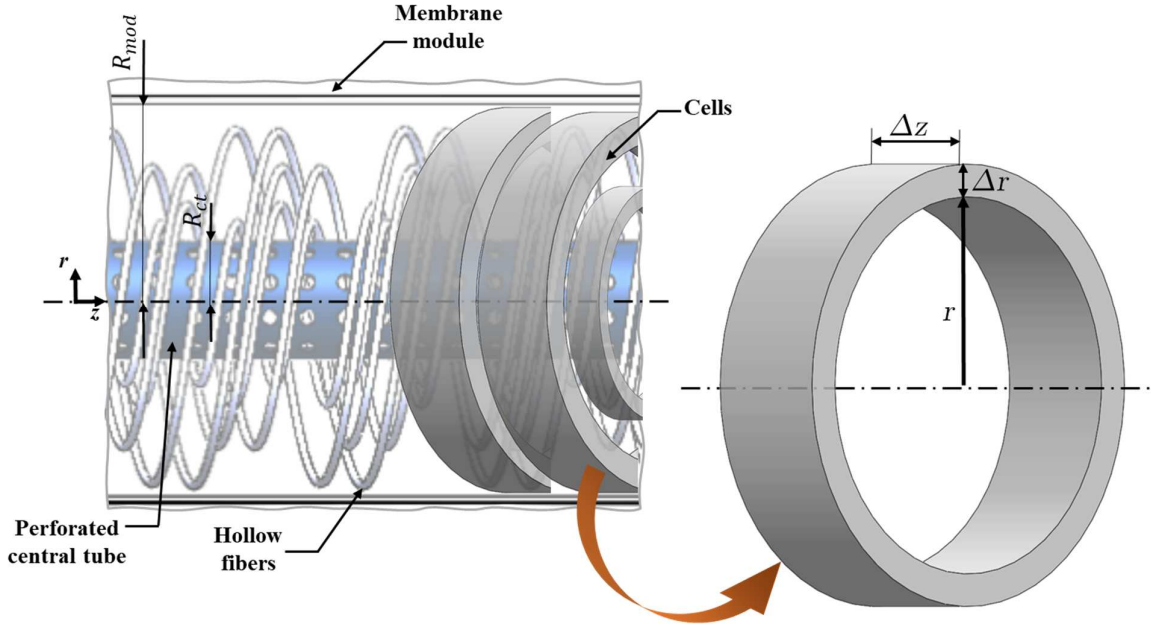


Figure 3.2: Sample of cells within the membrane module and related dimensions.

The orientation for the flows in the cells was considered to be in the axial and radial directions only. That is, the model was two-dimensional. An illustration of the segmentation method used is shown in Figure 3.3. An external view of the membrane module is displayed in Figure 3.3a. A detailed view of the interior of the membrane module with the hollow fibers can be seen in Figure 3.3b. A more convenient and closer view of a section within the membrane module shows the cells used in this segmentation method (Figure 3.3c). Figure 3.3d presents a section view of some sample cells with the variables calculated here. The location where each variable was computed in the cells is given by the superscripts i and j , which represents their row and column indexes, respectively. $\dot{m}_{w,sh}$ and $\dot{m}_{s,sh}$ are the mass flow rates of water and salt in the shell, whereas $\dot{m}_{w,fib}$ and $\dot{m}_{s,fib}$ are the mass flow rates of water and salt in the fibers. These variables are calculated at the edges of the cells since they are inputs for computing other variables. The pressure boundary conditions $P_{fib,in}$, $P_{fib,out}$, $P_{sh,in}$ and $P_{sh,out}$, which are the prescribed pressures for the inlet and outlet streams in the fibers and for the incoming and outgoing flows in the shell, respectively, are given at the border of the most inner and outer cells. At the center of the cells, J_w and J_s

represent the fluxes of water and salt, C_m is the concentration at the membrane; and P_{fib} and P_{sh} are the pressures in the fibers and in the shell at a given cell.

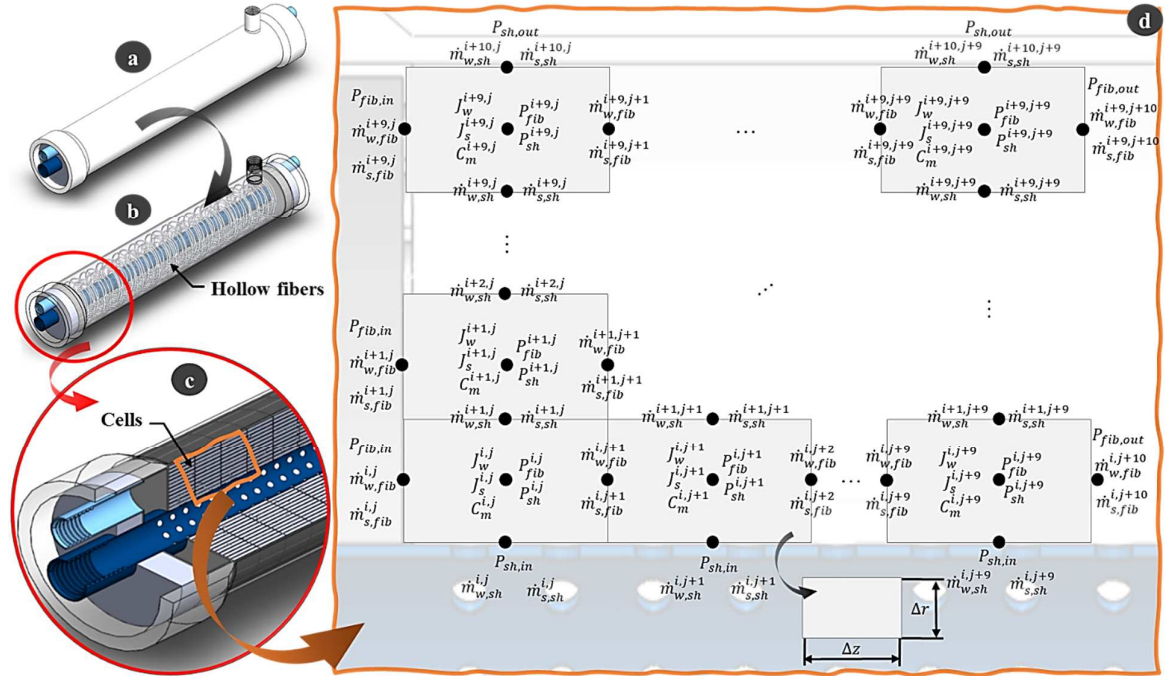


Figure 3.3: Illustration of the method used for segmentizing the hollow fiber membrane module.

The volume of each cell is related to its radial coordinate. Considering that the total membrane area is equally distributed through volume, the active membrane area per unit of volume is described by:

$$A_{m,vol} = \frac{A_m}{\pi(R_{mod}^2 - R_{ct}^2)L_{mod}}, \quad (3.3)$$

where $A_{m,vol}$ is the active membrane area per unit of volume; and A_m is the total active membrane area within the module, which is given by the membrane module manufacturer.

The number of fibers in each cell is given by:

$$n_{fib,cell} = n_{fib} \frac{(r + \Delta r)^2 - r^2}{(R_{mod}^2 - R_{ct}^2)} = \frac{A_{m,vol}}{d_{fib,ext}} (r + \Delta r)^2 - r^2, \quad (3.4)$$

where $n_{fib,cell}$ is the number of fibers per cell; n_{fib} is the number of fibers within the membrane module, which is also provided by the membrane module manufacturer; and r is the inner radius of a given cell.

3.2 Model development

The physical behavior of the fluids within the membrane module was modeled by employing the equations presented in chapter 2. This section exhibits the main considerations for developing the models and demonstrates how those equations were applied for each cell within the membrane module.

3.2.1 Main assumptions

In order to reach feasible computational costs during the simulations, some assumptions were established to decrease the complexity of the models. These considerations are described below as:

- a) In actual membrane modules, the hollow fibers present different lengths depending on their radial position within the shell because they are assembled in a cross-wound arrangement around the central tube. However, this study considered an average length for all hollow fibers based on geometric characteristics (internal and external diameters of the fibers, void fraction and length of the membrane module) of commercially used membrane modules [61-63];
- b) Both RO and PRO models were considered to operate in steady state condition, since it is usually reached quickly in such processes [64];
- c) As the focus of this study is on what occurs within the membrane modules in RO and PRO processes, the pressure losses inside the inlet and outlet pipes of the membrane module were neglected;
- d) The values for pressures were considered to be an average value everywhere inside a cell either within the fibers or on the shell side;
- e) Some membrane parameters which might vary locally inside a membrane module depending on concentration and/or pressure (i.e. A , B , S and D_s), were assumed to be an average value for the whole membrane module [65, 66].

3.2.2 Mass balances

Mass balances were applied to describe the amount of water and salt within the hollow fibers and in the shell for each cell for the RO and PRO processes. In the following equations, the notation J was used for fluxes and refers to transfer across the hollow fiber membranes and \dot{m} was used for flows within one stream. Both symbols were used for salt and water. Also, the axial (fibers) and radial (shell) directions of flows in a single cell are shown in different pictures for a better understanding.

3.2.2.1 RO mass balances

Figure 3.4 illustrates the mass balances and fluxes with their respective directions over a single cell for the RO process. In this figure, the mass flow rate inlets are represented by green arrows, the mass flow rates outlets are depicted as red arrows, and the fluxes of water and salt are shown as purple and gray arrows, respectively. In the RO process, water and salt fluxes have the same direction because both are leaving the shell to cross the hollow fibers and there is no incoming freshwater entering the membrane module.

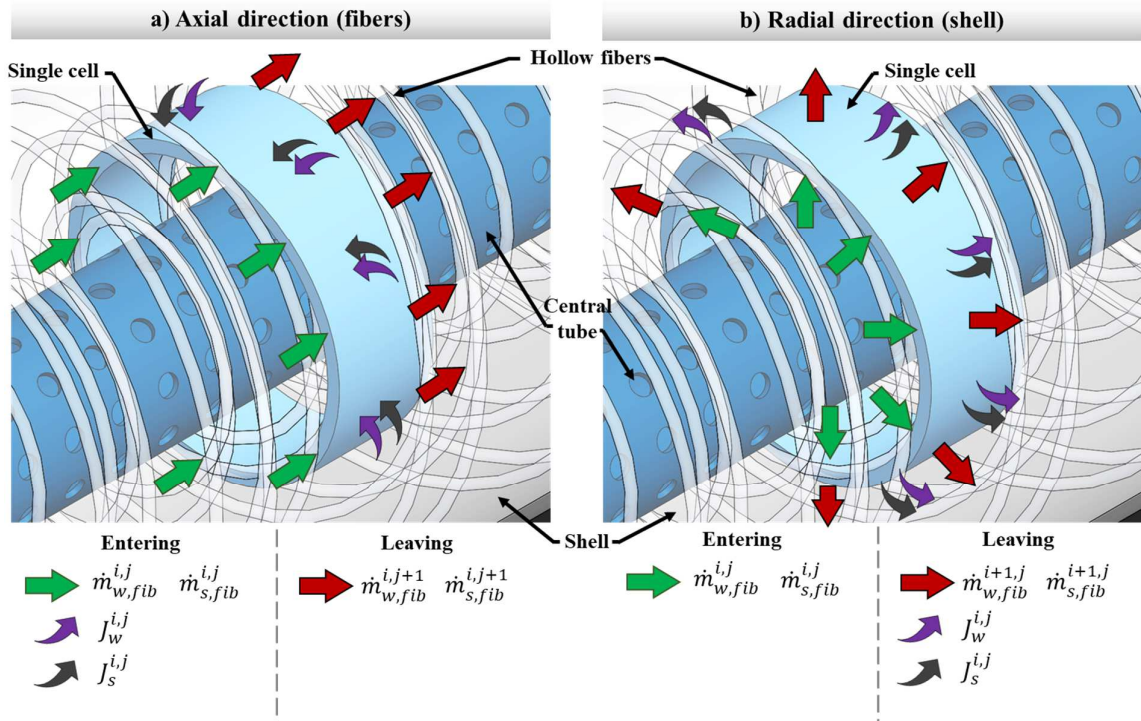


Figure 3.4: Mass balances of water and salt over a single cell for the RO process.

The mass balances of water and salt inside the hollow fibers in the axial direction are the sum of the inlet mass flow rates coming from previous cells and the water and salt fluxes that crossed the hollow fibers as depicted in Figure 3.4a. In these cells, the mass balances of water and salt are given respectively as:

$$\dot{m}_{w, fib}^{i,j+1} = \dot{m}_{w, fib}^{i,j} + \rho_{pw} J_w^{i,j} A_{m, vol} V_{cell}^{i,j} , \quad (3.5)$$

and

$$\dot{m}_{s, fib}^{i,j+1} = \dot{m}_{s, fib}^{i,j} + J_s^{i,j} A_{m, vol} V_{cell}^{i,j} , \quad (3.6)$$

where $V_{cell}^{i,j}$ is the volume of the cell ($\pi [(r + \Delta r)^2 - r^2] \Delta z$).

The mass balances of water and salt on the shell side in the radial direction exiting the cells is the difference between the inlet mass flow rates and the fluxes of water and salt that left the shell side to cross the hollow fibers as shown in Figure 3.4b. The mass balances of water and salt in the shell are described respectively as:

$$\dot{m}_{w,sh}^{i+1,j} = \dot{m}_{w,sh}^{i,j} - \rho_{pw} J_w^{i,j} A_{m,vol} V_{cell}^{i,j} \quad , \quad (3.7)$$

and

$$\dot{m}_{s,sh}^{i+1,j} = \dot{m}_{s,sh}^{i,j} - J_s^{i,j} A_{m,vol} V_{cell}^{i,j} \quad . \quad (3.8)$$

3.2.2.2 PRO mass balances

For the PRO process, the mass balances are similar to those used for the RO system with slight differences. First, there is incoming freshwater entering the membrane module, which flows within the hollow fibers in the first radial cells. Second, due to the flow of freshwater from the fibers to the shell side, the directions of water and salt fluxes are swapped in the mass balance equations. Figure 3.5 exhibits the mass balances and fluxes with their respective directions over a single cell for the PRO process. The mass flow rate inlets are shown by green arrows, the mass flow rates outlets are represented as red arrows, and the fluxes of water and salt are depicted as purple and gray arrows, respectively. Note that in PRO, water and salt fluxes present opposite directions in the cells due to the characteristic of this process. That is, water molecules are drawn from within the fibers towards the shell side and some salt crosses the fibers coming from the shell.

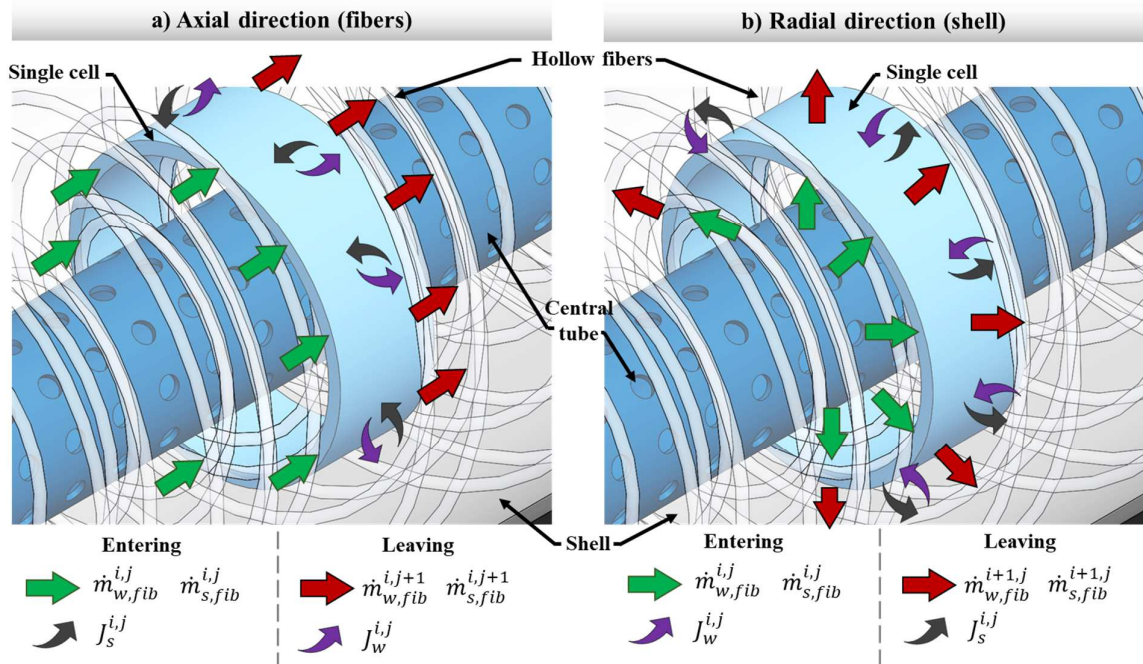


Figure 3.5: Mass balances of water and salt over a single cell for the PRO process.

Within the hollow fibers in the axial direction, the mass flow rate of water leaving the cell is given by the difference between the incoming mass flow rate of water and the flux of water that crossed the hollow fibers towards the shell side. On the other hand, the mass flow rate of salt leaving the cell is equals to the incoming mass flow rate of salt plus the flux of salt that crossed the hollow fibers coming from the shell side. The mass balances of water and salt for the hollow fibers inside the cell shown in Figure 3.5a are given respectively as:

$$\dot{m}_{w, fib}^{i,j+1} = \dot{m}_{w, fib}^{i,j} - \rho_{pw} J_w^{i,j} A_{m, vol} V_{cell}^{i,j} \quad , \quad (3.9)$$

and

$$\dot{m}_{s, fib}^{i,j+1} = \dot{m}_{s, fib}^{i,j} + J_s^{i,j} A_{m, vol} V_{cell}^{i,j} \quad . \quad (3.10)$$

On the shell side in the radial direction, the mass flow rate of water leaving the cell is described as the sum of the mass flow rate of water coming from the previous cell and the flux of water received from the hollow fibers. Whereas the mass flow rate of salt leaving the cell is the difference between inlet mass flow rate of salt from other cell and the flux of salt that crossed the hollow fibers. The mass balances of water and salt for the cell on the shell side displayed in Figure 3.5b are given respectively as:

$$\dot{m}_{w, sh}^{i+1,j} = \dot{m}_{w, sh}^{i,j} + \rho_{pw} J_w^{i,j} A_{m, vol} V_{cell}^{i,j} \quad , \quad (3.11)$$

and

$$\dot{m}_{s, sh}^{i+1,j} = \dot{m}_{s, sh}^{i,j} - J_s^{i,j} A_{m, vol} V_{cell}^{i,j} \quad . \quad (3.12)$$

3.2.3 Flow rates

As mentioned earlier in section 3.2.1, in this model some variables as volume flow rates, pressures, fluxes and mass concentrations of bulk solutions were calculated as averages for each cell. This was because the model was set up to use the mass flow rates computed at the edge of the cells and prescribed inlet hydraulic pressures as inputs to be able to find results for such quantities. The volume flow rates of the solutions within the hollow fibers and on the shell side for the membrane module working on both RO and PRO systems are:

$$\dot{V}_{fib}^{i,j} = \frac{(\dot{m}_{w, fib}^{i,j} + \dot{m}_{s, fib}^{i,j}) + (\dot{m}_{w, fib}^{i,j+1} + \dot{m}_{s, fib}^{i,j+1})}{2 \rho^{i,j}} \quad (3.13)$$

and

$$\dot{V}_{sh}^{i,j} = \frac{(\dot{m}_{w, sh}^{i,j} + \dot{m}_{s, sh}^{i,j}) + (\dot{m}_{w, sh}^{i+1,j} + \dot{m}_{s, sh}^{i+1,j})}{2 \rho^{i,j}} \quad , \quad (3.14)$$

where $\dot{V}_{fib}^{i,j}$ and $\dot{V}_{sh}^{i,j}$ are respectively the volume flow rates within the hollow fibers and on the shell side at a given cell; $\rho^{i,j}$ is the density of the solution at a given cell as a function of its temperature, salinity and pressure, which was obtained using MATLAB functions from experimental research [25]. Other properties of the solutions such as enthalpies and entropies were also acquired from the same source.

3.2.4 Concentrations

The mass concentrations of the solutions within the hollow fibers and on the shell side are determined as averages of incoming and outgoing mass concentrations. They are expressed respectively as:

$$C_{fib}^{i,j} = \frac{1}{2} \left(\frac{\dot{m}_{s,fib}^{i,j}}{\dot{m}_{w,fib}^{i,j} + \dot{m}_{s,fib}^{i,j}} + \frac{\dot{m}_{s,fib}^{i,j+1}}{\dot{m}_{w,fib}^{i,j+1} + \dot{m}_{s,fib}^{i,j+1}} \right), \quad (3.15)$$

and

$$C_{sh}^{i,j} = \frac{1}{2} \left(\frac{\dot{m}_{s,sh}^{i,j}}{\dot{m}_{w,sh}^{i,j} + \dot{m}_{s,sh}^{i,j}} + \frac{\dot{m}_{s,sh}^{i+1,j}}{\dot{m}_{w,sh}^{i+1,j} + \dot{m}_{s,sh}^{i+1,j}} \right). \quad (3.16)$$

In Eqs. (3.15) and (3.16), the first terms in parenthesis describe the mass concentrations of salt entering a cell, while the second terms express the mass concentrations leaving that cell.

For both osmotic processes, the mass concentrations of the solutions within the fibers and on the shell side for a given cell are related to their salinities as:

$$sal_{fib}^{i,j} = \frac{C_{fib}^{i,j}}{\rho^{i,j}}, \quad (3.17)$$

and

$$sal_{sh}^{i,j} = \frac{C_{sh}^{i,j}}{\rho^{i,j}}. \quad (3.18)$$

here $sal_{fib}^{i,j}$ and $sal_{sh}^{i,j}$ are the salinities of the solutions within the hollow fibers and on the shell side at a given cell, respectively.

3.2.5 Membrane transport

This section describes the membrane transport equations used for modeling the fluxes within the membrane module of the RO and PRO processes, which are segmented versions of equations presented previously in section 2.6. Note that depending on the process, the direction of water and salt fluxes may vary.

3.2.5.1 RO transport equations

For the RO process, both water and salt fluxes are in the same direction. The transport of water through the membrane is written as a segmented version of Eq. (2.28):

$$J_w^{i,j} = A(\Delta P^{i,j} - \varphi^{i,j} \Delta \Pi^{i,j}) = A(P_{sh}^{i,j} - P_{fib}^{i,j}) - A\varphi^{i,j}(\Pi_{sh,m}^{i,j} - \Pi_{fib}^{i,j}) \quad , \quad (3.19)$$

where the concentration polarization coefficient for a given cell ($\varphi^{i,j}$) is segmented as a form of Eq. (2.29):

$$\varphi^{i,j} = \frac{C_{sh,m}^{i,j} - C_{fib}^{i,j}}{C_{sh}^{i,j} - C_{fib}^{i,j}} = \exp\left(\frac{J_v^{i,j}}{k^{i,j}}\right) \quad , \quad (3.20)$$

where the flux of permeate across the membrane at a given cell ($J_v^{i,j}$) is given by its segmented form as a version of Eq. (2.30):

$$J_v^{i,j} = \frac{J_s^{i,j} + (J_w^{i,j} \rho_{pw})}{\rho^{i,j}} \quad , \quad (3.21)$$

while the mass transfer coefficient of salt through the membrane at a given cell ($k^{i,j}$) is written as a segmented form of Eq. (2.12):

$$k^{i,j} = \frac{Sh^{i,j} D_s}{d_{fib,ext}} \quad , \quad (3.22)$$

and the Sherwood number at a given cell is calculated as a segmented version of Eq. (2.13):

$$Sh^{i,j} = 0.048 (Re^{i,j})^{0.6} (Sc^{i,j})^{1/3} \quad , \quad (3.23)$$

where the Schmidt ($Sc^{i,j}$) and Reynolds ($Re^{i,j}$) numbers at a given cell are expressed respectively as segmented forms of Eqs. (2.17) and (2.14) by:

$$Sc^{i,j} = \frac{\nu_{sh}^{i,j}(T, C)}{\rho^{i,j} D_s} \quad , \quad (3.24)$$

and

$$Re^{i,j} = \frac{d_{fib,ext} U_{sh}^{i,j} \rho^{i,j}}{\nu_{sh}^{i,j}(T, C)} \quad , \quad (3.25)$$

where $\nu_{sh}^{i,j}(T, C)$ is the dynamic viscosity of the solution, which is an empirical relation given as a function of its temperature and concentration obtained using MATLAB functions from experimental research [25]. The segmented form of the velocity of the solution in the shell is described as a segmented version of Eq. (2.15):

$$U_{sh}^{i,j} = u_{sh}^{i,j} \varepsilon , \quad (3.26)$$

where, the superficial velocity of the solution on the shell side at a cell ($u_{sh}^{i,j}$) is given by a segmented form of Eq. (2.16) as:

$$u_{sh}^{i,j} = \frac{\dot{V}_{sh}^{i,j}}{2\pi\Delta r\Delta z} . \quad (3.27)$$

The transport of salt across the membrane is defined as a segmented version of Eq. (2.31):

$$J_s^{i,j} = B\varphi^{i,j}(C_{sh,m}^{i,j} - C_{fib}^{i,j}) , \quad (3.28)$$

where the concentration of the permeate solution within the hollow fibers reads:

$$C_{fib}^{i,j} = \frac{J_s^{i,j}}{(J_s^{i,j} + J_w^{i,j} \rho_{pw})} . \quad (3.29)$$

Finally, the concentration at the membrane on the shell side for a given cell can be written as a segmented form of Eq. (2.11):

$$C_{sh,m}^{i,j} = \left(C_{sh}^{i,j} - \frac{J_s^{i,j}}{J_w^{i,j}} \right) \exp\left(\frac{J_w^{i,j}}{k^{i,j}} \right) + \frac{J_s^{i,j}}{J_w^{i,j}} . \quad (3.30)$$

3.2.5.2 PRO transport equations

For the PRO process, the fluxes of water and salt across the membrane present opposite directions. These fluxes are expressed as segmented versions of Eqs. (2.32) and (2.33) respectively by:

$$J_w^{i,j} = A(\Delta\Pi^{i,j} - \Delta P^{i,j}) = A[(\Pi_{sh,m}^{i,j} - \Pi_{fib,m}^{i,j}) - (P_{sh}^{i,j} - P_{fib}^{i,j})] , \quad (3.31)$$

and

$$J_s^{i,j} = B(C_{sh,m}^{i,j} - C_{fib,m}^{i,j}) . \quad (3.32)$$

The external concentration polarization on the feed and draw sides of the membrane are expressed as segmented forms of Eqs. (2.19) and (2.20) respectively as:

$$C_{fib,m}^{i,j} = \left(C_{fib}^{i,j} + \frac{J_s^{i,j}}{J_w^{i,j}} \right) \exp \left(\frac{J_w^{i,j}}{k^{i,j}} \right) - \frac{J_s^{i,j}}{J_w^{i,j}}, \quad (3.33)$$

and

$$C_{sh,m}^{i,j} = \left(C_{sh}^{i,j} + \frac{J_s^{i,j}}{J_w^{i,j}} \right) \exp \left(-\frac{J_w^{i,j}}{k^{i,j}} \right) - \frac{J_s^{i,j}}{J_w^{i,j}}. \quad (3.34)$$

The internal concentration polarization in a segmented form of Eq. (2.22) reads:

$$C_I^{i,j} = \left(C_{fib,m}^{i,j} + \frac{J_s^{i,j}}{J_w^{i,j}} \right) \exp(J_w^{i,j} K^{i,j}) - \frac{J_s^{i,j}}{J_w^{i,j}}. \quad (3.35)$$

3.2.6 Pressure drops

The pressure difference between the membrane module inlet and outlet is a key factor for the operation of the processes, since it determines the amount of flow rates of each fluid entering and leaving the membrane module. Another important parameter is the pressure drop within the membrane module because it describes the behavior of the pressure of the fluids inside the hollow fibers and on the shell side.

Since the pressure drop Eqs. (2.37) and (2.38) are given in their differential forms, Taylor series was applied to expand them and create finite difference approximations to meet the segmentation method used in this work for both RO and PRO processes. Higher order terms after second order were neglected as their effect on the final pressure values were negligible. To find the pressure drops for the first cells in the axial and radial directions, the forward difference approximation method was used. The pressure drop within the hollow fibers for the first axial cells reads:

$$9P_{fib}^{i,j} = 8P_{fib,in} + P_{fib}^{i,j+1} - \frac{384 \nu_{fib}^{i,j} d_{fib,ext} \dot{V}_{fib}^{i,j} L_{fib,avg}}{\pi d_{fib,int}^4 A_{m,vol} [(r + \Delta r)^2 - r^2] L_{mod}}. \quad (3.36)$$

It is important to mention that the length of the hollow fibers has no significant influence on the global pressure drop through the membrane module when it is divided in small segments [61]. Therefore, an average length for the hollow fibers ($L_{fib,avg}$) was used for the pressure drop within fibers in each cell.

The pressure drop on the shell side in the first radial cells is given by:

$$9P_{sh}^{i,j} = 8P_{sh,in} + P_{sh}^{i+1,j} - \left[\frac{150 (1 - \varepsilon)^2 \nu_{sh}^{i,j} u_{sh}^{i,j}}{\varepsilon^3 (1.5 d_{fib,ext})^2} + \frac{1.75 (1 - \varepsilon) \rho_{sh}^{i,j} (u_{sh}^{i,j})^2}{\varepsilon^3 (1.5 d_{fib,ext})} \right] 3\Delta r. \quad (3.37)$$

The central difference approximation method was applied to find the pressure drops for the intermediate cells in the axial and radial directions. The pressure drop within the hollow fibers for the intermediate axial cells in the hollow fibers reads:

$$P_{fib}^{i,j+1} = P_{fib}^{i,j} - \frac{384 \nu_{fib}^{i,j} d_{fib,ext} \dot{V}_{fib}^{i,j} L_{fib,avg}}{\pi d_{fib,int}^4 A_{m,vol} [(r + \Delta r)^2 - r^2] L_{mod}} \quad (3.38)$$

The pressure drop on the shell side in the intermediate radial cells is given by:

$$P_{sh}^{i+1,j} = P_{sh}^{i,j} - \left[\frac{150 (1 - \varepsilon)^2 \nu_{sh}^{i,j} u_{sh}^{i,j}}{\varepsilon^3 (1.5 d_{fib,ext})^2} + \frac{1.75 (1 - \varepsilon) \rho_{sh}^{i,j} (u_{sh}^{i,j})^2}{\varepsilon^3 (1.5 d_{fib,ext})} \right] \Delta r. \quad (3.39)$$

To find the pressure drops for the last cells in the axial and radial directions, the backward difference approximation method was used. The pressure drop within the hollow fibers for the last axial cells reads:

$$9P_{fib}^{i,j} = 8P_{fib,out} + P_{fib}^{i,j-1} + \frac{384 \nu_{fib}^{i,j} d_{fib,ext} \dot{V}_{fib}^{i,j} L_{fib,avg}}{\pi d_{fib,int}^4 A_{m,vol} [(r + \Delta r)^2 - r^2] L_{mod}}. \quad (3.40)$$

While the pressure drop on the shell side in the last radial cells is given by:

$$9P_{sh}^{i,j} = 8P_{sh,out} + P_{sh}^{i-1,j} + \left[\frac{150 (1 - \varepsilon)^2 \nu_{sh}^{i,j} u_{sh}^{i,j}}{\varepsilon^3 (1.5 d_{fib,ext})^2} + \frac{1.75 (1 - \varepsilon) \rho_{sh}^{i,j} (u_{sh}^{i,j})^2}{\varepsilon^3 (1.5 d_{fib,ext})} \right] 3\Delta r. \quad (3.41)$$

3.3 Membrane module parameters

A 5-inch scale Toyobo HP5255SI-H3K hollow fibers membrane module [67] was selected as reference (see Appendix A). Unfortunately, its specification sheet does not explicitly provide all dimensions, then some quantities such as L_{mod} , R_{mod} and R_{ct} were estimated based on its schematic. Further membrane parameters were acquired from membrane modules with similar characteristics from literature. Table 3.1 presents the main membrane parameters with their references.

Parameter	Symbol	Value	Unit	Reference
Water permeability	A	7.5×10^{-13}	m/s-Pa	[31, 46]
Salt permeability	B	9.72×10^{-9}	m/s	[31, 46]
Structure factor	S	1024×10^{-6}	-	[31, 46]
Diffusion coefficient	D_s	1.48×10^{-9}	m ² /s	[66]
Fiber internal diameter	$d_{fib,int}$	90×10^{-6}	m	[67]
Fiber external diameter	$d_{fib,ext}$	200×10^{-6}	m	[67]
Active module length	L_{mod}	0.6227	m	[67]
Active module radius	R_{mod}	0.0775	m	[67]
Central tube radius	R_{ct}	0.0107	m	[67]
Void fraction	ε	0.5	-	[31, 46]
Number of fibers	n_{fib}	200,000	-	[31, 46]
Total membrane area	A_m	60.0	m ²	[67]

Table 3.1: Membrane module parameters used in the RO and PRO simulations.

The constant values considered in the simulations are exhibited in Table 3.2. These quantities are commonly used by many authors in the analyzed literature [31, 41, 46].

Parameter	Symbol	Value	Unit
Outlet hydraulic pressure on the fibers side	$P_{fib,out}$	101.325	kPa
Pressure at reference state	P_0	101.325	kPa
Temperature of the solutions	T	298.15	K
Molar gas constant	\bar{R}	8.3145	J/mol-K
Density of pure water	ρ_{pw}	1000	kg/m ³

Table 3.2: Constants used in the RO and PRO simulations.

The models were developed considering inlet and outlet pressures as inputs instead of flow rates. This alternative was necessary to solve the system of nonlinear equations because MATLAB's solver encountered issues to find a solution when dealing with constrained flow rates. In order to implement the possibility of inputting a range of operational parameters to the models, their values were computed indirectly using factors and difference parameters. Table 3.3 displays the range of operational input parameters to the membrane module of the RO process based on the reviewed literature and practical operation in industry.

Parameter	Symbol	Value range	Unit	Step
Salinity of inlet salt water	$sal_{sh,in}$	0.020 - 0.050	kg/kg	0.001 kg/kg
Pressure difference across the module	ΔP_{sh}	0.1 - 5.0	kPa	0.1 kPa
Osmotic pressure factor	Π_{fac}	1.10 - 2.50	-	0.05

Table 3.3: Operational input parameters to the membrane module of the RO process.

The osmotic pressure factor (Π_{fac}) and the hydraulic pressure difference across the membrane module on the shell side (ΔP_{sh}) for the RO process, which are only definitions used for allowing a range of inputs to the model, are respectively related to the inlet ($P_{sh,in}$) and outlet ($P_{sh,out}$) hydraulic pressures of feed solution as:

$$P_{sh,in} = \Pi_{fac} \Pi(T, C) , \quad (3.42)$$

$$P_{sh,out} = P_{sh,in} - \Delta P_{sh} , \quad (3.43)$$

A similar approach for selecting the input parameters for the PRO process was conducted in accordance with the reviewed literature. The range of input parameters used are given in Table 3.4.

Parameter	Symbol	Value range	Unit	Step
Salinity of inlet draw solution	$sal_{sh,in}$	0.020 - 0.050	kg/kg	0.001 kg/kg
Salinity of inlet feed solution	$sal_{fib,in}$	0.00083 - 0.001858	kg/kg	-
Pressure difference on the shell side	ΔP_{sh}	0.1 - 5.0	kPa	0.1 kPa
Osmotic pressure factor - shell	$\Pi_{fac,sh}$	0.10 - 0.90	-	0.025
Osmotic pressure factor - fibers	$\Pi_{fac,fib}$	1.5	-	-

Table 3.4: Operational input parameters to the membrane module of the PRO process.

It is important to mention that the values for the salinity of inlet feed solution were obtained from the RO model. Additionally, the osmotic pressure factors on the shell side are smaller than unity to allow hydraulic pressure difference inferior to the osmotic pressure difference due to a requirement of the PRO process. Also, the inlet pressure of feed solution was kept constant at a value below 30 kPa in accordance with the investigated literature [31, 68]. This resulted in a constant value for the osmotic pressure factor for the fibers side.

As in the RO process, the osmotic pressure factor ($\Pi_{fac,sh}$) and the hydraulic pressure difference (ΔP_{sh}) on the shell side for the PRO process are respectively related to the inlet ($P_{sh,in}$) and outlet ($P_{sh,out}$) hydraulic pressures of draw solution by the same Eqs. (3.42) and (3.43). However, the osmotic pressure factor ($\Pi_{fac,fib}$) along the hollow fibers of the membrane module for the PRO process is related to the inlet ($P_{fib,in}$) pressure of feed solution by:

$$P_{fib,in} = \Pi_{fac,fib} \Pi(T, C) , \quad (3.44)$$

The outlet pressure on the fiber side was considered as a reference pressure for the other pressures. Therefore, all inlet and outlet pressures are gauge pressures relative to the outlet pressure on the fiber side ($P_{fib,out}$). Table 3.5 summarizes all the input and output parameters provided to and obtained from the membrane module models working in the RO and PRO processes, respectively:

Process	Input parameters	Output parameters
RO	<ul style="list-style-type: none"> • $s_{sh,in}$ • $P_{sh,in}$ and $P_{sh,out}$ • $P_{fib,out}$ • T • Values from Tables 3.1 and 3.2 	<ul style="list-style-type: none"> • $s_{sh,out}$ • $\dot{m}_{sh,in}$ and $\dot{m}_{sh,out}$ • $s_{fib,out}$ • $\dot{m}_{fib,out}$
PRO	<ul style="list-style-type: none"> • $s_{sh,in}$ • $P_{sh,in}$ and $P_{sh,out}$ • $s_{fib,in}$ • $P_{fib,in}$ and $P_{fib,out}$ • T • Values from Tables 3.1 and 3.2 	<ul style="list-style-type: none"> • $s_{sh,out}$ • $\dot{m}_{sh,in}$ and $\dot{m}_{sh,out}$ • $s_{fib,out}$ • $\dot{m}_{fib,in}$ and $\dot{m}_{fib,out}$

Table 3.5: Input and output parameters for the RO and PRO models.

3.4 Validation

In order to verify the accuracy of the proposed RO model, it was run with data acquired from experimental research. An experimental study conducted by Sekino (1995) [42] was then selected as a reference to validate the RO model, by reason of Sekino (1995) [42] used a membrane module with similar characteristics to the one here. The proposed RO model worked under the same conditions and input parameters as in their study. Some parameters, which were not provided in Sekino's (1995) [42] research, were considered to be the same values as those found in the analyzed literature, since the membrane modules are similar. All these inlet parameters, as well as the references they were obtained from are shown in Table 3.6. The results of flow rate of permeate produced ($\dot{V}_{fib,out}$) and ratio of concentrations between permeate and incoming salt water ($C_P/C_{sh,in}$) varying with the inlet pressure of salt water into the membrane module ($P_{sh,in}$) were compared against the results presented by Sekino (1995) [42].

Parameter	Symbol	Value	Unit	Reference
Water permeability	A	2.89×10^{-13}	m/s-Pa	
Salt permeability	B	8.12×10^{-9}	m/s	
Structure factor	S	1024×10^{-6}	-	[31, 46]
Diffusion coefficient	D_s	1.48×10^{-9}	m ² /s	[66]
Fiber internal diameter	$d_{fib,int}$	70×10^{-6}	m	
Fiber external diameter	$d_{fib,ext}$	163×10^{-6}	m	
Active module length	L_{mod}	0.99	m	
Active module radius	R_{mod}	0.095	m	
Central tube radius	R_{ct}	0.02	m	
Void fraction	ε	0.5	-	[31, 46]
Number of fibers	n_{fib}	598,000	-	
Total membrane area	A_m	361	m ²	
Shell side inlet concentration	$C_{sh,in}$	35	kg/m ³	
Temperature of the process	T	298.15	K	

Table 3.6: Input parameters for validating the RO model from [42], unless otherwise noted.

Similarly, the PRO model was also verified by comparing the results obtained with results from experimental research carried out by Tanaka *et al* (2018) [31] using the same system inputs. Tanaka *et al* (2018) [31] used a membrane module with similar features to the one chosen for this work and its parameters are given in Table 3.7. Missing parameters in Tanaka's *et al* (2018) [31] research were considered to be equivalent to those found in literature for membrane modules with same characteristics and are provided in the last column of the aforementioned table.

Parameter	Symbol	Value	Unit	Reference
Water permeability	A	7.5×10^{-13}	m/s-Pa	[66]
Salt permeability	B	9.72×10^{-9}	m/s	
Structure factor	S	1024×10^{-6}	-	
Diffusion coefficient	D_s	1.48×10^{-9}	m ² /s	
Fiber internal diameter	$d_{fib,int}$	85×10^{-6}	m	
Fiber external diameter	$d_{fib,ext}$	175×10^{-6}	m	
Active module length	L_{mod}	0.682	m	
Active module radius	R_{mod}	0.0635	m	
Central tube radius	R_{ct}	0.0107	m	
Void fraction	ε	0.458	-	
Number of fibers	n_{fib}	220,000	-	
Total membrane area	A_m	70.5	m ²	
Shell side inlet concentration	$C_{sh,in}$	35	kg/m ³	
Fibers side inlet concentration	$C_{fib,in}$	<1	kg/m ³	
Temperature of the process	T	298.15	K	
Volume flow rate of draw solution	$\dot{V}_{sh,in}$	8	l/min	
Volume flow rate of feed solution	$\dot{V}_{fib,in}$	8	l/min	

Table 3.7: Input parameters for validating the PRO model from [31], unless otherwise noted.

The average flux in the membrane module ($J_{w,avg}$), calculated as:

$$J_{w,avg} = \frac{\dot{V}_{sh,in} - \dot{V}_{sh,out}}{A_m}, \quad (3.45)$$

was compared with the results obtained by Tanaka *et al* (2018) [31] varying the values of inlet pressure of salt water into the membrane module ($P_{sh,in}$)

3.5 Computational resources

In possession of the systems of equations and membrane parameters, the models for the membrane module were developed using MATLAB (R2020b) software provided by the University of Victoria running on an Intel Core i7 (8th generation), 16 GB RAM system. The built-in MATLAB's *fsolve* function, which finds the roots of nonlinear equations, was employed to solve the system equations. The initial guess provided to the *fsolve* function was used only for the very first cell (indexes $i = j = 1$) and consisted in the same equations presented in this chapter with some simplifications as:

- a) Values of flows and fluxes close to zero;
- b) Negligible concentration polarization;
- c) Linear approximation for osmotic pressure (Eq. (2.8));
- d) Constant values for mass density (ρ) and dynamic viscosity (ν) of the solution set as 1000 kg/m³ and 1x10⁻³ Pa-s, respectively.

After obtaining the results for the very first cell, the *fsolve* function redid all calculations without the simplifications mentioned above. Then, it proceeded using the previously obtained results as inputs for the system of equations presented in this chapter to compute the results for next cell and so on.

Chapter 4

Results and discussion

In this chapter, the results obtained are presented and discussed in dedicated sections for both RO and PRO processes. Initially, the proposed models of membrane module are validated. Afterwards, the results that describe the behavior of the fluids within the membrane module are analyzed. Finally, the performance curves obtained from the models are exhibited and their performance are examined. In order to allow a compact notation on the axes of the plots, in this section the values for pressures, volume flow rates, water and salt fluxes are given in bar, lpm (liters per minute), lpm/m² and mg/m²-s, respectively. Besides, these units are also usual in literature and industry for this topic [31, 46, 47].

4.2 Results for the RO membrane module

This section presents and discusses the results obtained from simulations of the membrane module for the RO process.

4.2.1 Validation for RO

As explained in section 3.4, the membrane module model for the RO process was validated. Firstly, the experimental research led by Sekino (1995) [42] was used for validating the RO model. Figure 4.1 compares the results acquired after using the same input values as Sekino (1995) [42] presented in Table 3.6.

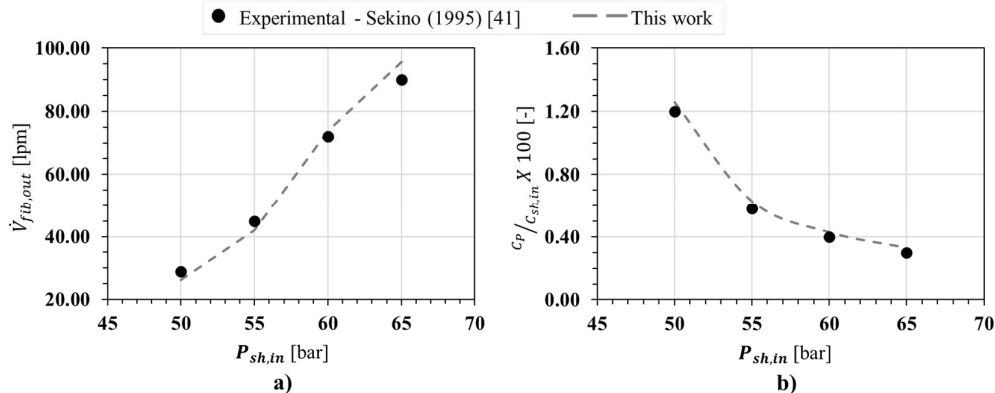


Figure 4.1: Comparison between experimental and produced results from the proposed RO model.

The vertical left axes in Figures 4.1a and b present the volume flow rate of permeate produced ($\dot{V}_{fib,out}$) and the ratio of concentrations between permeate and incoming salt water ($C_P/C_{sh,in}$), respectively. Whereas the horizontal bottom axes show the inlet pressure of salt water into the membrane module ($P_{sh,in}$). An observation to point out is that Sekino (1995) [42] does not provide the exact values of their experimental results, therefore the values were estimated from charts. Results of the simulation demonstrate that the proposed model provides relatively reasonable fit to the experimental data with differences between 2.40% and 9.47% for the results of volume flow rate of permeate ($\dot{V}_{fib,out}$) displayed in Figure 4.1a. Also, discrepancies from 4.76% to 9.52% were observed in the results of ratio of concentrations ($C_P/C_{sh,in}$) exhibited in Figure 4.1b. Despite of the deviations found in the results generated by the proposed model, the overall trend of results is similar to Sekino (1995) [42].

The main reason for the differences found in the results was due to a variable diffusion coefficient of salt (D_s) obtained from trial and error used by Sekino (1995) [42]. This parameter influences the mass transfer coefficients and consequently, the concentration polarization profile within the membrane module and mass transport across the membrane. To find closer results, it would be necessary to use experimental variable diffusion coefficient of salt (D_s) as Sekino (1995) [42], however, performing experiments is out of the scope of this study.

4.2.2 Sectional distribution of pressures, flows and fluxes for RO

Before presenting the performance curves for the membrane module working in the RO process, this section presents the behavior of fluxes, flow rates and pressures within the membrane module to clarify the performance results obtained for the process. To reach this, the model worked with the average inlet values presented in section 3.3 as shown in Table 4.1.

Parameter	Symbol	Value	Unit
Salinity of inlet salt water	$sal_{sh,in}$	0.035	kg/kg
Pressure difference across the module	ΔP_{sh}	0.0255	bar
Osmotic pressure factor	Π_{fac}	1.80	-

Table 4.1: Average inlet parameters for understanding the behavior of certain quantities within the membrane module of the RO process.

A sectional distribution of the values in each cell of fluxes, flow rates and pressures was plotted along the axial (from left to right) and radial (from right to left) directions of the membrane module as depicted in Figures 4.2 to 4.5. The presentation and discussion of these figures are provided in the following paragraphs.

Figure 4.2 presents a sectional distribution of pressure within the membrane module in each cell. Figure 4.2a shows that the hydraulic pressure of feed solution on the shell side is uniformly distributed along the axial direction of the module, which agrees with the principle of transmission of fluid-pressure (Pascal's principle) [69]. In Figure 4.2b the hydraulic pressure is higher on the fibers side in the first radial and a few axial cells before the middle of the membrane module because these cells are closer to the central perforated tube and are the first cells to receive fluid at higher hydraulic pressure coming from the shell side. The number of hollow fibers in each cell also influenced the pressure drops because the cells closer to the central perforated tube present smaller number of fibers and consequently, less fibers were susceptible to pressure drop. Both Figures 4.2a and b also demonstrate that the segmented versions of Ergun Eqs. (3.37), (3.39) and (3.41), as well as Hagen-Poiseuille Eqs, (3.36), (3.38) and (3.40) were able to show reasonable and expected pressure drops on the shell (radial direction) and fibers (axial direction) sides caused by frictional losses, agreeing with literature [31, 46, 47].

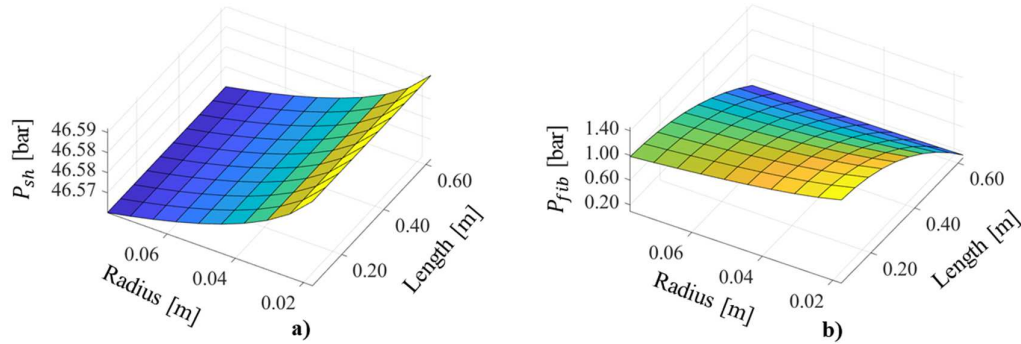


Figure 4.2: Sectional distribution of pressures for each cell within the membrane module.

The behavior of the solution within the membrane module was also evaluated from the point of view of the sectional distribution of flow rates as shown in Figure 4.3. Figure 4.3a shows that the most inner cells on the shell side presented higher amounts of volume flow rate due to their proximity with the central perforated tube. The volume flow rate of fluid decreased along the radial direction, as part of the solution crossed the hollow fibers. The axial values of flow rates were homogeneous due to no fluid accumulation in this direction. On the fibers side displayed in Figure 4.3b, the volume flow rate of permeate in the axial direction increased for every cell because of accumulation of fluid coming from the previous cells. The volume flow rate of permeate also increased in the radial direction because of the larger number of hollow fibers at higher radius within the membrane module, which allowed a larger volume of solution to cross the fibers. Finally, the highest flow rate values occurred at the most outer radius and length due to a combination of fluid accumulation and larger number of fibers on that location.

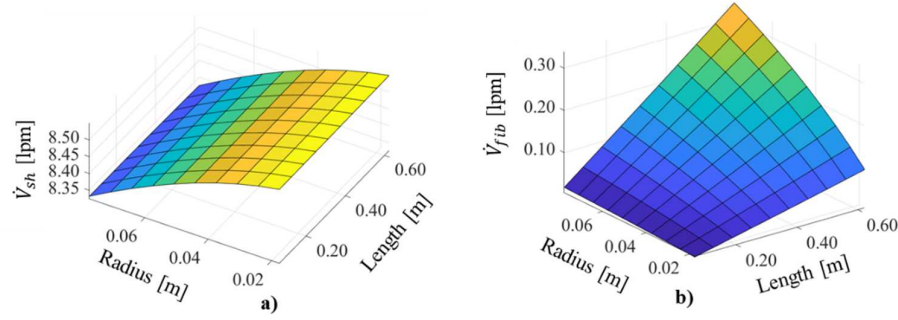


Figure 4.3: Sectional distribution of volume flow rates for each cell within the membrane module.

Another important aspect to comprehend the behavior of the solutions within the membrane module is shown in Figure 4.4. This figure shows that the salinity increased in the radial direction either on the membrane surface (Figure 4.4a) and within the hollow fibers (Figure 4.4b).

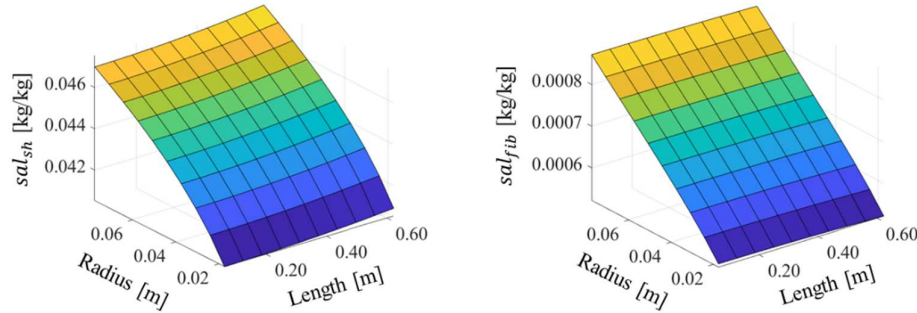


Figure 4.4: Sectional distribution of salinities for each cell within the membrane module.

Figure 4.4a shows that the salinity on the membrane surface was higher than the inlet salinity of the feed solution since the first axial cells due to concentration polarization. These salinity values increased by steps of 6.5 kg/kg (13.85%) towards the outer radius of the membrane module because the most part of water in the shell had already crossed the hollow fibers by the center of the radius of the module, leaving a concentrated brine solution in the upper part of the membrane module. This allowed large amounts of salt to accumulate on the membrane surface in that region. On the other hand, salinity raised by average steps of 0.00035 kg/kg (39.45%) along the radial direction on the fibers side as shown in Figure 4.4b because of the particles of salt that crossed the not perfectly selective hollow fibers along with water molecules. The amount of salt in the permeate solution increased towards the upper part of the membrane module in the radial direction due to the salt coming from the concentrated brine solution in that region that crossed a large number of fibers positioned there. This issue unveiled that the hollow fibers in the upper part of the membrane module were not used as efficiently as possible. Working with membrane modules with smaller dimensions might be beneficial to improve usage of the membrane area provided by the hollow fibers, which agrees with related literature [31].

Figure 4.5 shows sectionally how the fluxes of water and salt were distributed in each cell within the membrane module. According Figure 4.5a, the fibers closer to the central perforated tube received larger flux of water because the salinities of salt water and permeate in this region presented lower values, consequently, their osmotic pressures were lower as well. This allowed a small osmotic pressure gradient in that region and made the difference between hydraulic and osmotic pressures to reach higher values, which resulted in a larger flux of water through the fibers in the first cells in the axial direction. The flux of water decreased towards the outer radius of the membrane module because most part of the water molecules had already crossed the hollow fibers located in the first cells on the radial direction. As a result, less water was left to cross the hollow fibers located in the outer radius and it became more concentrated. This led the osmotic pressure difference between water in the shell and fibers sides to increase, which reduced the difference between hydraulic and osmotic pressures and consequently, the water flux through the fibers in that region.

As shown in Figure 4.5b, the flux of salt was smaller in the first cells nearer to the central tube because the solution was more diluted in that region and the salinity gradient was smaller. Nonetheless, the salt flux increased along the radial direction by reason of most part of water molecules had already crossed the hollow fibers in the first cells, leaving a more concentrated solution in the upper part of the membrane module as explained earlier. This led the salinity gradient of the solution between the shell and fibers side to reach higher values, which allowed larger amount of salt to cross the fibers in that region.

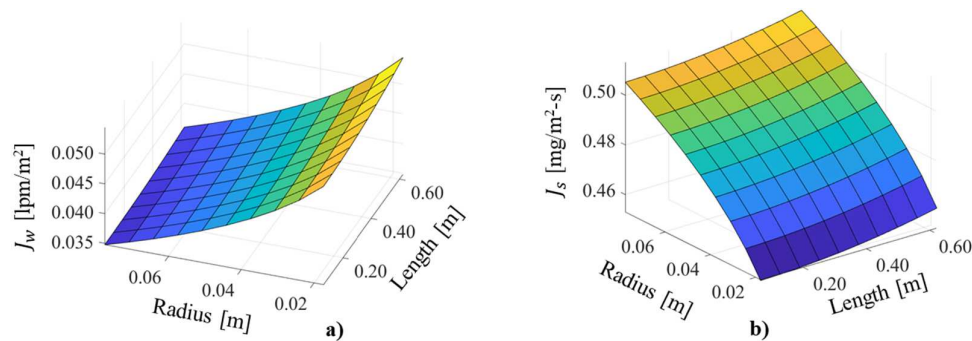


Figure 4.5: Sectional distribution of fluxes for each cell within the membrane module.

The issue of having a more concentrated solution in the upper part of the membrane module was also observed in terms of water and salt fluxes as presented in Figure 4.5. This is a point of attention for membrane module designers to improve the utilization of the available membrane area in future development of this component. Depending on the proposed enhancements to reach this goal, for instance, reduction in the radius of the module and/or number of fibers, membrane modules might become more financially attractive for new desalination projects and research about RO.

4.2.3 Performance curves for RO

After acquiring a clearer understanding of the behavior of pressures, volume flow rates, salinities and fluxes within the membrane module, the major focus of this work is presented and discussed in this section. After simulating the membrane module model for the RO process using the input parameters presented in section 3.3, the results obtained for the key performance parameters were combined into meaningful plots.

In the following figures, the base axes represent the two most important input parameters, which are the inlet volume flow rate of salt water (feed solution) ($\dot{V}_{sh,in}$) plotted on the left bottom axis and its hydraulic pressure ($P_{sh,in}$) plotted on the right bottom axis. The vertical axis provides the results for different output parameters obtained from the simulations, which varies depending on the analyzed figure. Lastly, the figures also provide an additional output parameter represented as a color scale to display the results for the salinity of the permeate solution ($sal_{fib,out}$), which is a crucial parameter to measure the quality of permeate produced. A preliminary analysis demonstrated that all the results acquired from the simulations for the 5-inch scale Toyobo HP5255SI-H3K membrane module presented similar trend when using the operational input parameters presented earlier in Table 3.3. In order to make this section more concise, only the results using the inlet salinity of feed solution of 0.035 kg/kg are shown and discussed in this section. This value is the salt water salinity used as reference [22]. Further results for lower and higher salinities of inlet feed solution are provided in Appendix B.

The amount of permeate produced by a RO process is one of the most important indicators of the system performance. Figure 4.6 shows the volume flow rate and salinity of permeate produced using the selected membrane module.

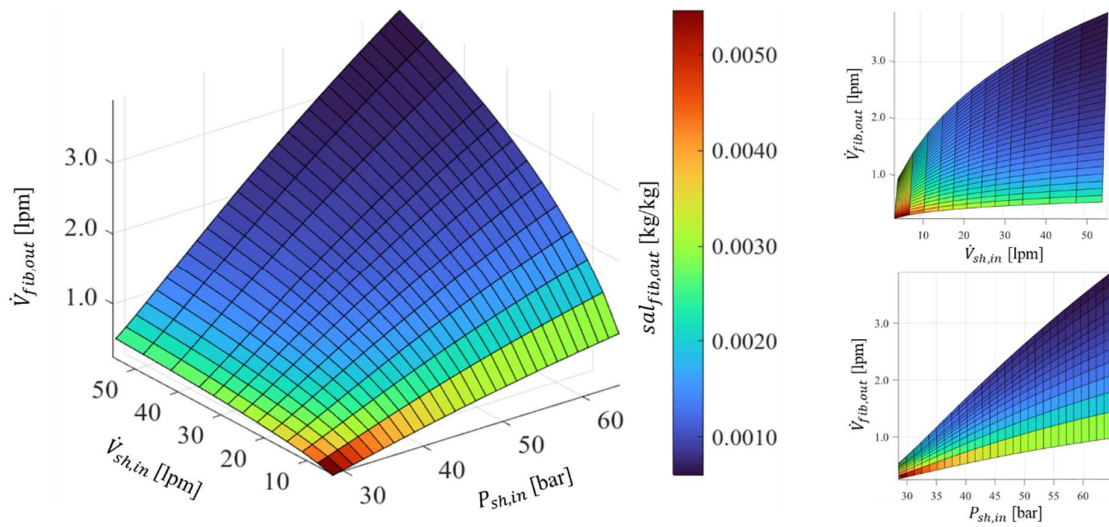


Figure 4.6: Performance curve for the Toyobo HP5255SI-H3K membrane module in terms of permeate outlet volume flow rate and salinity for different inlet parameters.

Figure 4.6 shows that increments in the inlet volume flow rate of feed solution did not significantly affect the amount of permeate solution produced compared to increases in its inlet hydraulic pressure. In other words, when the membrane module worked with the feed solution at inlet hydraulic pressures up to 45 bar, the amount of permeate produced was not very expressive even for larger inlet volume flow rates of feed solution. To produce higher volume of permeate solution, the feed solution had to be pressurized at higher inlet hydraulic pressures above 45 bar. This behavior revealed that the amount of permeate produced was mainly affected by the inlet hydraulic pressure of feed solution than by its inlet volume flow rate because the water flux through the membrane is a function of hydraulic and osmotic gradients only. It is necessary to carefully analyze in which circumstance it would be beneficial to increase the inlet hydraulic pressure of feed solution to produce more volume of permeate. Unfortunately, this would require more power input to the system and also raise the operation costs, beyond increasing the entropy generation within the membrane module, producing more losses.

Figure 4.6 also demonstrates that the salinity of permeate relies more on the inlet volume flow rate of feed solution than on its inlet hydraulic pressure. That means, for inlet volume flow rates of feed solution higher than approximately 18 lpm, the salinity of permeate produced dropped substantially to around 0.0035 kg/kg, which is nearly half of the highest value reached by a combination of low inlet volume flow rate and hydraulic pressure of the feed solution. After this point, the salinity of permeate reduces even more as either the inlet volume flow rate or hydraulic pressure of feed solution is increased. Therefore, the notable influence of the inlet volume flow rate over the salinity of permeate output is explained by the fact that the velocity of the feed solution within the membrane module is high, which did not allow enough time for large quantities of salt to cross the hollow fibers.

As expected, Figure 4.6 shows that increasing the inlet hydraulic pressure and volume flow rate of feed solution led to a larger production of permeate with lower salinity by reason it provided higher flow velocities within the membrane module and did not allow enough time for salt to cross the hollow fibers. This case is clearly advantageous from the point of view of the amount of permeate produced at proper quality. On the other hand, low values of inlet hydraulic pressure and inlet volume flow rate resulted in low amounts of permeate produced with very high salinity because the velocity of the inlet flow rate of feed solution within the membrane module was also low. The feed solution spent more time within the module, allowing salt to be in contact with the hollow fiber membranes for a longer period and increasing the chances of salt to cross the membrane. Hence, Figure 4.6, provides ways to find an optimum and feasible combination of input parameters, which will lead to the highest amount of permeate produced with the lowest salinity possible.

Besides the amount of permeate produced by a RO process, another key indicator of the membrane module performance is the recovery ratio. Figure 4.7 presents the recovery ratio and salinity of permeate produced by the Toyobo HP5255SI-H3K membrane module.

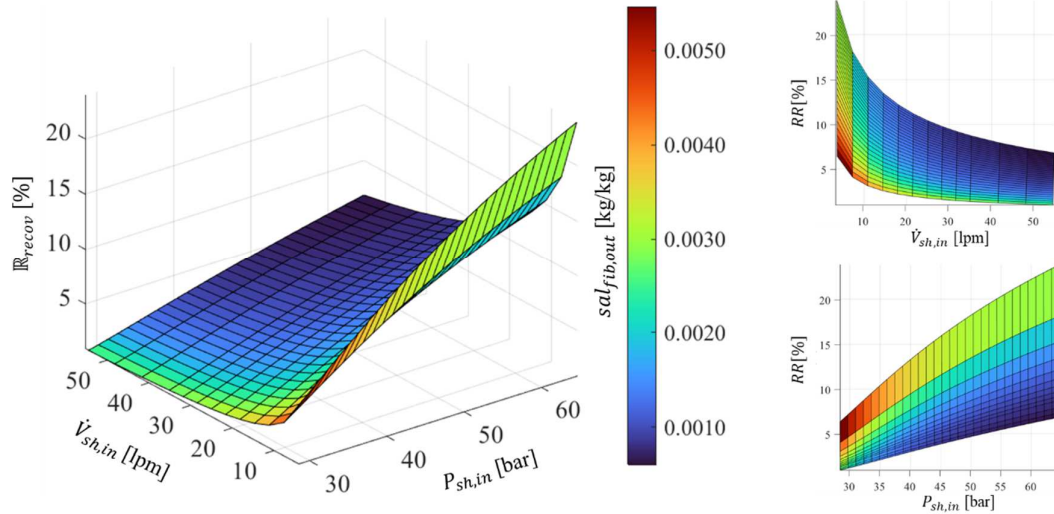


Figure 4.7: Performance curve for the Toyobo HP5255SI-H3K membrane module in terms of recovery ratio and permeate salinity for different inlet parameters.

Figure 4.7 demonstrates that for low values of inlet volume flow rate and hydraulic pressure of feed solution, the recovery ratio was only around 5%, while the salinity of permeate produced reached high values, above 0.0050 kg/kg. This occurred due to the combination of small amount of feed solution entering the membrane module at low velocity, which led the feed solution to spend a long time within the membrane module in contact with the fibers. This resulted in a small and highly concentrated production of permeate. Figure 4.7 also shows that increasing the inlet volume flow rate of feed solution resulted in lower recovery ratio values at lower salinities. This is explained by the larger amount of feed solution entering the membrane module and not having enough time for crossing the hollow fibers, since it spent less time there.

A suitable way to increase the recovery ratio was by raising the inlet hydraulic pressure of feed solution because it increased the flux of water through the fibers and decreased the effect of concentration polarization. The highest recovery ratio results occurred when a high inlet hydraulic pressure was applied when working with low inlet volume flow rates of feed solution. This was caused by a small amount of feed solution being highly pressurized against the surface of the fibers for long enough to force, not only water molecules, but also salt particles to penetrate it. Therefore, working with a combination of high inlet hydraulic pressures (between 55 bar and 60 bar) and lower volume flow rates (up to 10 lpm) of feed solution is the best alternative to reach higher recovery ratios (above 15%) despite the moderate values for salinity of permeate

produced (from 0.0020 to 0.0030 kg/kg). However, as mentioned in the previous paragraphs, it would require more power to be provided to the system and would generate more losses.

Equally important to the above indicators, the salt rejection of the membrane module was also evaluated. Figure 4.8 presents the results obtained for salt rejection and salinity of permeate using the membrane module selected here.

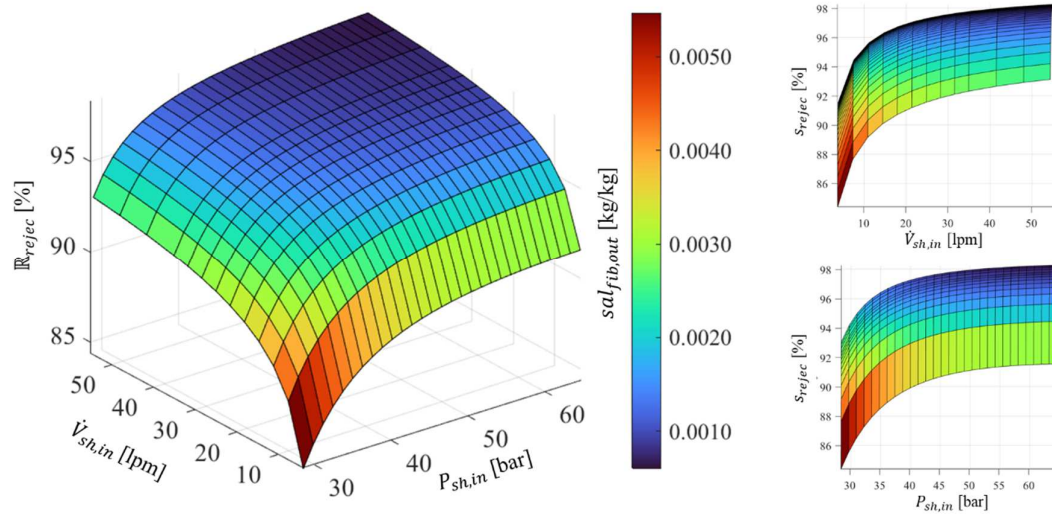


Figure 4.8: Performance curve for the Toyobo HP5255SI-H3K membrane module in terms of salt rejection and permeate salinity for different inlet parameters.

As described in the last paragraphs, low incoming amount of feed solution at low velocity provided by lower values of inlet hydraulic pressures and volume flow rate of feed solution was not advantageous in terms of salt rejection rate as shown in Figure 4.8 because this condition allows enough time for salt to penetrate the hollow fibers. Increasing the inlet hydraulic pressure of feed solution only, did not provide significant increase in salt rejection rate for lower inlet volume flow rates (below 10 lpm) because the feed solution was strongly forced against the hollow fibers, allowing more salt particles to cross the membranes together with water molecules. Consequently, salt rejection was not very high and the permeate solution presented high salinity.

On the other hand, increasing either the inlet volume flow rate or hydraulic pressure of feed solution decreased the influence of concentration polarization on the water flux and led to higher salt rejection rates and lower salinity values of permeate outflow. This was due to lesser accumulation of salt on the membrane surface and higher flux of water crossing the hollow fibers, which is a function of the hydraulic pressure gradient through the membrane. Hence, to achieve salt rejection rates above 96% with a favorable salinity below 0.0020 kg/kg, it is not necessary to work at very high values of inlet volume flow rate and hydraulic pressure of feed solution, since values around 18 lpm and 35 bar, respectively, would be enough to reach these results for the analyzed membrane module.

The behavior of the Toyobo HP5255SI-H3K membrane module was also assessed in terms of power loss. The results acquired for this parameter are exhibited in Figure 4.9 together with salinity of outgoing permeate solution.

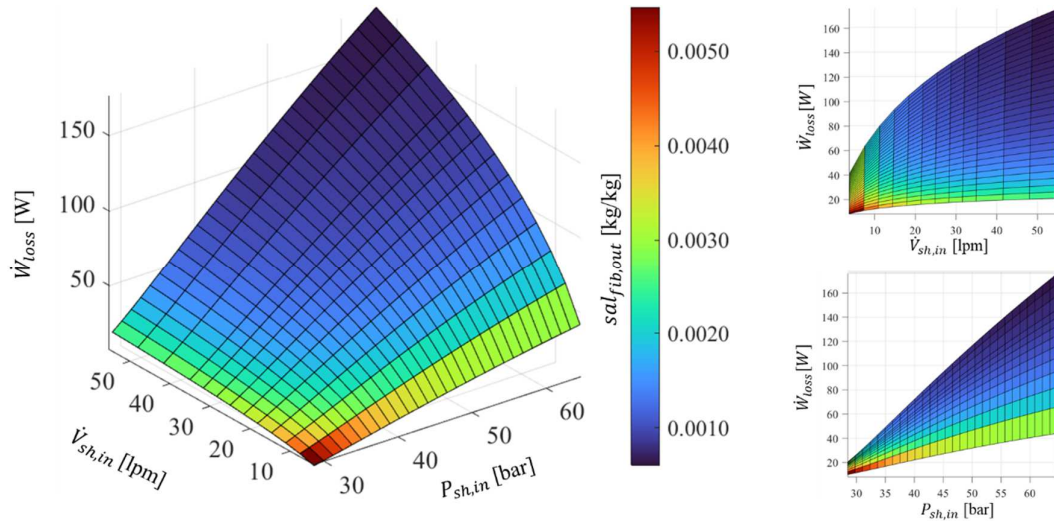


Figure 4.9: Performance curve for the Toyobo HP5255SI-H3K membrane module in terms of power loss and permeate salinity for different inlet parameters.

At a first look, Figure 4.9 resembles the plot for the results on volume flow rate of permeate solution produced previously discussed in this section (see Figure 4.6). It is totally reasonable since the outflow volume permeate is related to the work loss within the membrane module in the sense that higher values of inlet hydraulic pressure of feed solution are required to produce larger amounts of permeate. This increases the flow velocities within the membrane module generating more entropy, which leads to larger internal losses in the process. Increments in the inlet volume flow rate also raised the internal losses because higher volume flow rates of feed solution are associated with higher values of entropy entering the membrane module. It was noticed that inlet hydraulic pressure changes were dominant over inlet volume flow rate of feed solution in terms of power losses because internal losses within the membrane module were more sensitive to changes in inlet hydraulic pressure compared to inlet volume flow rate. Finally, as explained earlier in this section, low values of inlet volume flow rate and hydraulic pressure led to saltier permeate solution. Thanks to low inlet hydraulic pressure and flow rate, the internal losses within the membrane module were not significant.

Another parameter analyzed was the extra work to be added to the membrane module in order to overcome the internal losses. Figure 4.10 presents the extra cost work per liter of permeate solution produced with its salinity.

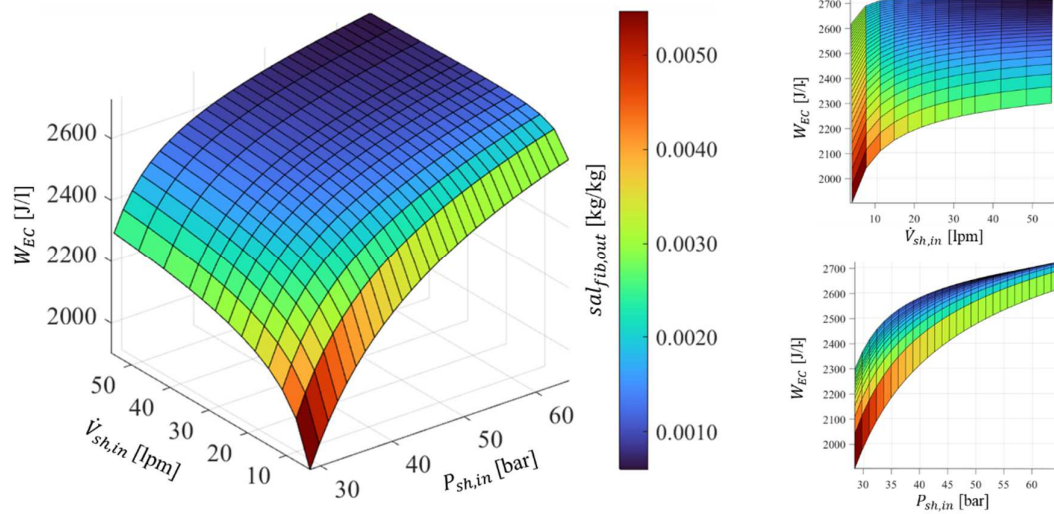


Figure 4.10: Performance curve for the Toyobo HP5255SI-H3K membrane module in terms of extra cost work and permeate salinity for different inlet parameters.

Figure 4.10 also resembles the shape of a previously presented performance curve seen in this section (Figure 4.8), however, there are some differences. As shown in Figure 4.10, low inlet hydraulic pressure values and volume flow rate of feed solution required little work to overcome internal losses within the membrane module. The quality of permeate was not desirable in this case due to its high salinity. On the other hand, the work necessary to overcome internal losses per liter of permeate produced increased more significantly with increments in the inlet hydraulic pressure compared to raises in the inlet volume flow rate of feed solution. This occurred because of entropy generation increased more with hydraulic pressure increments, producing higher amounts of internal losses within the membrane module. This led to larger values of work required by the pumping system to overcome the losses within the membrane module. Increasing inlet volume flow rate also contributed for extra cost work, but in less extension compared to inlet hydraulic pressure increments. Therefore, balancing the production of permeate and its salinity with a low value of extra cost work is quite challenging, since to obtain satisfactory results for a certain output parameter requires to sacrifice others.

4.3 Results for the PRO membrane module

This section demonstrates and analyzes the results obtained from simulations of the membrane module for the PRO process. The discussion was performed as follows.

4.3.1 Validation for PRO

For the PRO process, an experimental research carried out by Tanaka *et al* (2018) [31], was used to validate the proposed model. A comparison between the results

obtained using the same input parameters as the authors (see Table 3.7) is exhibited in Figure 4.11. In this curve, the vertical left axes provide the average flux in the membrane module ($J_{w,avg}$) presented in Eq. (3.45).

Figure 4.11 shows that the obtained results from the PRO model were in reasonable agreement with the experimental data, with deviation ranging from 1.67% to 13.64%. These differences are explained by some simplifications adopted in the proposed model mentioned in section 3.2.1 (i.e. constant membrane parameters, steady state condition, average fiber length, etc.) which do not occur in actual applications. However, this membrane module model provides a reasonable idea on what to expect in terms of performance when working in PRO systems.

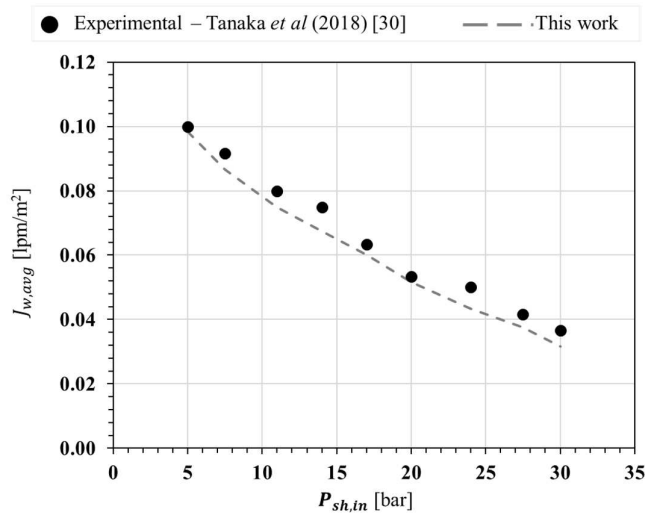


Figure 4.11: Comparison between experimental and produced results from the proposed PRO model

4.3.2 Sectional distribution of pressures, flows and fluxes for PRO

Analogously to the analysis performed to understand the behavior of the RO model previously in section 4.2.2, the proposed membrane module model for PRO was also assessed in order to comprehend what occurs within it in terms of pressures, salinities, flow rates and fluxes. The PRO model worked with the average values of the inlet parameters provided in section 3.3 as displayed in Table 4.2.

Parameter	Symbol	Value	Unit
Salinity of inlet draw solution	$sal_{sh,in}$	0.035	kg/kg
Salinity of inlet feed solution	$sal_{fib,in}$	0.001344	kg/kg
Pressure difference across the module	ΔP_{sh}	0.0255	bar
Osmotic pressure factor of draw solution	$\Pi_{fac,draw}$	0.50	-
Osmotic pressure factor of feed solution	$\Pi_{fac,feed}$	1.50	-

Table 4.2: Average inlet parameters for understanding the behavior of certain quantities within the membrane module of the PRO process.

For the PRO process, a sectional distribution of the values in each cell of the forementioned quantities was plotted along the axial and radial directions of the membrane module as exhibited in Figures 4.12 to 4.15.

Figure 4.12 provides a sectional distribution of hydraulic pressure within the membrane module in each cell. The hydraulic pressure of both draw (Figure 4.12a) and feed (Figure 4.12b) solutions were uniformly distributed along the radial and axial directions, respectively, within the membrane module, which agrees with the principle of transmission of fluid-pressure [69]. Also in Figure 4.12b, the cells closer to the central perforated tube, which have less fibers, presented slightly lower values of pressure drops because of the smaller amount of fibers. Similarly for the PRO process, the segmented versions of Ergun Eqs. (3.37), (3.39) and (3.41), as well as Hagen-Poiseuille Eqs, (3.36), (3.38) and (3.40) predicted the pressure drops on the shell (radial direction) and fibers (axial direction) caused by frictional losses as expected and this agrees with the reviewed literature [31, 46, 47].

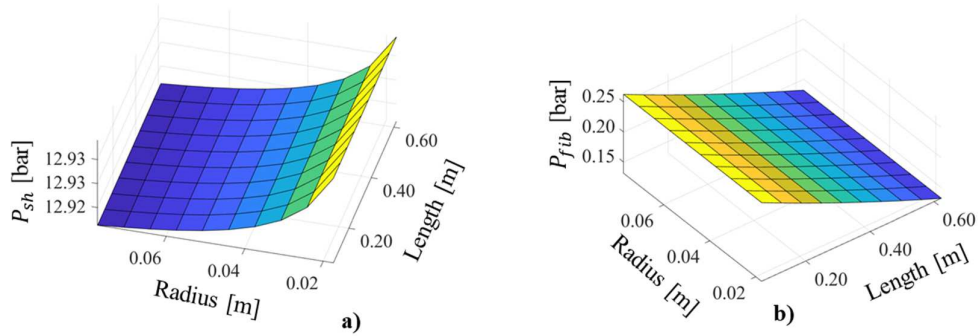


Figure 4.12: Sectional distribution of pressures for each cell within the membrane module.

The sectional distribution of flow rates within the membrane module was also analyzed and it is depicted in Figure 4.13. Figures 4.13a and b present a similar pattern for both draw and feed solutions across the membrane module. That is, both fluids on the shell and fibers sides increased their flow rates radially but decreased it axially within the membrane module. The reasons for this are explained as follows.

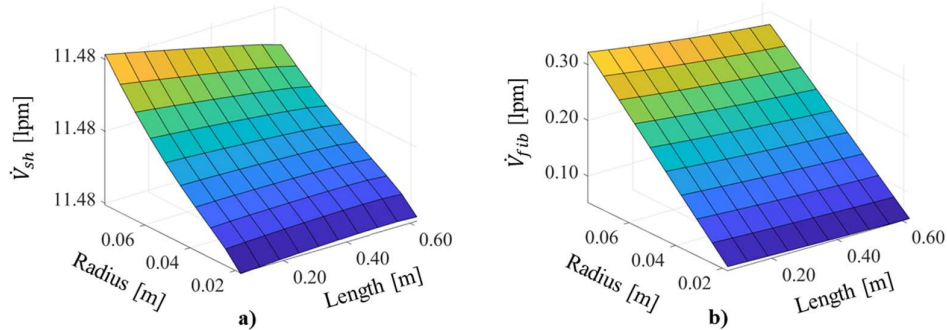


Figure 4.13: Sectional distribution of volume flow rates for each cell within the membrane module

The radial increment on volume flow rate of draw solution on the shell side shown in Figure 4.13a is due to the mixture of the existent draw solution with the flow of feed solution crossing the hollow fibers. The volume of this mixture of fluids increased along the radial direction where the number of hollow fibers is larger and consequently, there was higher amount of feed solution crossing the fibers and dilute the draw solution due to the difference in chemical potential. The volume flow rate of the mixture between draw and feed solutions slightly decreased towards the axial length of the membrane module near the outer radius because the mixture in that region was leaving the membrane module by the outlet pipe. Similarly, Figure 4.13b shows that the volume flow rate of feed solution within the hollow fibers also increase along the radial direction of the membrane module. The reason for this was due to a geometric characteristic of the membrane module in which a larger number of fibers are placed towards the outer radius. As a result, the larger is the radius within the membrane module, the higher was the amount of feed solution able to flow through the cells in that particular radial section. Also, the volume flow rate of feed solution within the hollow fibers decreased along the axial direction because part of the fluid crossed the fibers towards the shell side due to the chemical potential gradient.

From the perspective of salinities of the draw and feed solutions, the sectional distribution for each cell is exhibited in Figure 4.14. In this figure, the salinities on the shell and fibers sides present opposite behavior.

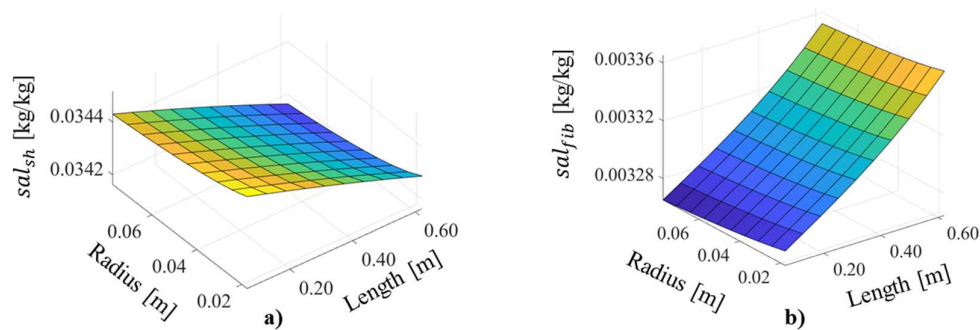


Figure 4.14: Sectional distribution of salinities for each cell within the membrane module.

In Figure 4.14a, the salinity of draw solution on the shell side decreased in the axial direction because it was becoming more diluted as water molecules crossed the fibers driven by the chemical potential gradient along the membrane module. Also, the highest salinity values on the shell side were found on those cells close to the central perforated tube. This occurred by reason of the number of hollow fibers in that region was lower, leading to a smaller flux of water through them. The salinity on the shell side slightly decreased towards the radial direction because there were more fibers in those regions, which allowed for higher flux of water coming from the fibers to dilute the draw solution. Figure 4.14b shows that the feed solution entered the membrane module at the lowest salinity values, and it increased towards the axial direction due to

the reverse salt flux crossing the fibers from the draw solution on the shell side, which is an effect of the concentration polarization phenomenon. The impact of this salinity distribution reflected on water and salt fluxes presented in the next paragraphs.

Finally, Figure 4.15 presents how the fluxes of water and salt were distributed in each cell within the membrane module for the PRO process. These plots and their explanation are supported by the previous plots discussed in this section.

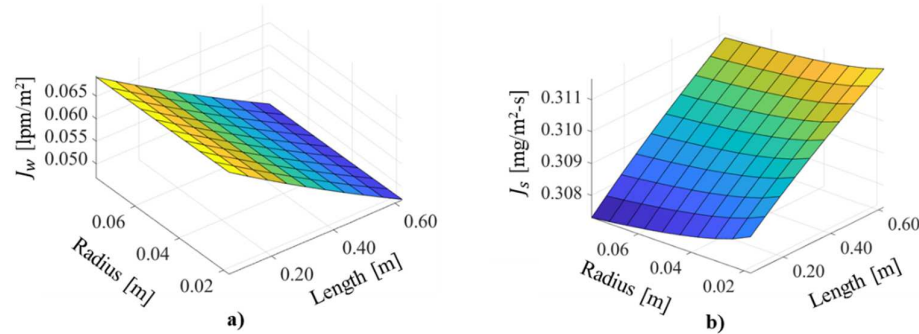


Figure 4.15: Sectional distribution of fluxes for each cell within the membrane module.

According to Figure 4.15a, the water flux was larger in the first radial cells because the difference of salinities between draw and feed solution was greater in this region and consequently, their osmotic pressure difference. Since the hydraulic pressure difference is smaller than the osmotic pressure difference in PRO processes, the higher osmotic pressure gradient in this region allowed a larger amount of water to cross the fibers towards the shell side to dilute the draw solution for balancing the chemical potential of the fluids on the feed and draw sides. The reverse salt flux increased the salinity of the solution within the hollow fibers and decreased the water flux towards the shell side along the axial direction of the membrane module, which was affected by the reduction in the osmotic pressure difference between feed and draw solutions. From the salt flux point of view presented in Figure 4.15b, the amount of salt flux, which is a function of concentrations, increased along the axial direction of the membrane module. This occurred due to increments in the concentration gradient between draw and feed solutions caused by the reverse salt flux and concentration polarization phenomenon. An alternative to mitigate these issues would be designing shorter membrane modules with the purpose of reducing the salt flux that crosses the hollow fibers from the shell side along the axial length of the module.

4.3.3 Performance curves for PRO

After performing the simulations of the membrane module model for the PRO process with the input parameters presented in section 3.3, the results acquired for the key performance indicators were presented into significant plots, analogously to what was done in section 4.2.3 for the RO process.

In the subsequent figures, the base axes represent two input parameters, which are the inlet volume flow rate of draw solution ($\dot{V}_{sh,in}$) plotted on the left bottom axis and its inlet hydraulic pressure ($P_{sh,in}$) or the inlet hydraulic pressure difference between the feed and draw solutions ($\Delta P_{sh-fib,in}$) depending on the plot. These last two parameters were plotted on the right bottom axis. The vertical axis presents the results for output parameters obtained from the simulations, which is different for each figure. The plots also provide another output parameter represented as a color scale. As in the RO model, the PRO results for the 5-inch scale Toyobo HP5255SI-H3K membrane module presented similar trend when using the operational input parameters given in Table 3.4. To make this section more compact, only the results using the inlet salinity of draw solution of 0.035 kg/kg, which is the reference value for salt water used here [22], are shown and discussed. Additional results for lower and higher salinities of inlet draw solution using this membrane module are provided ahead in Appendix C.

The amount of power produced per unit membrane area (power density) is an indicator widely used in literature [5, 41, 68] for describing the membrane module efficiency in PRO processes. Figure 4.16 presents the power density and the irreversible net power output produced using the selected membrane module.

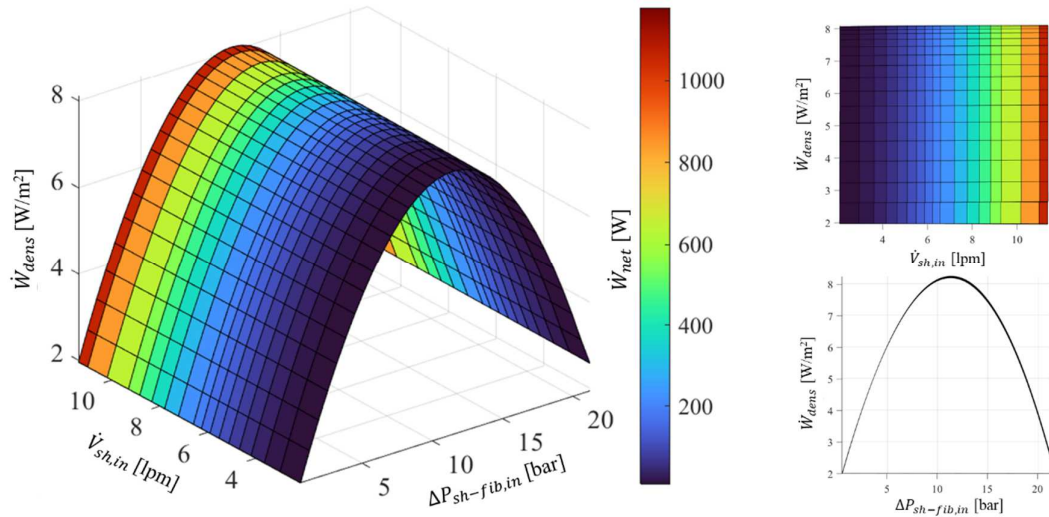


Figure 4.16: Performance curve for the Toyobo HP5255SI-H3K membrane module in terms of power density and net power output for different inlet parameters.

As shown in Figure 4.16, the Toyobo HP5255SI-H3K membrane module working in the PRO process reached a maximum power density of 8.1 W/m², which was achieved when $\Delta P = \Delta \Pi / 2$ [70]. After this maximum point, as the hydraulic pressure difference kept increasing, it went towards equilibrium with the osmotic pressure difference. This reduced the water flux through the hollow fibers and consequently, the osmotic driving force across the membrane and the power density of the membrane module. This behavior agrees to results found in literature [5, 68]. Also, the maximum net power output occurred at higher flow rates because a larger amount of feed solution

was drawn from the fibers, allowing a larger amount of diluted fluid to flow out of the membrane and produce more power. Hence, for the membrane module to perform at its best in terms of power density and net power output, it is interesting to work with the inlet hydraulic pressure difference near 12 bar together with inlet volume flow rates of draw solution above 10 lpm.

The net power output was evaluated along with the power loss within the membrane module as shown in Figure 4.17. This plot demonstrates that the net power output produced increased with increments in the inlet volume flow rate of draw solution only. The amount of net power output produced was more influenced by increments in the inlet volume flow rate of draw solution than on its inlet hydraulic pressure because larger amount of draw solution within the membrane module induced a higher water flux across the fibers to equilibrate the chemical potential on draw and feed sides. Then, larger amounts of diluted solution flowed out of the membrane module to generate power. Although power loss did not significantly affect the amount of output net power produced by the PRO process, lower inlet hydraulic pressures of draw solution generated higher amounts of power losses, which were reduced as the inlet hydraulic pressure was raised.

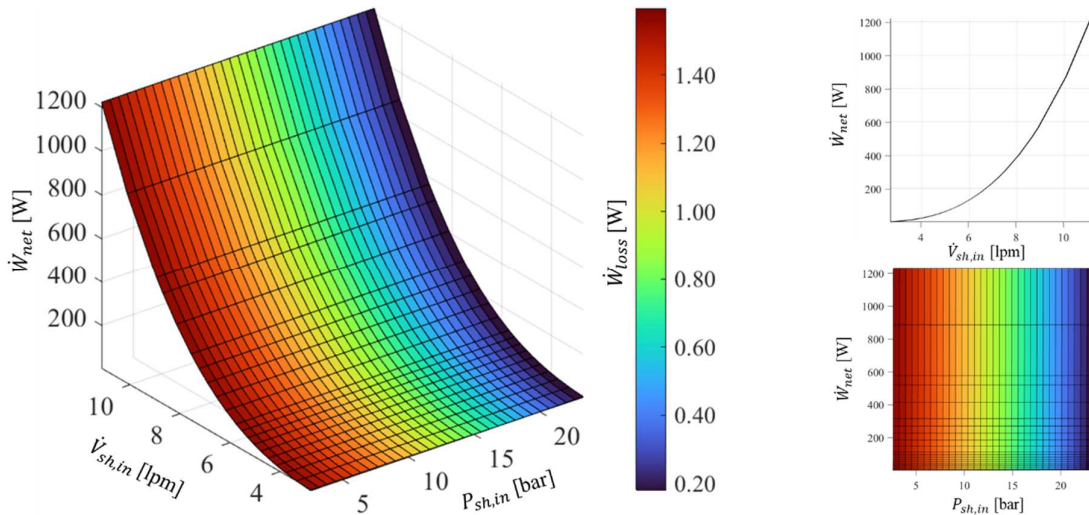


Figure 4.17: Performance curve for the Toyobo HP5255SI-H3K membrane module in terms net power output and power loss for different inlet parameters.

4.4 Remarks on integrated RO-PRO systems

Over the years, several studies have been conducted on the development of PRO systems aiming to improve their practical and economical feasibility [5, 19, 20, 31, 32, 43, 68, 71-73]. Also, the very first PRO pilot plant built and operated by the Norwegian company Statkraft AS from 2009 to 2014 was an unsuccessful attempt of producing and selling electricity due to the high production and operation costs [74,

75]. Before this scenario, there is no doubt that PRO systems are still a concept and need to be improved before being put into actual application.

Integration of RO and PRO systems has also been studied over the time. The aim of these research was to desalinate salt water using the RO and store the resulting freshwater and brine in separate tanks, then produce power by joining them into a PRO system. Unfortunately, proposed systems found in recent literature presented very low efficiencies around 10% [18, 47, 76]. In light of the investigation carried out in this study, combining RO and PRO systems would not work at least with current technology due to the following reasons:

- a) After desalinating salt water, the obtained permeate solution would present some salinity, which would reduce the osmotic pressure difference in a PRO system, leading to less power generation;
- b) Depending on the size of the RO system, the amount of permeate produced might not be enough for the necessity of the PRO system to be worthy to generate power;
- c) After the RO process, there might be accumulation of salt in both brine and permeate tanks and at certain point, these fluids would have to be discharged because it would not be advantageous to use them in the PRO system. The saltier permeate and brine would have to go through treatment before being discharged, increasing operational costs. Trying to use brine and/or permeate with high salinities in PRO systems impact directly on the operational costs of the combined RO-PRO system. First, brine at very high salinity requires higher inlet hydraulic pressures into the system and consequently, larger amounts of power input, increasing costs. Secondly, using permeate with high salinity is also a problem because it presents high osmotic pressure, therefore the osmotic pressure gradient for the PRO process will be lower because of lower flux of water through the fibers and less power would be produced.

Chapter 5

Conclusions and suggestions for future work

The development of this work provided interesting insights and the main ones are listed as follows:

- a) Working with membrane modules with smaller radius in RO processes might be advantageous to decrease unused membrane area, leading to more permeate production and reducing costs related to this component;
- b) The performance curves for the RO process provide feasible ways to find the optimum values of inlet parameters to produce the highest amount of permeate with the lowest salinity;
- c) The amount of permeate produced is majority affected by the inlet hydraulic pressure of feed solution than by its inlet volume flow rate;
- d) The velocity of feed solution within the membrane module in the RO process determines how long water molecules and salt particles will be in contact with the fibers, which is one of the factors that determines fluxes across the membrane;
- e) The influence of concentration polarization in the membrane module of RO systems decreases by raising the inlet hydraulic pressure of feed solution;
- f) Higher salt rejection rates with low salinity values in RO do not require very high inlet flow rates and hydraulic pressures of feed solution;
- g) Internal losses in the membrane module of RO process are more sensitive to changes in inlet hydraulic pressure than in inlet volume flow rate;
- h) Higher flow velocities within the membrane module of a RO system produces more entropy and leads to larger internal losses in the process;
- i) The extra cost work in RO processes is directly related to increments in both inlet hydraulic pressure and flow rate of feed solution;
- j) Shorter membrane modules might be a suitable alternative to mitigate the reverse salt flux through the hollow fibers in PRO applications;
- k) To extract the highest power density from a membrane module in PRO systems it is not necessary to work with high input hydraulic pressures or volume flow rates of draw solution. The same is valid for power production;

- l) The amount of net power output produced in PRO processes is more influenced by increments in the inlet volume flow rate of draw solution than on its inlet hydraulic pressure;
- m) A combined RO-PRO system would not work with currents technology due to limitations on the initial salinity and amount of feed solution to run the PRO system, as well as high costs with operation, storage and treatment of feeding fluids for the PRO process.

The simplifications adopted in this work certainly reflected on the obtained results. Therefore, there is a great opportunity to refine and improve it to bring the models closer to an actual membrane module operation. The main suggestions for future work are given below:

- a) Improve the model to account for the whole length of each individual hollow fiber may lead to more accurate results;
- b) Use water (A), salt (B) and diffusion (D_s) coefficients as functions of concentration of the solution would lead to a more realistic model;
- c) Use different temperatures for the inlet fluids and account for the temperature change within the membrane module during the processes;
- d) Use transient state operation at the beginning of the simulation;
- e) Use higher number of axial and radial divisions to increase accuracy of the models;
- f) Find the optimum operating conditions for the membrane module working in the RO and PRO processes using the resulting performance curves.

Bibliography

- [1] M. Elimelech and W. A. Phillip, “The future of seawater desalination: Energy, technology, and the environment,” *Science (80-.)*, vol. 333, no. 6043, pp. 712–717, 2011, doi: 10.1126/science.1200488.
- [2] M. A. Shannon, P. W. Bohn, M. Elimelech, J. G. Georgiadis, B. J. Mariñas, and A. M. Mayes, “Science and technology for water purification in the coming decades,” *Nature*, vol. 452, no. 7185, pp. 301–310, 2008, doi: 10.1038/nature06599.
- [3] K. Touati and F. Tadeo, “Green energy generation by pressure retarded osmosis: State of the art and technical advancement—review,” *Int. J. Green Energy*, vol. 14, no. 4, pp. 337–360, 2017, doi: 10.1080/15435075.2016.1255633.
- [4] BPSTATS, “BP Statistical Review of World Energy Statistical Review of World, 68th edition,” *Ed. BP Stat. Rev. World Energy*, pp. 1–69, 2019, [Online]. Available: <https://www.bp.com/content/dam/bp/business-sites/en/global/corporate/pdfs/energy-economics/statistical-review/bp-stats-review-2019-full-report.pdf>.
- [5] F. Helfer, C. Lemckert, and Y. G. Anissimov, “Osmotic power with Pressure Retarded Osmosis: Theory, performance and trends - A review,” *J. Memb. Sci.*, vol. 453, pp. 337–358, 2014, doi: 10.1016/j.memsci.2013.10.053.
- [6] International Energy Agency, “Global Energy Review 2021,” *Glob. Energy Rev. 2020*, pp. 1–36, 2021, [Online]. Available: <https://iea.blob.core.windows.net/assets/d0031107-401d-4a2f-a48b-9eed19457335/GlobalEnergyReview2021.pdf>.
- [7] E. Jones, M. Qadir, M. T. H. van Vliet, V. Smakhtin, and S. mu Kang, “The state of desalination and brine production: A global outlook,” *Sci. Total Environ.*, vol. 657, pp. 1343–1356, 2019, doi: 10.1016/j.scitotenv.2018.12.076.
- [8] M. Parfit, N. G. S. (U.S.), and W. Graves, *Water: The Power, Promise, and Turmoil of North America’s Fresh Water*. National Geographic Society, 1993.
- [9] A. D. Khawaji, I. K. Kutubkhanah, and J. M. Wie, “Advances in seawater desalination technologies,” *Desalination*, vol. 221, no. 1–3, pp. 47–69, 2008, doi: 10.1016/j.desal.2007.01.067.
- [10] A. Sapalidis, *Membrane Desalination*. CRC Press, 2020.
- [11] E. Koncagül, M. Tran, R. Connor, and S. Uhlenbrook, “The United Nations world water development report 2019: leaving no one behind, facts and figures,” 2019.
- [12] Z. Hadadian, S. Zahmatkesh, M. Ansari, A. Haghghi, and E. Moghimipour, “Mathematical and experimental modeling of reverse osmosis (RO) process,” *Korean J. Chem. Eng.*, vol. 38, no. 2, pp. 366–379, 2021, doi: 10.1007/s11814-020-0697-9.

- [13] M. Qasim, M. Badrelzaman, N. N. Darwish, N. A. Darwish, and N. Hilal, "Reverse osmosis desalination: A state-of-the-art review," *Desalination*, vol. 459, no. March, pp. 59–104, 2019, doi: 10.1016/j.desal.2019.02.008.
- [14] A. Tamburini, A. Cipollina, M. Papapetrou, A. Piacentino, and G. Micale, *Salinity gradient engines*. Elsevier Ltd., 2016.
- [15] D. Bharadwaj, T. M. Fyles, and H. Struchtrup, "Multistage Pressure-Retarded Osmosis," *J. Non-Equilibrium Thermodyn.*, vol. 41, no. 4, pp. 327–347, 2016, doi: 10.1515/jnet-2016-0017.
- [16] H. Struchtrup, *Thermodynamics and Energy Conversion*, 1st ed. Berlin, Heidelberg: Springer Berlin Heidelberg, 2014.
- [17] I. E. A. (IEA), "Electricity Market Report, July 2021," Paris, 2021. doi: 10.1787/f4044a30-en.
- [18] D. Bharadwaj and H. Struchtrup, "Large scale energy storage using multistage osmotic processes: Approaching high efficiency and energy density," *Sustain. Energy Fuels*, vol. 1, no. 3, pp. 599–614, 2017, doi: 10.1039/c6se00013d.
- [19] Q. A. Khasawneh, B. Tashtoush, A. Nawafleh, and B. Kan'an, "Techno-economic feasibility study of a hypersaline pressure-retarded osmosis power plants: Dead sea-red sea conveyor," *Energies*, vol. 11, no. 11, 2018, doi: 10.3390/en11113118.
- [20] R. Soltani and H. Struchtrup, "Modeling and simulation of the dual stage pressure retarded osmosis systems," *Desalination*, vol. 460, no. January, pp. 28–40, 2019, doi: 10.1016/j.desal.2019.02.010.
- [21] J. Kim, J. Lee, and J. H. Kim, "Overview of pressure-retarded osmosis (PRO) process and hybrid application to sea water reverse osmosis process," *Desalin. Water Treat.*, vol. 43, no. 1–3, pp. 193–200, 2012, doi: 10.1080/19443994.2012.672170.
- [22] National Ocean Service, "Why is the ocean salty?," 2021. <https://oceanservice.noaa.gov/facts/whysalty.html>.
- [23] S. H. Touati, K.; Tadeo, F.; Kim, J.; Silva, O. A. A.; Chae, *Pressure Retarded Osmosis*, 1st ed. Elsevier Science, 2017.
- [24] A. S. Kim and H. Kim, "Membrane Thermodynamics for Osmotic Phenomena," in *Desalination*, no. August, InTech, 2017.
- [25] K. G. Nayar, M. H. Sharqawy, L. D. Banchik, and J. H. Lienhard, "Thermophysical properties of seawater: A review and new correlations that include pressure dependence," *Desalination*, vol. 390, pp. 1–24, 2016, doi: 10.1016/j.desal.2016.02.024.
- [26] F. J. Millero, R. Feistel, D. G. Wright, and T. J. McDougall, "The composition of Standard Seawater and the definition of the Reference-Composition Salinity Scale," *Deep Sea Res. Part I Oceanogr. Res. Pap.*, vol. 55, no. 1, pp. 50–72, Jan. 2008, doi: 10.1016/j.dsr.2007.10.001.

- [27] E. M. Kramer and D. R. Myers, “Five popular misconceptions about osmosis,” *Am. J. Phys.*, vol. 80, no. 8, pp. 694–699, 2012, doi: 10.1119/1.4722325.
- [28] D. P. S. Ribeiro, “Desenvolvimento e caracterização de membranas para aplicação no processo de produção de energia por Osmose Retardada por Pressão (PRO),” University of Lisbon, 2014.
- [29] R. W. Baker, *Membrane Technology and Applications*, 3rd ed. Chichester, UK: John Wiley & Sons, Ltd, 2012.
- [30] N. Wang, L., Chen, J., Hung, Y., Shammas, Ed., *Membrane and Desalination Technologies*. New York: Humana Press, 2011.
- [31] Y. Tanaka *et al.*, “Experimental and simulation studies of two types of 5-inch scale hollow fiber membrane modules for pressure-retarded osmosis,” *Desalination*, vol. 447, no. December 2017, pp. 133–146, 2018, doi: 10.1016/j.desal.2018.09.015.
- [32] A. Achilli and K. L. Hickenbottom, *Pressure retarded osmosis: Applications*. Elsevier Ltd., 2016.
- [33] Z. Berk, *Food Process Engineering and Technology*, 3rd ed. London: Elsevier, 2018.
- [34] J. Balster, “Plate and Frame Membrane Module,” in *Encyclopedia of Membranes*, Springer, Berlin, Heidelberg, 2015, pp. 2006–2008.
- [35] J. Kucera, *Reverse Osmosis*. Hoboken, NJ, USA: John Wiley & Sons, Inc., 2015.
- [36] S. Zhang, G. Han, X. Li, C. Wan, and T. S. Chung, *Pressure retarded osmosis: Fundamentals*. 2016.
- [37] N. Bolong, A. F. Ismail, and M. R. Salim, “Spinning Effect of Polyethersulfone Hollow Fiber Membrane Prepared by Water or Polyvinylpyrrolidone in Ternary Formulation,” in *Sustainable Membrane Technology for Energy, Water, and Environment*, 1st ed., Hoboken, NJ, USA: John Wiley & Sons, Inc., 2012, pp. 1–10.
- [38] S. Sarp, Z. Li, and J. Saththasivam, “Pressure Retarded Osmosis (PRO): Past experiences, current developments, and future prospects,” *Desalination*, vol. 389, pp. 2–14, 2016, doi: 10.1016/j.desal.2015.12.008.
- [39] S. Sablani, M. Goosen, R. Al-Belushi, and M. Wilf, “Concentration polarization in ultrafiltration and reverse osmosis: a critical review,” *Desalination*, vol. 141, no. 3, pp. 269–289, Dec. 2001, doi: 10.1016/S0011-9164(01)85005-0.
- [40] A. H. Haidari, S. G. J. Heijman, and W. G. J. van der Meer, “Optimal design of spacers in reverse osmosis,” *Sep. Purif. Technol.*, vol. 192, no. October 2017, pp. 441–456, 2018, doi: 10.1016/j.seppur.2017.10.042.
- [41] K. Touati, C. Hänel, F. Tadeo, and T. Schiestel, “Effect of the feed and draw solution temperatures on PRO performance: Theoretical and experimental study,” *Desalination*, vol. 365, pp. 182–195, 2015, doi: 10.1016/j.desal.2015.02.016.

- [42] M. Sekino, "Study of an analytical model for hollow fiber reverse osmosis module systems," *Desalination*, vol. 100, no. 1–3, pp. 85–97, 1995, doi: 10.1016/0011-9164(96)00010-0.
- [43] S. Xu, Y. Liu, Y. Wang, M. Zhang, Q. Xiao, and Y. Duan, "Influential analysis of concentration polarization on water flux and power density in PRO process: Modeling and experiments," *Desalination*, vol. 412, pp. 39–48, 2017, doi: 10.1016/j.desal.2017.02.020.
- [44] C. Klaysom, T. Y. Cath, T. Depuydt, and I. F. J. Vankelecom, "Forward and pressure retarded osmosis: potential solutions for global challenges in energy and water supply," *Chem. Soc. Rev.*, vol. 42, no. 16, p. 6959, 2013, doi: 10.1039/c3cs60051c.
- [45] E. Nagy, *Basic Equations of the Mass Transport through a Membrane Layer*, 1st ed. London: Elsevier, 2012.
- [46] M. Shibuya *et al.*, "Experimental and theoretical study of a forward osmosis hollow fiber membrane module with a cross-wound configuration," *J. Memb. Sci.*, vol. 504, pp. 10–19, 2016, doi: 10.1016/j.memsci.2015.12.040.
- [47] A. Vickerman, "Energy Storage Using Osmotic Processes: A Thermodynamics Based Model," University of Victoria, 2020.
- [48] H. K. Lonsdale, U. Merten, and R. L. Riley, "Transport properties of cellulose acetate osmotic membranes," *J. Appl. Polym. Sci.*, vol. 9, no. 4, pp. 1341–1362, 1965, doi: 10.1002/app.1965.070090413.
- [49] L. Fortunato, A. H. Alshahri, A. S. F. Farinha, I. Zakzouk, S. Jeong, and T. O. Leiknes, "Fouling investigation of a full-scale seawater reverse osmosis desalination (SWRO) plant on the Red Sea: Membrane autopsy and pretreatment efficiency," *Desalination*, vol. 496, no. March, 2020, doi: 10.1016/j.desal.2020.114536.
- [50] A. Matin, F. Rahman, H. Z. Shafi, and S. M. Zubair, "Scaling of reverse osmosis membranes used in water desalination: Phenomena, impact, and control; future directions," *Desalination*, vol. 455, no. January, pp. 135–157, 2019, doi: 10.1016/j.desal.2018.12.009.
- [51] W. Yin, X. Li, S. R. Suwarno, E. R. Cornelissen, and T. H. Chong, "Fouling behavior of isolated dissolved organic fractions from seawater in reverse osmosis (RO) desalination process," *Water Res.*, vol. 159, pp. 385–396, Aug. 2019, doi: 10.1016/j.watres.2019.05.038.
- [52] S. Zhao *et al.*, "Engineering antifouling reverse osmosis membranes: A review," *Desalination*, vol. 499, no. November 2020, 2021, doi: 10.1016/j.desal.2020.114857.
- [53] E. Nagy, I. Hegedüs, E. W. Tow, and J. H. Lienhard V, "Effect of fouling on performance of pressure retarded osmosis (PRO) and forward osmosis (FO)," *J. Memb. Sci.*, vol. 565, no. June, pp. 450–462, 2018, doi: 10.1016/j.memsci.2018.08.039.

- [54] R. W. Baker, *Membrane Technology and Applications*, 3rd ed. John Wiley & Sons, Incorporated, 2012.
- [55] J. G. Wijmans and R. W. Baker, “The solution-diffusion model: a review,” *J. Memb. Sci.*, vol. 107, no. 1–2, pp. 1–21, Nov. 1995, doi: 10.1016/0376-7388(95)00102-I.
- [56] H. Ismail, A. F.; Kusworo, T. D.; Mustafa, A.; Hasbullah, “Understanding the Solution-Diffusion Mechanism in Gas Separation Membrane for Engineering Students,” in *Regional Conference on Engineering Education*, 2005, pp. 155–159.
- [57] S. C. George and S. Thomas, “Transport phenomena through polymeric systems,” *Prog. Polym. Sci.*, vol. 26, no. 6, pp. 985–1017, 2001, doi: 10.1016/S0079-6700(00)00036-8.
- [58] R. W. Baker, *Membrane Technology and Applications*, 3rd ed. Chichester, UK: John Wiley & Sons, Ltd, 2012.
- [59] M. Sekino, “Precise analytical model of hollow fiber reverse osmosis modules,” *J. Memb. Sci.*, vol. 85, no. 3, pp. 241–252, 1993, doi: doi.org/10.1016/0376-7388(93)85278-5.
- [60] S. Ergun and A. A. Orning, “Fluid Flow through Randomly Packed Columns and Fluidized Beds,” *Ind. Eng. Chem.*, vol. 41, no. 6, pp. 1179–1184, Jun. 1949, doi: 10.1021/ie50474a011.
- [61] Q. Xu, G. K. Pearce, and R. W. Field, “Pressure driven inside feed (PDI) hollow fibre filtration: Optimizing the geometry and operating parameters,” *J. Memb. Sci.*, vol. 537, no. May, pp. 323–336, 2017, doi: 10.1016/j.memsci.2017.05.010.
- [62] R. Schopf, F. Schmidt, and U. Kulozik, “Impact of hollow fiber membrane length on the milk protein fractionation,” *J. Memb. Sci.*, vol. 620, no. August 2020, p. 118834, 2021, doi: 10.1016/j.memsci.2020.118834.
- [63] M. A. Junker, W. M. de Vos, R. G. H. Lammertink, and J. de Groot, “Bridging the gap between lab-scale and commercial dimensions of hollow fiber nanofiltration membranes,” *J. Memb. Sci.*, vol. 624, no. November 2020, p. 119100, 2021, doi: 10.1016/j.memsci.2021.119100.
- [64] L. Gómez Palacín, “Modelling , simulation and advanced control of small-scale Reverse Osmosis desalination plants,” University of Valladolid, 2014.
- [65] E. Sivertsen, T. Holt, and W. R. Thelin, “Concentration and temperature effects on water and salt permeabilities in osmosis and implications in pressure-retarded osmosis,” *Membranes (Basel)*, vol. 8, no. 3, 2018, doi: 10.3390/membranes8030039.
- [66] V. Lobo, “Mutual Diffusion Coefficients in Aqueous Electrolyte Solutions,” *Pure Appl. Chem.*, vol. 65, no. 12, pp. 2613–2640, 1993.
- [67] Toyobo CO. LTD., “Hollow Fibers Membrane Module HP5255SI-H3K.” Toyobo CO. LTD., p. 1.

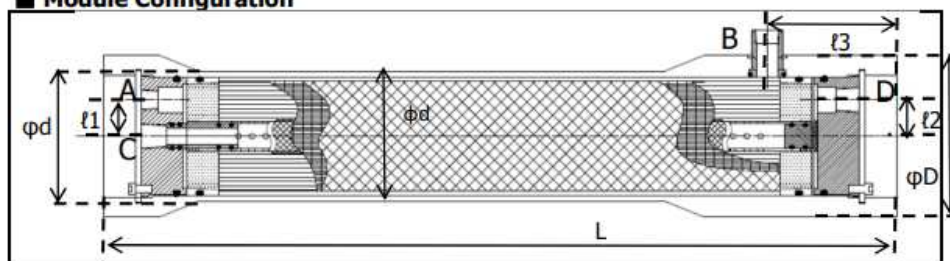
- [68] A. Achilli, T. Y. Cath, and A. E. Childress, “Power generation with pressure retarded osmosis: An experimental and theoretical investigation,” *J. Memb. Sci.*, vol. 343, no. 1–2, pp. 42–52, 2009, doi: 10.1016/j.memsci.2009.07.006.
- [69] P. J. Pritchard, *Fox and McDonald’s Introduction to Fluid Mechanics*, 8 ed. Wiley, 2011.
- [70] K. V. Peinemann, K. Gerstandt, S. E. Skilhagen, T. Thorsen, and T. Holt, “Membranes for Power Generation by Pressure Retarded Osmosis,” *Membr. Energy Convers.*, vol. 2, pp. 263–273, 2008, doi: 10.1002/9783527622146.ch9.
- [71] J. Maisonneuve, C. B. Laflamme, and P. Pillay, “Experimental investigation of pressure retarded osmosis for renewable energy conversion: Towards increased net power,” *Appl. Energy*, vol. 164, pp. 425–435, 2016, doi: 10.1016/j.apenergy.2015.12.007.
- [72] A. P. Straub, A. Deshmukh, and M. Elimelech, “Pressure-retarded osmosis for power generation from salinity gradients: Is it viable?,” *Energy Environ. Sci.*, vol. 9, no. 1, pp. 31–48, 2016, doi: 10.1039/c5ee02985f.
- [73] H. W. Chung, J. Swaminathan, and J. H. Lienhard, “Multistage pressure-retarded osmosis configurations: A unifying framework and thermodynamic analysis,” *Desalination*, vol. 476, no. July 2019, 2020, doi: 10.1016/j.desal.2019.114230.
- [74] H. W. Chung, J. Swaminathan, L. D. Banchik, and J. H. Lienhard, “Economic framework for net power density and levelized cost of electricity in pressure-retarded osmosis,” *Desalination*, vol. 448, no. September, pp. 13–20, 2018, doi: 10.1016/j.desal.2018.09.007.
- [75] J. Benjamin, M. E. Arias, and Q. Zhang, “A techno-economic process model for pressure retarded osmosis based energy recovery in desalination plants,” *Desalination*, vol. 476, no. November 2019, 2020, doi: 10.1016/j.desal.2019.114218.
- [76] A. Altaee, G. Zaragoza, and A. Sharif, “Pressure retarded osmosis for power generation and seawater desalination: Performance analysis,” *Desalination*, vol. 344, pp. 108–115, 2014, doi: 10.1016/j.desal.2014.03.022.

Appendix A



HP5255SI-H3K

■ Module Configuration



■ Specification

Model	HP5255SI-H3K	
Membrane Material	Cellulose Triacetate (CTA)	
Membrane Type	Hollow Fiber Membrane	
OD of Hollow Fiber(Nominal)	200 μm^{*1}	
ID of Hollow Fiber(Nominal)	90 μm^{*1}	
Membrane Surface Area(Nominal)	60 m^2^{*2}	
Module	FRP	
Material of Vessel	FRP	
Dimension ϕD, ϕd, L	$\phi 176$ mm, $\phi 155$ mm, 825 mm	
$\ell 1$, $\ell 2$, $\ell 3$	40 mm, 40 mm, 107.5 mm	
Connection	A: PT 3/8 (Inlet), D: PT 1/2 (Outlet) : Bore Side C: PT 1/2 (Inlet), B: PT 1/2 (Outlet) : Shell Side	
Operating Conditions	Pressure (Max) Shell Side: 5.4 MPa Bore Side: 0.2 MPa	
	Temperature 5-40 °C	
	pH 3 - 8 ^{*3}	
	Residual Chlorine (Max) 1 mg/L ^{*3}	

*1 Please contact TOYOBO regarding the size of Hollow Fiber.

*2 Membrane surface area is calculated with OD of Hollow Fiber.

*3 The pH and residual chlorine are limited by the quality and the temperature of feed water.

■ Operation Discription (to prevent from breakage of module, parts and membrane element)

- Pressure on bore side should be lower than pressure on shell side.
- Pressure difference on shell side should be kept below 0.1 MPa.
- For start up, feed solution should flow first. For shutdown, draw solution should be stopped first.

rev.0 2017.4.12

Figure A.1 Toyobo HP5255SI-H3K membrane module specification sheet [67].

Appendix B

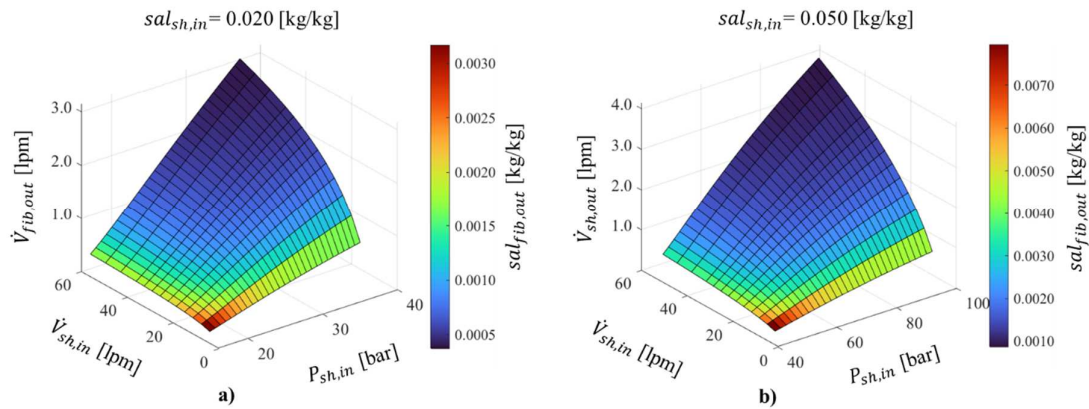


Figure B.1: Performance curves for the Toyobo HP5255SI-H3K membrane module working in the RO process in terms of permeate outlet volume flow rate and its salinity for inlet feed solution with salinities of 0.020 kg/kg (a) and 0.050 kg/kg (b).

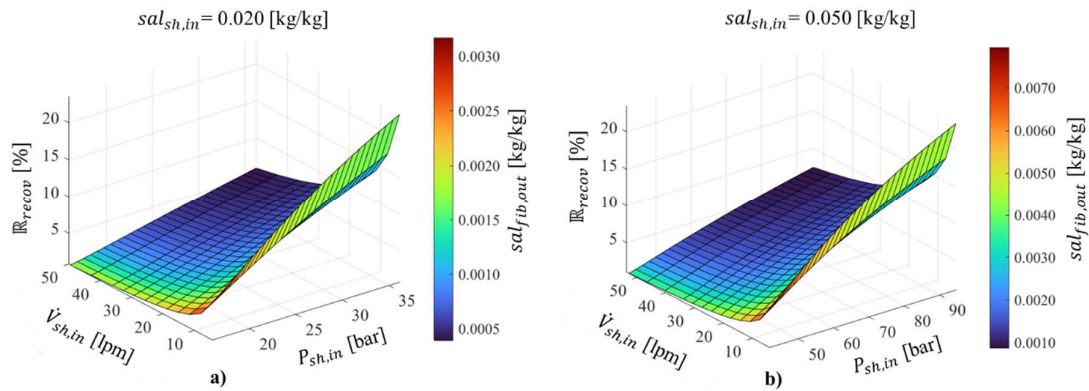


Figure B.2: Performance curves for the Toyobo HP5255SI-H3K membrane module working in the RO process in terms of recovery ratio and permeate salinity for inlet feed solution with salinities of 0.020 kg/kg (a) and 0.050 kg/kg (b).

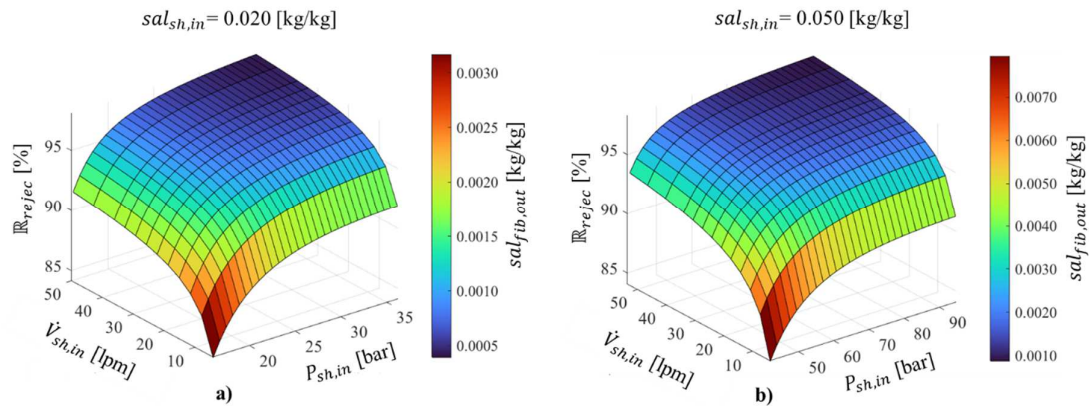


Figure B.3: Performance curves for the Toyobo HP5255SI-H3K membrane module working in the RO process in terms of salt rejection and permeate salinity for inlet feed solution with salinities of 0.020 kg/kg (a) and 0.050 kg/kg (b).

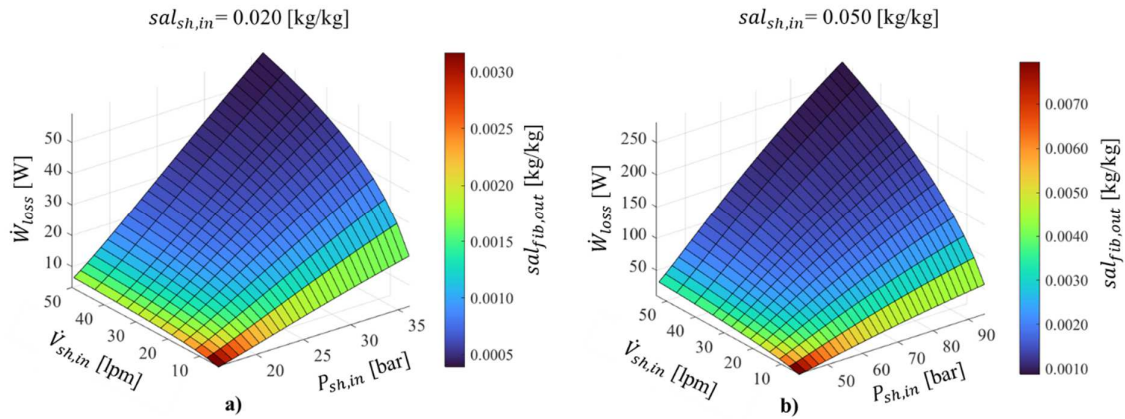


Figure B.4: Performance curves for the Toyobo HP5255SI-H3K membrane module working in the RO process in terms of power loss and permeate salinity for inlet feed solution with salinities of 0.020 kg/kg (a) and 0.050 kg/kg (b).

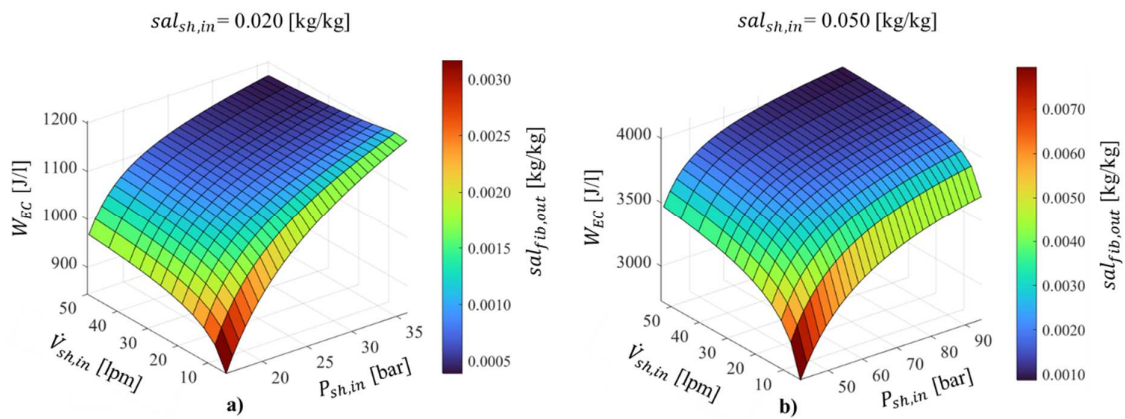


Figure B.5: Performance curves for the Toyobo HP5255SI-H3K membrane module working in the RO process in terms of extra cost work and permeate salinity for inlet feed solution with salinities of 0.020 kg/kg (a) and 0.050 kg/kg (b).

Appendix C

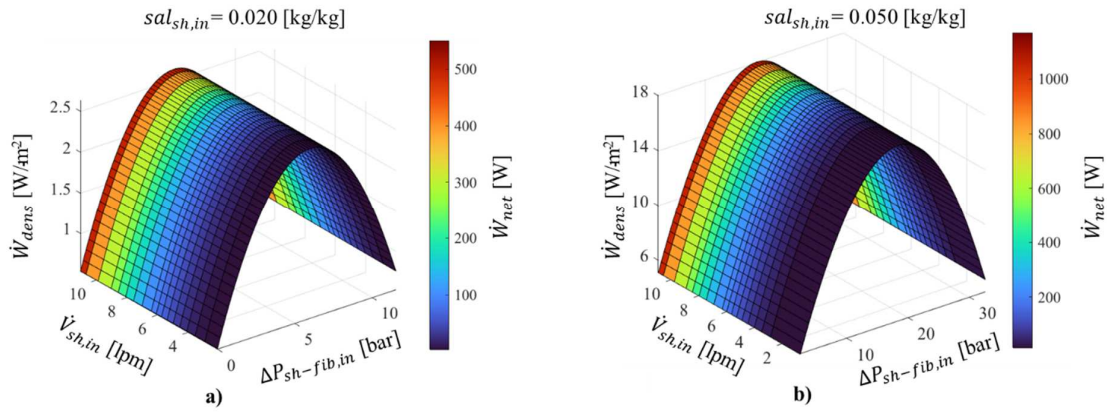


Figure C.1: Performance curve for the Toyobo HP5255SI-H3K membrane module working in the PRO process in terms of power density and net power output for inlet draw solution with salinities of 0.020 kg/kg (a) and 0.050 kg/kg (b).

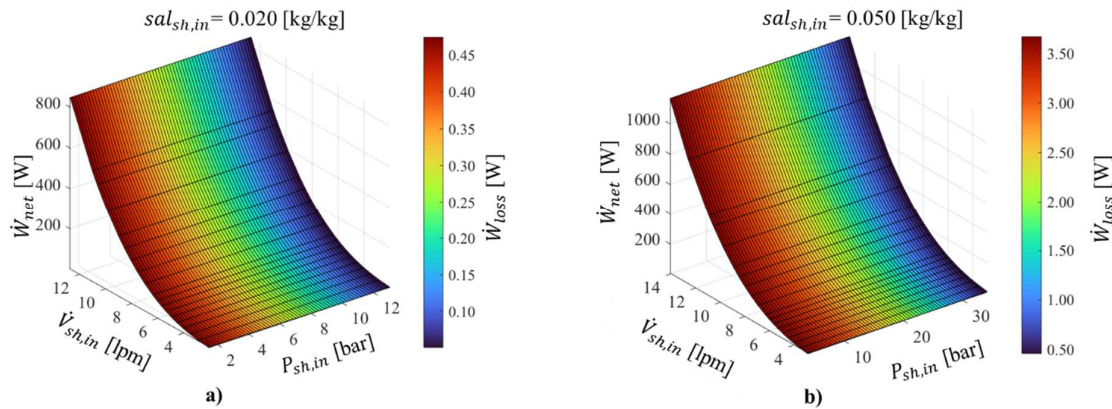


Figure C.2: Performance curve for the Toyobo HP5255SI-H3K membrane module working in the PRO process in terms net power output and power loss for inlet draw solution with salinities of 0.020 kg/kg (a) and 0.050 kg/kg (b).